A K Band E.S.R. Spectrometer using an Ammonia Maser as a Pre-Amplifier.

Thesis submitted for the Degree of
Doctor of Philosophy at the University
of Southampton

by

R.J. Collier.

1966

O Lord, how manifold are Thy works!

In wisdom hast Thou made them all;

The earth is full of Thy creation.

Psalm 104 - 24.

Acknowledgments

The author wishes to thank his supervisor - Dr. T.H. Wilmshurst - for all his thoughtful and stimulating help in this work, and also to thank Professor W.A. Gambling for his invitation to do this work and his co-operation throughout.

The author also wishes to thank Experimental Officer E.R.L. Bassett and his technical staff for their frequent assistance, and also to Chief Technician G. Newell and his technical staff who built all the mechanical parts of the maser.

Finally, the author would like to thank Mrs. E.R.L. Bassett for her work with the typing, and Miss J.P. Blundell for her work with the printing of this thesis.

R.J. Collier

University of Southampton September 1966

Contents

Introduction

The object of this research has been to continue the work begun by Dr. T.H. Wilmshurst[1] to improve the sensitivity of an E.S.R. Spectrometer. An E.S.R. (Electron Spin Resonance) Spectrometer is an instrument used to investigate electronic structure and in particular the presence of free radical electrons in a sample of a substance. The instrument consists of a microwave cavity containing a sample of a substance which is placed between the poles of a magnet. The electron energy levels are split by the Zeeman effect of the magnetic field, and, if a microwave field of the correct frequency is present in the cavity, transitions will occur between the levels usually resulting in an absorption of energy. The sensitivity depends on the ability of the detecting system to distinguish between the small coherent electronic absorption signal and the normal background thermal noise. Feher[2] has showed that theoretically the sensitivity is proportional to $f^{\frac{7}{2}}$ for a constant sample volume and $f^{\frac{1}{2}}$ if the sample volume always fills the cavity by the same fraction, where f is the frequency of the microwave field.

The first method used to improve the sensitivity used in this work was to increase the frequency from the conventional X Band to a K Band frequency. This increase in frequency also involved an increase in the magnetic field required, which was about 8,500 Gauss at K Band.

The second method was to put a suitable pre-amplifier in the microwave circuit before the first detector to reduce the noise figure of the detecting system. At this frequency there are few suitable amplifiers. Most solid state masers and parametric amplifiers are available at frequencies below 10 Gc/s. This is because they need a high pump power at a frequency greater than the signal frequency. The amplifier chosen was the original maser invented by Gordon et allia in 1955[3]. This device, the ammonia maser, has two advantages over the others as well. It does not need a separate pump and it does not need liquid helium to cool it. However, for normal purposes it has serious disadvantages as it has a narrow bandwidth - 300 c/s, a small saturation input power - 10^{-15}W and is practically untunable. These compare with 10 Mc/s bandwidth and 10^{-7}W input saturation power of a solid state maser. Only one of these disadvantages is serious and that is the low saturation. This is because the E.S.R. Spectrometer usually uses a bandwidth of about 1 c/s to reduce noise. Also, frequency determination is now trivial as the ammonia maser is untunable.

The first part of this work has been to develope a theory for the ammonia maser amplifier from the existing theory on the ammonia maser oscillator. Also an equivalent circuit has been found which simplifies the theory of the ammonia maser. Some work has also been done on the hyperfine structure in the maser amplifier characteristic.

The final part of the work has been to use an existing K Band Spectrometer and measure the improvement in sensitivity. A frequency stabilised microwave supply has been developed to achieve this, the required stability being 1 in 10^9. This work has then been compared with other possible systems.

References for the Introduction

1. W.A. Gambling and T.H. Wilmshurst - "An Electron Spin Resonance Spectrometer using an Ammonia Maser as a Pre-Amplifier".
Physics Letters Vol. 5 No. 4 15th July 1963. page 228.

2. G. Feher - "Sensitivity Considerations in Microwave Paramagnetic Resonance Absorption Techniques". page 460
The Bell Syst. Tech. Jor. March 1957.

3. J.P. Gordon, H.J. Zeiger and C.H. Townes - "The Maser - New Type of Microwave Amplifier, Frequency Standard and Spectrometer".
Physical Review Vol. 99 No. 4 August 15 1955. page 1264

Chapter 1

Basic Theory of the Ammonia Maser Amplifier

1.1 Introduction

The Ammonia Maser is a device which uses the inversion property of the ammonia molecule to amplify signals by stimulated emission of radiation. Hence the acronym M.A.S.E.R.[1] - Microwave ~~Molecular~~ Amplification by Stimulated Emission of Radiation. The ammonia molecule has two different energy levels, such that when it changes from one level to the other, it absorbs or emits electromagnetic radiation in the microwave region. The maser consists of a beam of molecules which is first passed through a focusser and level (or state) separator which removes most of ~~all~~ the lower energy level molecules. The upper energy molecules are then passed through a suitable microwave cavity. A stimulating signal is put into the cavity to cause some of the molecules to give up their energy to the cavity. The beam leaves the cavity with some of its molecules in the lower energy level. Hence this input or stimulating signal is enhanced or amplified by the stimulated emission from the beam.

In this chapter a summary of the current theory of the ammonia molecule will first be given and then a theory of the ammonia maser amplifier will be developed.

1.2 The Ammonia Molecule

The ammonia molecule consists of three hydrogen atoms forming an equilateral triangle as the base of a pyramid which has the nitrogen atom at its apex. The nitrogen atom is capable, given sufficient energy, of tunnelling through the hydrogen base moving along the axis of symmetry (see figure 1.1). This process is called 'inversion' (which is not to be confused with population inversion). Since there is a finite probability of finding the nitrogen atom on either side of the base, the Schrödinger wave function for the atom must be a linear combination of the wave functions for each side alone. There are two solutions, one of antisymmetric and one of symmetric form with respect to the base, which will satisfy the boundary conditions. As the antisymmetric form has a slightly shorter wavelength than the other, the antisymmetric form has the higher energy[2]. If W_1 and W_2 are the energies of the two forms, then they are linked by the Bohr frequency condition:-

$$W_1 - W_2 = h\nu_o \qquad 1.21$$

where h is Plank's constant and ν_o is frequency of the quantum of microwave energy emitted or absorbed when a transition occurs. Inversion levels only occur in the double well region of the atom's potential energy diagram. For higher energies, there is the normal set of single levels for a single potential well (see figure 1.2).

The effect of molecular rotation will now be considered. As the molecule rotates with the discrete set of angular velocities

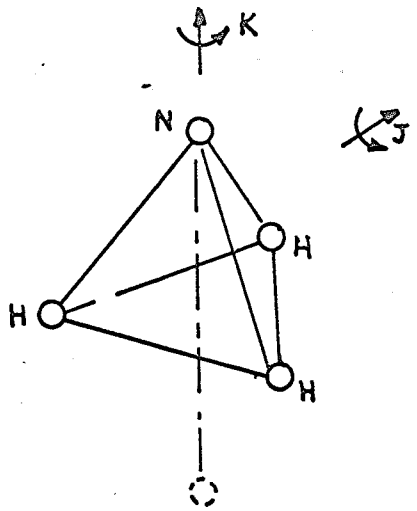

Figure 1.1 Structure of the Ammonia Molecule

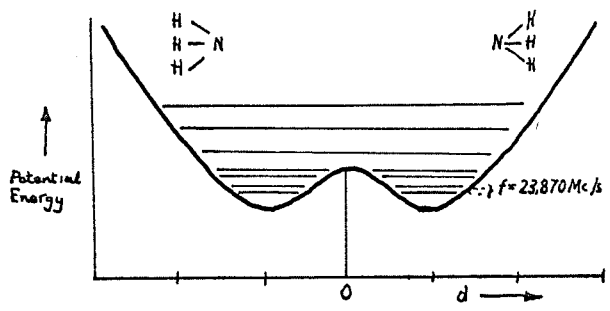

Figure 1.2 Potential Energy Diagram of the Ammonia Molecule. 'd' is the distance between the nitrogen atom and the plane of the hydrogen atoms.

predicted by quantum mechanics, the hydrogen base is distorted slightly, by centrifugal forces. This changes the shape of the potential energy diagram (see figure 1.2) and thus slightly alters the frequency of the inversion transition. As there is a discrete set of rotational states for the molecule this gives rise to a similar set of inversion frequencies or lines. All these rotational states are present in various proportions in any ammonia gas and an absorption spectrum shows the set of inversion lines. These lines are designated by two quantum numbers. The first is J which is the total angular momentum excluding nuclear spin. The second is K the component of J about the axis of symmetry. The strongest line so far observed is the J=3, K=3 line which occurs at a frequency of 23,870 Mc/s. This is the inversion line used in this present maser (see figure 1.3).

There are also two smaller effects which further split the inversion lines. The stronger effect is caused by the electric quadrupole moment of the nitrogen atom, and is described by a quantum number $F_1 = J + I_N$. (Where I_N is the nitrogen atom spin). The selection rules allow $\Delta F_1 = 0, \pm 1$ transitions. The $\Delta F_1 = \pm 1$ transitions give two pairs of satellites called the inner and outer quadrupole satellites. The $\Delta F_1 = 0$ give three lines in the main transition. The satellites are much weaker than the main transition and are not used in maser work. The weaker effect is due to the hydrogen and nitrogen magnetic interaction with the molecular rotation.

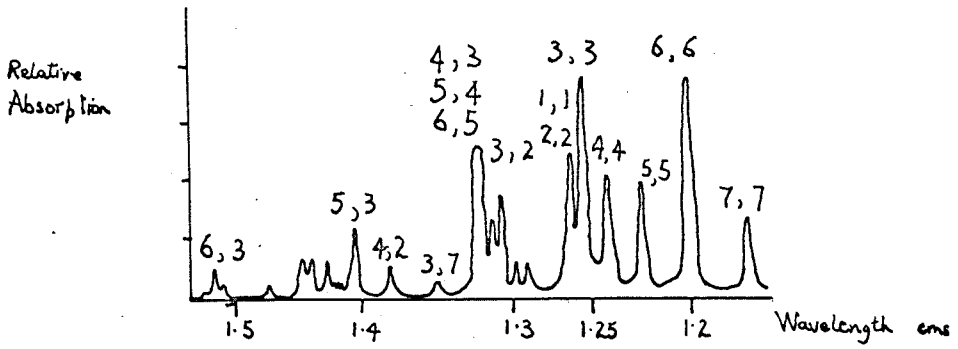

Figure 1.3 Ammonia Spectrum in the region of a wavelength of 1.25 cms.

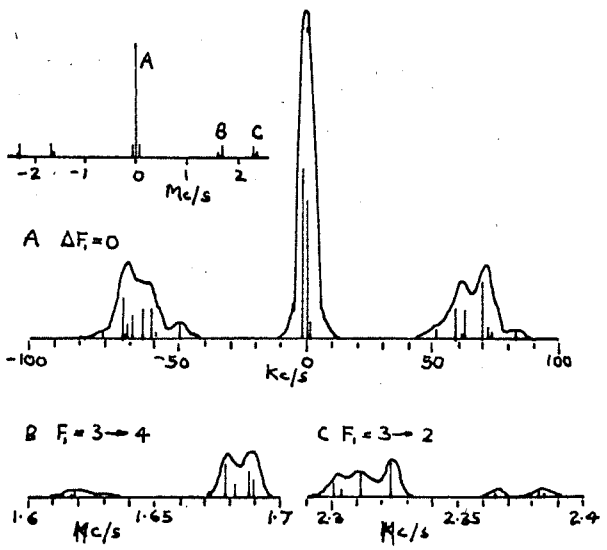

Figure 1.4 Hyperfine Structure of the J=3, K=3 Line. A - Main Line and Magnetic Satellites (Main line reduced by a factor of 5), B - Inner Quadrupole Satellites, C - Outer Quadrupole Satellites.

This effect splits all the energy levels into four components. For the main transition this gives 30 lines in all. Fortunately, 18 of these produce a pair of magnetic satellites lying either side of the main transition and the other 12 form 3 sets of 4 degenerate levels in the main transition (see figure 1.4). Thus the effect of this hyperfine structure is to weaken and broaden the main transition. There are other much weaker interaction effects which were fully treated by Gordon[3] but normally their effect can be neglected.

1.3 The Beam Focusser

The focusser or energy level separator is a device for focussing the upper energy level molecules into a molecular beam and defocussing the lower energy level molecules out of the beam. In figure 1.5 the focusser is shown to consist of an arrangement of parallel wires which produce an electric field when each one is alternately charged. The electric field increases radially outwards from the axis of the focusser. Now Shimoda[5] gives the equation for the electric field E in terms of the voltage between V for an 8 pole focusser as:-

$$E = \frac{2\,V}{R} \qquad 1.31$$

When a molecule is put in a strong electric field the inversion effect of cancelling the permanent dipole moment of the molecule μ is partly quenched and the molecule has a dipole moment. The energies of the inversion states are given by:-

$$W = W_o \pm \left[\left(\frac{h\,\nu_o}{2} \right)^2 + \left(\frac{\mu\,EMK}{J(J+1)} \right)^2 \right]^{\frac{1}{2}} \qquad 1.32$$

where W_o is the average energy of the upper and lower inversion levels. M is the projection of J onto the electric field vector. The force on a molecule f_r is given by the gradient of W:-

$$f_r = \left(\frac{\mu\,MK}{J(J+1)} \right)^2 \cdot \frac{2}{h\,\nu_o} \cdot \frac{4\,V^2}{R^2} \qquad 1.33$$

assuming that $\mu E \ll h\,\nu_o$.

Now if v_r is the radial velocity and v_z the axial velocity components of the molecular velocity, then the conditions for the

Figure 1.5

Block Diagram of the Maser Focusser and Cavity

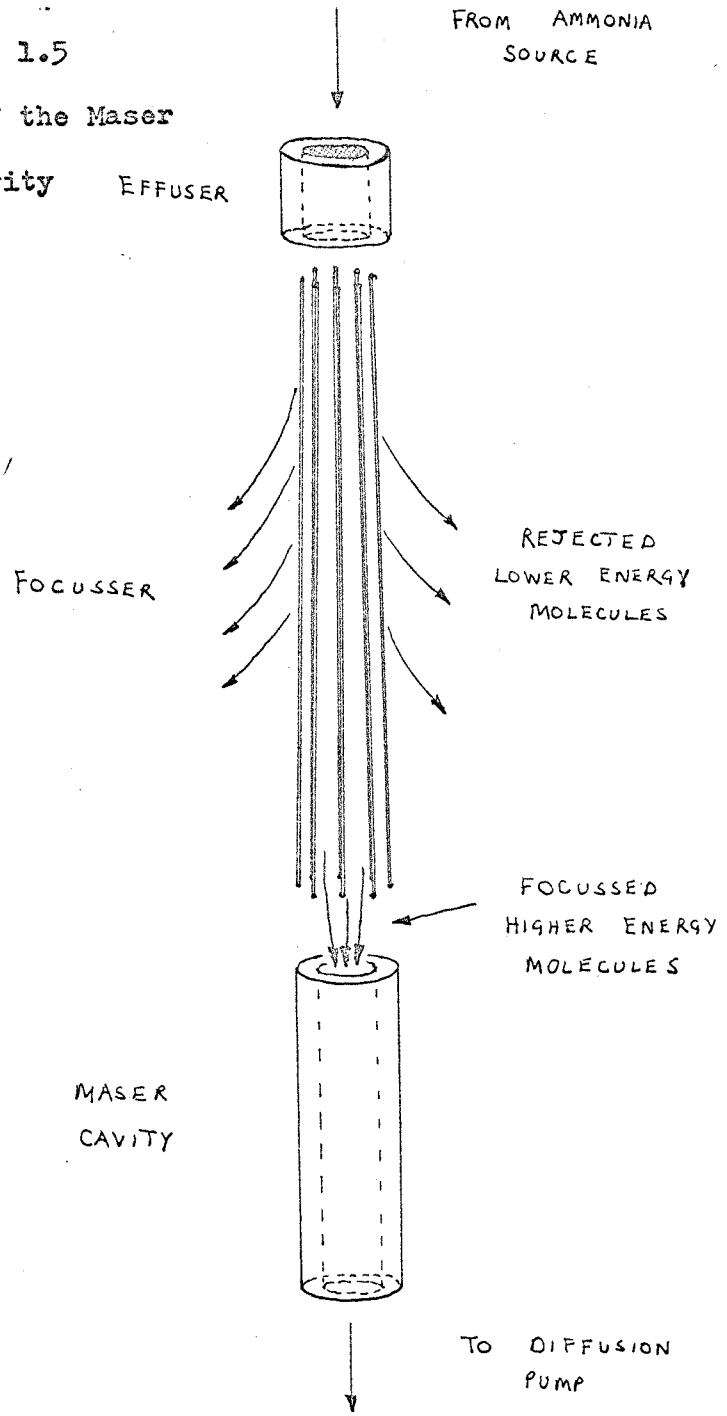

focusser to operate are:-

$$v_o = \frac{\mu MK}{J(J+1)} \cdot \left(\frac{8}{mh\,\nu_o}\right)^{\frac{1}{2}} \cdot \frac{V}{R} \geqslant v_r \qquad 1.34$$

$$v_c \geqslant v_z \cdot \frac{\pi}{2} \cdot \frac{R}{L_f} \qquad 1.35$$

where v_c is the critical radial velocity and L_f is the length of the focusser. A more exact treatment of the above has been achieved by Vonbun[4].

Now for any axial velocity v_z all molecules in a given M state are kept within the solid angle Ω where:-

$$\Omega = \pi \left(\frac{v_c}{v_z}\right)^2$$

and since this angle is small, the number of molecules in the angle is proportional to Ω and hence to v_c^2 and thus to M^2. Shimoda[5] suggests that instead of calculating the various values of v_c for the various M states a weighted value of:-

$$\langle M^2 \rangle = \frac{6J^3 + 9J^2 + J - 1}{5\,(2J+1)} = 7 \text{ for } J = 3 \qquad 1.36$$

simplifies the calculation. Further as a first approximation the most probable velocity $v_o = v_z$ where:-

$$v_o = \left(\frac{2KT}{m}\right)^{\frac{1}{2}} \qquad 1.37$$

where K is Boltzmann's constant and T is the beam temperature and m is the mass of a molecule. The above conditions are sufficient for the design of a practical focusser.

1.4 The Maser Cavity

The maser cavity is shown in figure 1.5 and is used for coupling the input signal to the molecular beam and also for coupling the amplified signal out, and on, to the detecting system. The power P_m emitted by molecular beam in the presence of a stimulating signal is:-

$$P_m = nh\nu_o a_1 \left| (t) \right|^2 \qquad 1.41$$

where n is the number of upper level molecules entering the cavity per second and $\left| a_1 (t) \right|^2$ is the probability that a downward transition has taken place. This probability is a function of E the microwave field in the cavity and $\bar{\mu}$ the matrix element between the two states for the component of dipole moment in the direction of E. The probability can be found from first order perturbation theory as:-[6]

$$\left| a_1 (t) \right|^2 = \frac{\left(\frac{\bar{\mu}E}{h}\right)^2}{(\nu - \nu_o)^2 + \left(\frac{\bar{\mu}E}{h}\right)^2} \sin^2 \left\{ \pi \left[(\nu - \nu_o)^2 + \left(\frac{\bar{\mu}E}{h}\right)^2 \right]^{\frac{1}{2}} t \right\} \qquad 1.42$$

Now the transit time of the molecules through the cavity is $\frac{L}{v_o}$ where L is the length of the cavity. The power emitted in the cavity is given by putting $t = \frac{L}{v_o}$ is equation 1.41 and, using equation 1.42, the equation becomes:-

$$P_m = nh\nu_o \frac{\theta^2}{\delta^2 + \theta^2} \sin^2 (\delta^2 + \theta^2)^{\frac{1}{2}} \qquad 1.43$$

where $\theta = \frac{\pi\bar{\mu}EL}{v_o h}$ and $\delta = \frac{\pi L(\nu - \nu_o)}{v_o}$ 1.44

A more rigorous treatment using the velocity distribution in the beam will be given in section 1.6. For small signals, equation 1.44 becomes:-

$$P_m = nh\nu_o\theta^2 \quad \frac{\sin^2\delta}{\delta^2} \qquad 1.45$$

And at $\delta = 0$ this becomes:-

$$P_m = nh\nu_o\theta^2$$

This is the midband power. The small signal approximation is the linear portion of the amplifier. At midband, for larger signals, the power emitted is:-

$$P_m = nh\nu_o \sin^2\theta \qquad 1.46$$

In section 1.2 it was shown that the main transition of the $J = 3$, $K = 3$ rotational state inversion line was split into three hyperfine lines. These lines are designated by the F_1 quantum number as the $F_1 = 2,3,4$ lines. This is because these transitions are the $\Delta F_1 = 0$ transitions. Shimoda[5] has worked out the amplitudes (c_2, c_3, c_4.) and the centre frequencies (ν_2, ν_3, ν_4) for these hyperfine lines. Equation 1.45 can now be modified to show this effect:-

$$P_m = nh\nu_o\theta^2 \left\{ \frac{c_2\sin^2\delta_2}{\delta_2^2} + \frac{c_3\sin^2\delta_3}{\delta_3^2} + \frac{c_4\sin^2\delta_4}{\delta_4^2} \right\} \qquad 1.47$$

where $\delta_2 = \dfrac{\pi L(\nu - \nu_2)}{v_o}$ etc.

These lines can only be resolved if $\frac{L}{v_o}$ is large. The effect of the velocity distribution about v_o is to smear out the zeros in the spectrum. This will be discussed in section 1.6. Normally

these lines are not resolved and the equation 1.47 becomes equation 1.45 with the condition that:-

$$c_2 + c_3 + c_4 = 1 \qquad 1.48$$

Transitions caused by spontaneous emissions are negligible at these frequencies as the spontaneous relaxation time is much greater than $\frac{L}{v_o}$. The only source of noise in the maser is the thermal noise of the cavity walls. If a large number of transitions is stimulated, noise can result as the device will begin to lose its coherent nature. The cause of this effect would be molecular collisions and molecular collisions with the cavity walls. At the normal pressure in the cavity, the mean free path of a molecule is much greater than the length of the cavity. Thus collision noise is a small effect.

1.5 The Mid-band Gain of the Maser Amplifier

In this section an expression for the mid-band Gain is derived using the equivalent circuit shown in figure 1.6. In order to find out how the Gain is effected by the various constants of the molecular beam a further expression is derived linking the maser equivalent circuit with the gas constants of the molecular beam, the cavity constants and the coupling coefficient. This expression is derived using the principle of superposition. A chart showing the various steps in this part of the theory is shown in figure 1.6. Following this theory the equations are developed to cover the saturation phenomena.

As the circulator (see figure 1.6) was also an isolator, the voltage reflection coefficient ρ_v in the maser arm is equal to the maser voltage gain. The reflection coefficient is:-

$$\rho_v = \frac{Z_m - R_o}{Z_m + R_o} = \frac{G_o - Y_m}{G_o + Y_m} \qquad 1.51$$

where R_o is the characteristic impedance of the guide and Z_m is the impedance of the cavity referred to the guide. G_o and Y_m are the respective conductances. In figure 1.6, the equivalent circuit of the coupling hole to the maser cavity is represented as a transformer of ratio m:1. This representation was used to simplify the expressions. Assuming a high 'Q' cavity then:-

$$Y_m = m^2 G_c \left\{ 1 + \frac{j\Delta\omega}{\Delta\omega_c} \right\} \qquad 1.52$$

where G_c is the lumped conductance of the cavity and $\Delta\omega$ and $\Delta\omega_c$ are given by the usual definitions:-

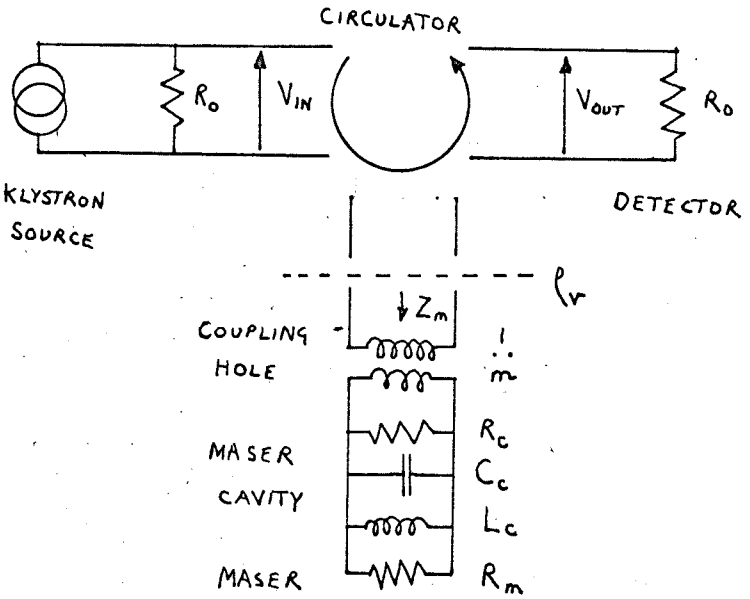

Figure 1.6a Maser Cavity Equivalent Circuit

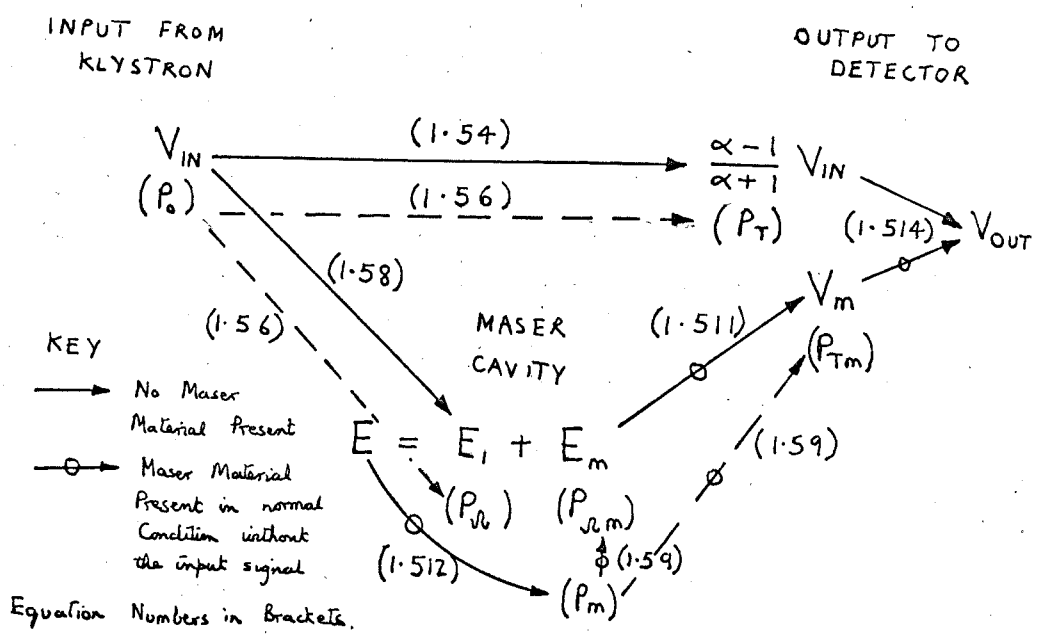

Figure 1.6b Diagram of the Principle of Superposition

$$\Delta\omega_c = \frac{\omega_c}{2Q_o} \qquad \text{and} \qquad \Delta\omega = \omega - \omega_c$$

and Q_o is the unloaded Q of the cavity, and ω_c is the resonant frequency of the cavity. Now if α is the coupling coefficient which is normally defined as $\frac{G_o}{m^2 G_c}$ then ρ_v is given by:-

$$\rho_v = \frac{\alpha - \left\{1 + j\frac{\Delta\omega}{\Delta\omega_c}\right\}}{\alpha + \left\{1 + j\frac{\Delta\omega}{\Delta\omega_c}\right\}} \qquad 1.53$$

and at midband:-

$$\rho_v = \frac{\alpha - 1}{\alpha + 1} \qquad 1.54$$

Now the addition of the molecular beam is equivalent to adding a negative conductance G_m in parallel with G_c. The expression for the maser gain G then becomes:-

$$G = \rho_v = \frac{\alpha - 1 - \beta}{\alpha + 1 + \beta} \qquad 1.55$$

where $\beta = \frac{G_m}{G_c}$

As $\beta \rightarrow -(1 + \alpha)$ the system oscillates as $\rho_v \rightarrow \infty$.

The Gain equation can also be found by a more complex method, and by comparing the two methods an expression for the negative conductance G_m can be found.

The complex method uses the principle of superposition. The system is first analysed without the molecular beam present. Secondly the system is analysed without any power coming from the klystron but with the maser beam present and emitting the power it

would be emitting if the klystron power was present. Finally the two results are added to give the complete system.

Part of the power P_o which the klystron source sends into the system goes into the cavity and is absorbed there. The rest is reflected at the coupling hole and is dissipated at the detector. If P_Ω and P_T are these powers respectively then:-

$$P_\Omega = \frac{4\alpha P_o}{(\alpha + 1)^2} \qquad \text{and } P_T = \frac{(\alpha - 1)^2 P_o}{(\alpha + 1)^2} \qquad 1.56$$

It is convenient to define the 'Q' factor of the cavity as:-

$$Q_o = \frac{\omega_c W}{P_\Omega} = \frac{\omega_c k E_1^2}{P_\Omega} \qquad 1.57$$

where W is the stored energy in the cavity, E_1 is the effective amplitude of the microwave field in the cavity, and k is some integrated capacitance for the cavity. The mode used in practice in the cavity was a simple one, E_{010}. This mode has a 'half wave' across any diameter and is constant along the molecular beam axis. For more complicated modes this theory is too simple, and this problem is further discussed in section 2.4. If the equivalent circuit for the cavity is used then $kE_1^2 = \frac{1}{2}C_c V^2$ where V is the voltage across the capacitance C_c. Now P_o can be expressed in terms of an input voltage using the normal definition:-

$$V_{in} = \sqrt{\frac{P_o}{G_o}}$$

and linking equations 1.56 and 1.57 gives the first expression required:-

$$E_1 = \sqrt{\frac{4\alpha Q_o G_o}{\omega_c k(1 + \alpha)^2}} \; V_{in} \qquad 1.58$$

If the molecular beam is present and the input power P_o is not and the beam is supposed to be emitting power P_m then this power will be dissipated in the cavity and in the detecting system. If $P_{\Omega m}$ and P_{Tm} are the powers respectively then:-

$$P_{\Omega m} = \frac{P_m}{1 + \alpha} \qquad \text{and } P_{Tm} = \frac{\alpha P_m}{1 + \alpha} \qquad 1.59$$

The power dissipated in the cavity, $P_{\Omega m}$, will also set up an oscillating field which can be derived from equation 1.57:-

$$E_m = \sqrt{\frac{Q_o P_m}{(1 + \alpha)\ \omega_c k}} \qquad 1.510$$

Where E_m is the amplitude of the field in the cavity.

The power dissipated in the detecting system, P_{Tm} can be expressed in terms of an output voltage V_m :-

$$V_m = \sqrt{\frac{P_{Tm}}{G_o}} = \sqrt{\frac{\alpha P_m}{(1 + \alpha) G_o}}$$

Linking equations 1.59 and 1.510 gives the second expression required:-

$$E_m = V_m \sqrt{\frac{Q_o G_o}{\alpha\ \omega_c\ k}} \qquad 1.511$$

One further equation can be obtained from the maser theory in the previous section. From equation 1.45, an expression for P_m is:-

$$P_m = AB^2E^2 \qquad 1.512$$

where $A = nh\nu_o$ and $B = \frac{\pi\mu L}{v_o h}$ (assuming at midband)

This can be expressed in terms of V_m as:-

$$V_m = \sqrt{\frac{\alpha AB^2}{(1 + \alpha)\ G_o}}\ E \qquad 1.513$$

Finally, by superposition, the total field E in the cavity is equal to E_1 and E_m. From equations 1.58, 1.511 and 1.513, and expression

for V_m in terms of V_{in} is:-

$$V_m = V_{in} \frac{\sqrt{\frac{4\alpha Q_o}{\omega_c k}}}{(1+\alpha)\left\{\sqrt{\frac{(1+\alpha)}{\alpha AB^2}} - \sqrt{\frac{Q_o}{\alpha\,\omega_c\,k}}\right\}}$$

Now the total output at the detector consists of V_m and the contribution from P_T which together form V_{out}:-

$$V_{out} = V_m + V_{in}\frac{(\alpha - 1)}{(\alpha + 1)} \qquad 1.514$$

Using the previous equation to simplify this equation, an expression for the gain is obtained as:-

$$G = \frac{V_{out}}{V_{in}} = \frac{\alpha - 1 + \gamma}{\alpha + 1 - \gamma} \qquad 1.515$$

where $\gamma = \sqrt{\frac{Q_o AB^2(1+\alpha)}{\omega_c k}}$

Comparing this equation with 1.55 shows that $\beta = -\gamma$. This gives an expression for G_m as:-

$$G_m = -G_c \sqrt{\frac{Q_o AB^2(1+\alpha)}{\omega_c k}} \qquad 1.516$$

So far in this theory only small signals have been considered. However, the principle of superposition also applies when the maser is saturated by a large input signal. The gain cannot be derived explicitly when the maser is saturated but the saturation characteristics can be obtained numerically. By applying the principle of superposition again and using equation 1.46 (which is the

mid-band saturation equation for the maser) an expression which can be solved numerically can be obtained. Using the same notation for A and B as used in equation 1.512, equation 1.46 becomes:-

$$P_m = A \sin^2 B E$$

Using equation 1.510 and the superposition equation $E = E_1 + E_m$ the required expression is:-

$$\left|\sin B(E_1 + E_m)\right| = CE_m \qquad 1.517$$

where $C = \sqrt{\dfrac{\omega_c k(1 + \alpha)}{A Q_o}}$

Equation 1.517 can be solved numerically to give a set of values of BE_1 and BE_m. The ratio of these two quantities can be defined as G_1 the implicit gain. This can be linked with the explicit gain G by the following equation (derived from equations 1.58, 1.511, and 1.514):-

$$G_1 = \frac{E_m}{E_1} = \frac{(1 + \alpha)}{2\alpha} \cdot \frac{V_m}{V_{in}} = \frac{(1 + \alpha) G - (\alpha - 1)}{2\alpha} \qquad 1.518$$

For small signals:-

$$G_1 = \frac{1}{\frac{C}{B} - 1} \qquad 1.519$$

The whole maser characteristic can be plotted on the same graph by plotting BE_m (which is proportional to the maser output voltage) against $\frac{B}{C}$ (which is proportional to the square root of the number of upper energy level molecules entering the cavity i.e. $\bar{n}$) for various values of BE_1 (which is proportional to the input voltage).

The modulus sign in equation 1.517 is a condition of quantum mechanics. These characteristics also include the case where the maser is oscillating (i.e. when BE_1 is zero). This oscillation characteristic was found by Shimoda[5] to be of similar form to:-

$$\frac{B}{C} = \frac{BE_m}{\sin BE_m} \qquad 1.520$$

Equation 1.520 can be obtained from 1.517 by putting $E_1 = 0$. The whole maser characteristic is plotted out in figure 1.7. The maximum output from the oscillator is given as $A \longrightarrow \infty$, and is $\frac{\pi}{2B}$. It can be seen from the diagram that for high gains $\frac{B}{C}$ must be almost unity. The maser characteristic does not really solve the condition when $\frac{B}{C} > 1$ and $E_1 \neq 0$ as the maser is then both oscillating and amplifying at different frequencies. A solution to this condition is beyond the scope of this work.

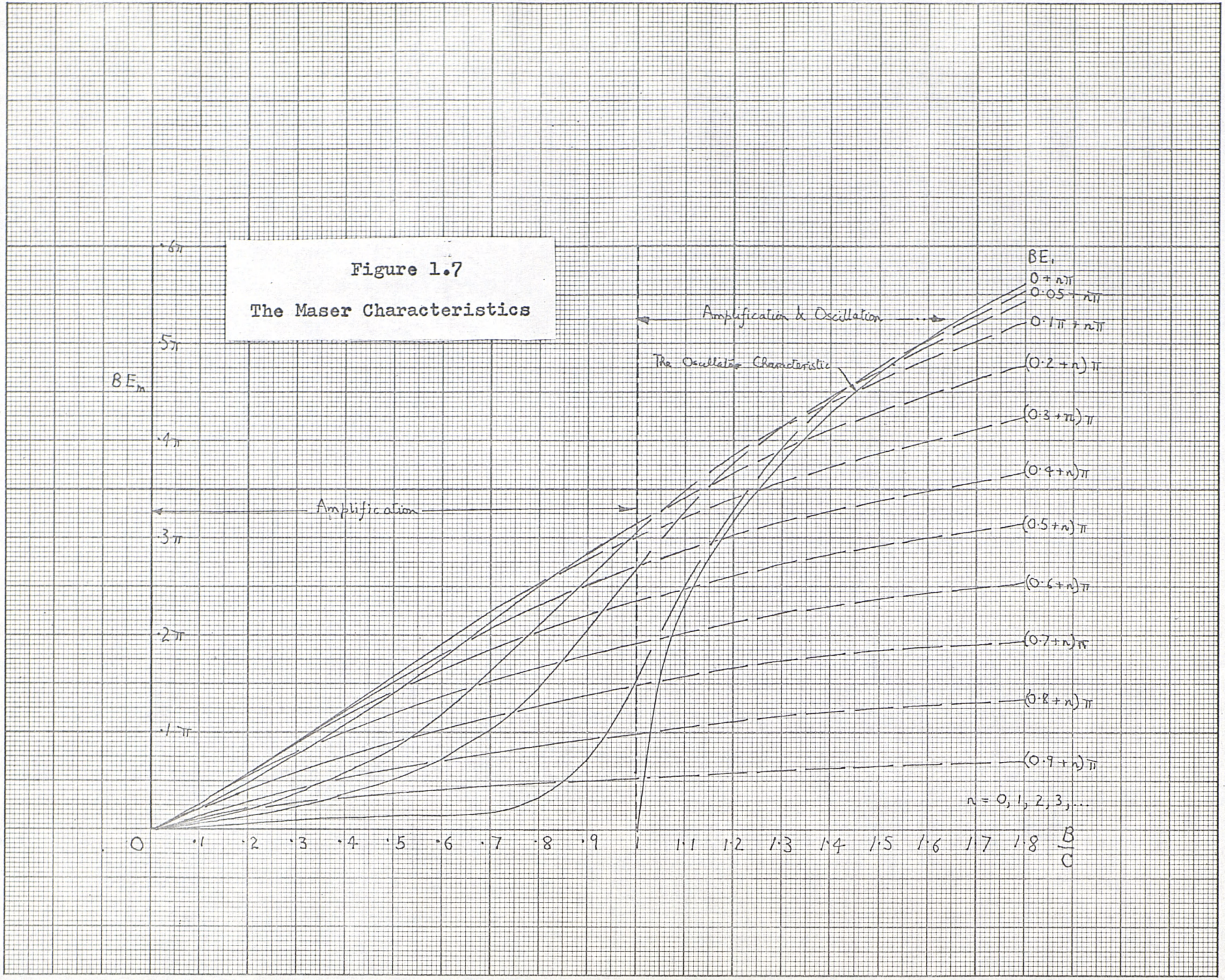
Figure 1.7
The Maser Characteristics
BE_n
BE_1
$0 + n\pi$
$0.05 + n\pi$
$0.1\pi + n\pi$
$(0.2 + n)\pi$
$(0.3 + n)\pi$
$(0.4 + n)\pi$
$(0.5 + n)\pi$
$(0.6 + n)\pi$
$(0.7 + n)\pi$
$(0.8 + n)\pi$
$(0.9 + n)\pi$
$n = 0, 1, 2, 3, \ldots$
Amplification & Oscillation
The Oscillator Characteristic
Amplification
$\cdot 6\pi$
$\cdot 5\pi$
$\cdot 4\pi$
$\cdot 3\pi$
$\cdot 2\pi$
$\cdot 1\pi$
0 ·1 ·2 ·3 ·4 ·5 ·6 ·7 ·8 ·9 1 1·1 1·2 1·3 1·4 1·5 1·6 1·7 1·8
$\frac{B}{C}$

1.6 Velocity Distribution Theory and the Focusser Characteristic

Shimoda[5] has investigated the effects of the velocity distribution on the performance of the Maser. His work will be given first, briefly, and then his equations will be used to find an expression for the efficiency of the focusser. The first assumption that Shimoda makes is that the molecules enter the focusser in a Maxwell-Boltzmann Distribution:-

$$N(v_r,v_z)\ dv_r dv_z = \frac{4Nv_r}{v_o^3\sqrt{\pi}}\ \exp(-\frac{v^2}{v_o^2})\ dv_r dv_z \qquad 1.61$$

where N is the number density of the molecules in the beam.

P_m - the power emitted from the beam is expressed in terms of P_1 - the power emitted by those molecules which travel straight through the cavity and P_2 - the power emitted from those which collide with the walls.

The condition that the molecules do not collide with the cavity walls is:-

$$\frac{v_z}{L} > \frac{v_r}{R} \qquad 1.62$$

Here it has been assumed that the radius of the inlet and outlet of both the cavity and the focusser are equal to R.

Shimoda's expressions for P_1 and P_2 are:-

$$P_1 = \bar{n}h\nu_o B^2 E^2\ \frac{4}{\sqrt{\pi}v_o^2} \int_o^{v_c} \int_{\left(\frac{L}{R}\right)v_r}^{\left(\frac{2L_f}{\pi R}\right)v_c} \frac{v_r}{v_z} \exp(-\frac{v^2}{v_o^2})\ dv_z dv_r \qquad 1.63$$

$$P_2 = \bar{n} h \nu_o B^2 E^2 \frac{1}{\sqrt{\pi}\, v_o^2} \int_o^{v_c} \int_o^{\left(\frac{L}{R}\right) v_r} \frac{v_z}{v_r} \exp\left(-\frac{v^2}{v_o^2}\right) dv_z dv_r \qquad 1.64$$

where $\bar{n}$ is the total number of upper level molecules entering the focusser per second. Both the above equations have been re-expressed in the terms used in this work. Using equation 1.45:-

$$P_m = P_1 + P_2 = nh\nu_o B^2 E^2 = AB^2 E^2$$

Now if η_f is efficiency of the focusser then:-

$$A = \bar{n}\, \eta_f h \nu_o \quad \text{or} \quad n = \bar{n}\, \eta_f$$

Using these results and the solution to equations for P_1 and P_2 in terms of exponential integrals which Shimoda derived, an expression for η_f becomes:-

$$\eta_f = \frac{v_c^2}{\sqrt{\pi}\, a^2 v_o^2} \left[1 - e^{-a^2} - (a^2 + 1)E_i(-a^2) + a^2 E_i(-b^2) + 2\log a + C_e\right] \qquad 1.65$$

where $a = \frac{Lv_c}{Rv_o}$; $b = \frac{2 L_f v_c}{\pi R v_o}$ and C_e is Eulers Constant which is 0.577 ....

This equation can be simplified for $a \ll 1$ to:-

$$\eta_f = \frac{2v_c^2}{\sqrt{\pi}\, v_o^2} \left[1 + \log\left(\frac{2L_f}{\pi L}\right)\right] \qquad 1.66$$

However for $a \sim 1$ then

$$\eta_f \sim \frac{R^2}{L^2} \sim \frac{v_c^2}{v_o^2} \quad \left(\text{if } L \sim \frac{2L_f}{\pi}\right) \qquad 1.67$$

And for $a > 1$ then:-

$$\eta_f \sim \frac{R^2}{L^2} \frac{1}{\sqrt{\pi}} (1.577 + 2\log a) \qquad 1.68$$

finally as $a \longrightarrow \infty$, $\eta_f \longrightarrow 1$.

It is also worth noting that the effect of the velocity distribution is also to smear out the zeros in the line shape equation given by equation 1.45. This means that for large values of δ the expression is averaged to give:-

$$P_m = \frac{AB^2E^2}{2\delta^2} \qquad 1.69$$

1.7 The Equivalent Circuit of an Ammonia Maser Amplifier and the Maser Bandwidth.

The use of equivalent circuits in electronics is normally to simplify the analysis of a system, particularly the frequency response of a system. In this section the molecular beam will be represented by a lumped electric susceptibility in the cavity. The normal convention is to define susceptibility by χ_e where:-

$$\chi_e = \chi'_e + j\chi''_e \qquad 1.71$$

In section 1.5 the maser cavity was represented by an equivalent circuit of C_c, L_c and G_c in parallel. The effect of the beam is to add to the total capacitance C_c to give:-

$$C_c (1 + \epsilon_o \chi'_e + j \epsilon_o \chi''_e) \qquad 1.72$$

where ϵ_o is the permittivity of free space. The susceptance of this capacitance is:-

$$j \omega C_c + j \omega C_c \epsilon_o \chi'_e - C_c \omega \epsilon_o \chi''_e \qquad 1.73$$

This shows that the beam adds a capacitance C'_m of value $\epsilon_o C_c \chi'_e$ and a conductance G_m of value $- \omega \epsilon_o \chi''_e C_c$.

Using equation 1.516, the line shape from equation 1.45 is:-

$$\chi''_e = + \frac{G_c}{\epsilon_o C_c} \sqrt{\frac{Q_o (1 + \alpha) A}{\omega_o^3 k}} B \left| \frac{\sin\delta}{\delta} \right| \qquad 1.74$$

This assumes that $\omega_c = \omega_o$. Now the Kronig-Kramers[7] relationships link the real and imaginary parts of the susceptibility and for a sharp resonance they are of the form:-

$$\chi''(\omega) = -\frac{2}{\pi}\int_0^\infty \frac{\chi'(\gamma)\ d\gamma}{(\gamma - \omega)}$$

$$\chi'(\omega) = \frac{2}{\pi}\int_0^\infty \frac{\chi''(\gamma)\ d\gamma}{(\gamma - \omega)} \qquad 1.75$$

From these expressions an equation for the real part of the susceptibility is:-

$$\chi'(\gamma) = \frac{2F}{\pi}\int_0^\infty \left| \frac{\sin \omega}{\omega} \right| \frac{1}{(\omega - \gamma)}\ d\omega$$

Where F is a constant.

This can be simplified using complex contour integrals. The modulus sign will be considered after the integration, as this is a simpler approach. Let $\omega = z$ (a complex variable).

Then:-

$$\chi'(\gamma) = \int \frac{2F}{\pi} \oint \frac{e^{iz}}{z\,(z - \gamma)}\ dz$$

The poles at $z = 0$ and $z = \gamma$ give residues:-

$$\mathcal{R}_{z=0} = -\frac{1}{\gamma} \quad ; \quad \mathcal{R}_{z=\omega} = \frac{e^{i\gamma}}{\gamma}$$

And from the Residue Theorem:-

$$\chi'(\gamma) = \int \frac{2F}{\pi} \cdot \frac{\pi i}{2}\left(-\frac{1}{\gamma} + \frac{e^{i\gamma}}{\gamma}\right)$$

$$= F\ \frac{(\cos \gamma - 1)}{\gamma}$$

Now when $0 \leqslant |\gamma| \leqslant \pi$ then the modulus sign has no effect. However when $\pi < |\gamma| < 2\pi$ then the effect of the modulus sign is to reverse the sign of the residue at $z = \gamma$. Thus the effect of taking the modulus is to modify the expression to:-

$$\chi'(\omega) = F\ \frac{|\cos \omega| - 1}{\omega} \qquad 1.76$$

The appropriate value of the constant F can be obtained from equation 1.74 and is:-

$$F = + \frac{1}{\epsilon_o} \sqrt{\frac{AB^2}{Q_L \omega_o k}} \qquad 1.77$$

where Q_L is the loaded 'Q' of the cavity.

The complete expressions for the susceptibilities are:-

$$\chi'_e = F \frac{|\cos\delta| - 1}{\delta} \qquad 1.78$$

$$\chi''_e = F \left| \frac{\sin\delta}{\delta} \right| \qquad 1.79$$

As before in section 1.6, the velocity distribution will smear out the function for large values of δ to give:-

$$\chi''_e = \frac{F}{\sqrt{2}\,\delta} \quad \text{and} \quad \chi'_e = \frac{F}{\delta} \left(\frac{1}{\sqrt{2}}\right) \qquad 1.710$$

These susceptibilities are plotted out in figure 1.8.

Now if the midband definition of G_m given in equation 1.516 is called G_{mo} to distinguish it from the general function of frequency, the original expression for gain (1.55) now becomes as a function of frequency:-

$$G = \frac{\alpha - \left(1 + j \frac{\Delta\omega}{\Delta\omega_c}\right) - \beta \left| \frac{\sin\delta}{\delta} \right| - j\beta \frac{|\cos\delta| - 1}{\delta}}{\alpha + \left(1 + j \frac{\Delta\omega}{\Delta\omega_c}\right) + \beta \left| \frac{\sin\delta}{\delta} \right| + j\beta \frac{|\cos\delta| - 1}{\delta}} \qquad 1.711$$

The equation is too complex to solve easily and so certain approximations will be made. To first order of magnitude, the terms involving $\Delta\omega$ can be neglected as $\Delta\omega_c$, the cavity bandwidth, is much greater than the maser bandwidth. To first order the equation

Figure 1.8 Maser Susceptibilities

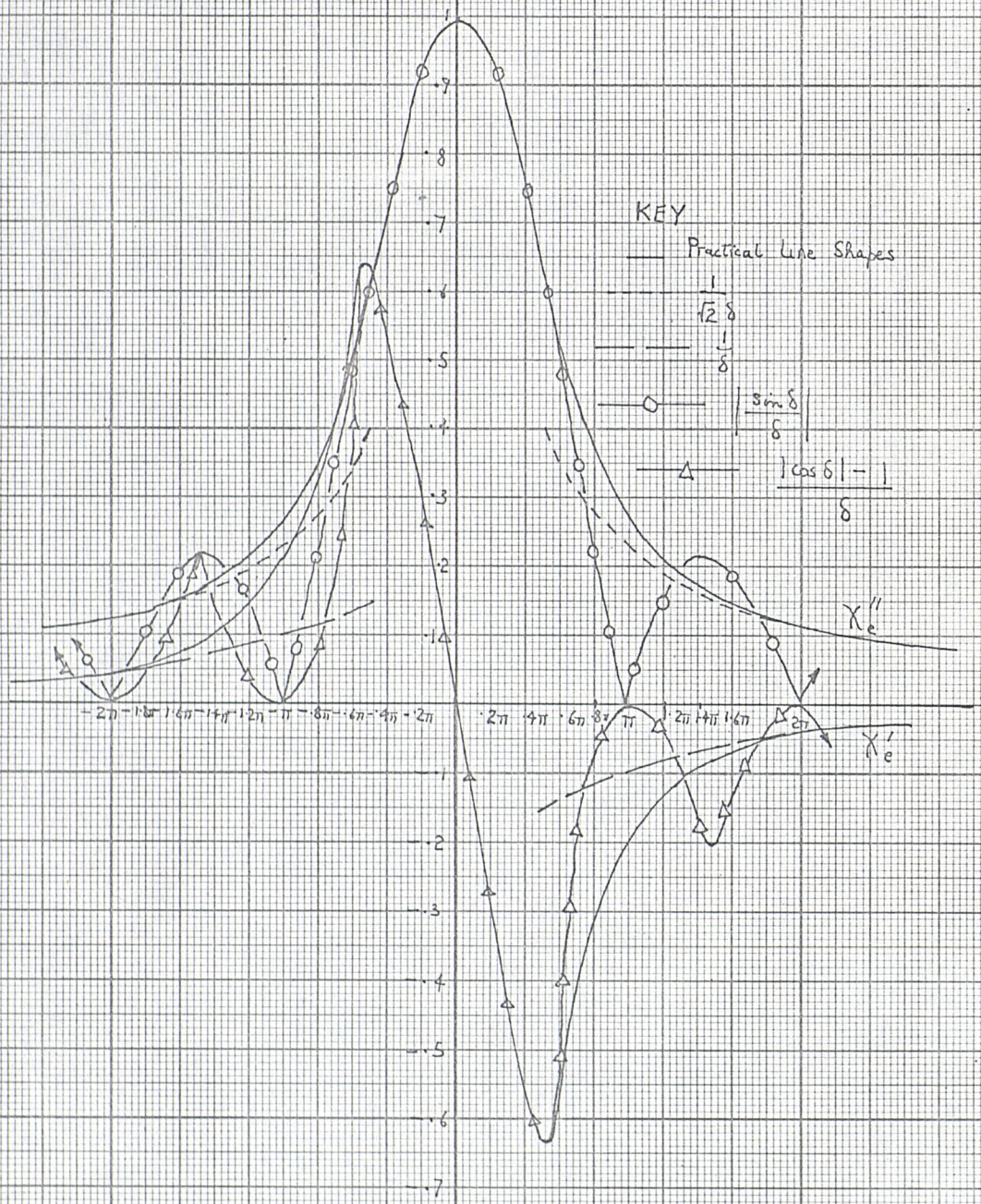

becomes:-

$$G = \frac{\alpha - 1 - \beta + j\frac{1}{2}\beta\delta}{\alpha + 1 + \beta - j\frac{1}{2}\beta\delta} \qquad 1.712$$

Now the term in δ in the numerator is less effective than the same term in the denominator, and thus the former term can be neglected. Now if δ_m is the bandwidth of the maser amplifier, the equation can be obtained from 1.712:-

$$\delta_m = \frac{4(\alpha + 1 + \beta)}{\beta} \qquad 1.713$$

As the gain increases, $\beta \rightarrow -(1 + \alpha)$ and so $\delta_m \rightarrow 0$. From this expression a gain bandwidth product is:-

$$G\delta_m = \frac{4(\alpha - 1 - \beta)}{\beta} \qquad 1.714$$

which as $\beta \rightarrow -(1 + \alpha)$ becomes:-

$$G\delta_m = \frac{8\alpha}{(1 + \alpha)} \qquad 1.715$$

Equation 1.715 shows that the best gain bandwidth is attained when $\alpha \rightarrow \infty$. However as $\alpha \rightarrow \infty$, the focusser voltage V required for the high gain condition increases. In chapter 2 section 3 the practical details of this are discussed so that the best practical compromise was achieved. The approximations taken to solve 1.711 are quite valid for the high gain condition, for smaller gains the expression 1.713 has to be modified if just the amplitude of the output voltage is detected. If the phase is detected then for high gain and small δ the phase ϕ_m is:-

$$\phi_m = + \tan^{-1}\left(\frac{\delta\beta}{2(1 + \alpha + \beta)}\right) \qquad 1.716$$

Finally, the hyperfine structure will be resolved to a greater degree by the high gain condition of the amplifier. This is because the effective bandwidth of each line of the three

hyperfine lines has been reduced. In the same way the dispersion signal will also show the hyperfine components and these should appear as separate non-linearities on the phase output of the maser. The general expressions for the equivalent circuit components are:-

$$G_m = G_{mo}\left\{\frac{\sqrt{c_i}}{c_o}\left|\frac{\sin\delta_i}{\delta_i}\right|\right. \quad \text{and} \quad C'_m = C'_{mo}\left\{\frac{\sqrt{c_i}}{c_o}\,\frac{|\cos\delta_i| - 1}{\delta_i}\right.$$

$$i = 2,3,4, \qquad\qquad i = 2,3,4,$$

$$\text{and} \quad c_o = \sum\sqrt{c_i} \qquad i = 2,3,4. \qquad\qquad 1.717$$

where G_{mo} is the value of G_m at midband and C'_{mo} is the value of the capacitance $\epsilon_o C_c F$.

A much simpler equivalent circuit can be found if the hyperfine structure is ignored and the maser susceptibilities are modified as shown in figure 1.8. With these conditions the maser can be represented by a series tuned circuit. This approximates the susceptibilities to the familiar lorentzian line shape. This equivalent circuit can be adjusted to have the right bandwidth but will be an approximation at other frequencies. The maser can be represented as a series tuned circuit with a 'Q' factor Q_m. This Q_m is the molecular Q and is defined in section 1.8. The inductance L_m and the capacitance C_m are given by:-

$$L_m = \frac{Q_m}{\omega_o G_m} \qquad 1.718$$

$$C_m = \frac{G_m}{\omega_o Q_m} \qquad 1.719$$

this equivalent circuit is evaluated in chapter 4 section 3.

1.8 Frequency Pulling Effects

So far in this theory, the cavity resonant frequency ω_c and the ammonia transition frequency ω_o have been assumed equal. A lot of work has been done on the ammonia oscillator to find the magnitude of the effect of 'frequency pulling' of the transition frequency by detuning the cavity. The resonant frequency of the cavity varies with temperature, as frequency of resonance is a function of physical size. The effect of frequency pulling on the Maser amplifier will be mainly one of phase change, but it changes the gain as well. The theory of this effect is simplified by the equivalent circuit theory. Using the results of equation 1.73, a resonant frequency for the whole system ω_s is:-

$$\omega_s = \frac{1}{\sqrt{L_c C_c (1 + \epsilon_o \chi'_e)}} \qquad 1.81$$

$$= \frac{\omega_c}{\sqrt{1 + \epsilon_o \chi'_e}}$$

then for small δ:-

$$\frac{\omega_c - \omega_s}{\omega_c} = \sqrt{\frac{AB^2}{Q_L \omega_c k}} \cdot \frac{\delta}{4}$$

using equation 1.78, and from equation 1.44 coupled with the high gain condition $\frac{C}{B} \rightarrow 1$, the effect becomes:-

$$\omega_c - \omega_s = \frac{\omega_c L}{8 v_o Q_L} (\omega_o - \omega_s) \qquad 1.82$$

Equation 1.82 can be simplified by means of a quantity called the molecular linewidth, $\Delta\omega_m$. Let δ_n be the value of δ which reduces P_m (as defined in equation 1.45) to half its midband value. δ_n can be found by solving:-

$$\frac{\sin^2\delta_n}{\delta_n^2} = \tfrac{1}{2} \quad \text{i.e. } \delta_n = 1.4$$

From equation 1.44:-

$$\delta_n = \frac{\pi L(\nu_n - \nu_o)}{v_o} = \frac{L\Delta\omega_m}{2v_o}$$

And defining a molecular 'Q' Q_m as:-

$$|Q_m| = \frac{\omega_o}{2\Delta\omega_m}$$

Equation 1.82 becomes (assuming $\omega_o \simeq \omega_c$):-

$$(\omega_c - \omega_s) = \frac{0.7|Q_m|}{Q_L}(\omega_o - \omega_s) \qquad 1.83$$

In practice $|Q_m| \gg Q_L$ so that:-

$$(\omega_c - \omega_o) = \frac{0.7|Q_m|}{Q_L}(\omega_s - \omega_o) \qquad 1.84$$

This equation shows that the frequency shift of the cavity causes a much smaller shift of the system resonant frequency. This clearly shows the magnitude of frequency pulling. As far as the amplifier characteristic is concerned the gain is unaffected for small δ. However the whole phase response is shifted along the frequency axis an amount $\omega_s - \omega_o$. In practice this is a small amount. This also explains the phenomenon of the maser oscillating at a different

frequency to ω_o. This frequency pulling effect, when applied to the maser amplifier theory, shows that the gain, G, is a function of the cavity resonant frequency. From equation 1.79 an expression for the conductance, G_m, of the maser can be derived:-

$$G_m = \beta_\delta G_c \left| \frac{\delta}{\sin \delta} \right| = \beta G_c$$

where β_δ is a function of δ, and $\beta_\delta = \beta$ when $\delta = 0$.

$$\beta_\delta = \frac{G_m}{G_c} \left| \frac{\sin \delta}{\delta} \right| = \beta \left| \frac{\sin \delta}{\delta} \right| \qquad 1.85$$

If $(\omega_c - \omega_o) = \Delta\omega$ then equation 1.84 can be rewritten as:-

$$\Delta \omega = \frac{\omega_o \delta}{4 Q_L}$$

$$\text{or} \quad \delta = \frac{2 \Delta \omega}{(1 + \alpha)} \qquad 1.86$$

From equations 1.85 and 1.86 the expression for β_δ is:-

$$\beta_\delta = \beta \left| \frac{\sin \left\{ \frac{2 \Delta \omega}{(1 + \alpha) \Delta \omega_c} \right\}}{\frac{2 \Delta \omega}{(1 + \alpha) \Delta \omega_c}} \right| \qquad 1.87$$

As the gain of the maser is a function of β (see equation 1.55) from equation 1.87 it follows that the gain is also a function of $\Delta\omega$.

A much smaller effect is caused by changes in the focusser voltage. The various amplitudes of the three hyperfine components are all functions of the focusser voltage. For a very low voltage the ratio of their amplitudes is $c_2 : c_3 : c_4 = 5:7:9$. These are the thermal equilibrium values at ambient. Shimoda[5] showed that under high field conditions in the focusser the ratio of intensities was changed to 0.047:1:0.9174. The position of the three lines about a

mean is +1Kc/s, -1.25Kc/s,+0.42Kc/s. It can be seen that the emission line shape and the value of ω_s will be a function of focusser voltage, (see figure 1.9). By having a small value of α a higher working voltage is needed. Shimoda has showed that for these high voltages these effects are second order ones. See figure 1.10.

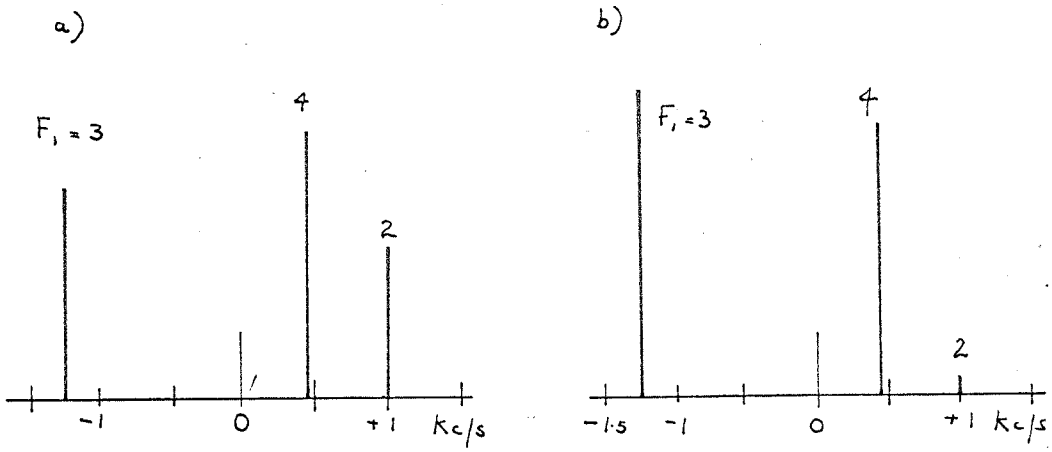

Figure 1.9 Focusser Effects on Hyperfine Structure. This diagram shows the relative intensities of the hyperfine components of the J=3, K=3, line of ammonia for a) Thermal Equilibrium and b) In the Maser Cavity.

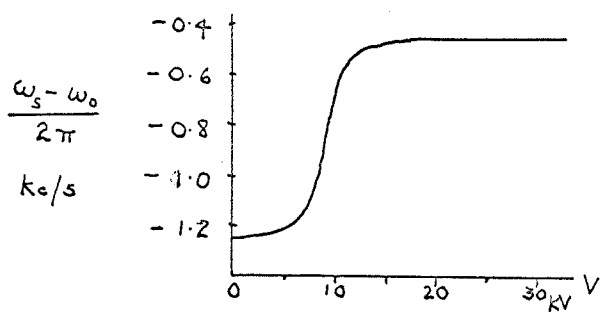

Figure 1.10 The Frequency shift due to Hyperfine Effects. Shimoda's calculated frequency shift for the J=3, K=3 line due to unresolved hyperfine structure. Changes in relative intensities by the saturation effect are neglected.

1.9 Saturation Effects

Up to this point in the theory, two independent parameters of the maser have been considered. These are midband-gain and bandwidth. The first part of the work on the linear operation of the maser was concerned with equation 1.45. Some of the theory for the saturation effect on the gain has already been considered in section 1.5 using equation 1.46. The results were shown in figure 1.7. In section 1.5 it was shown that the gain could be found by numerically solving equation 1.517. In saturation, the gain is a function of E_{in}, this is shown in figure 1.11, where the numerical solutions have been plotted out for various gains. It can be seen from that figure that over a certain range of values of E_1 the gain is constant. This is the linear range of the device. The range is defined as the range of E_1 within which the gain is 3db. or less from its mid-range value. In this work the gain is constant from $E_1 = 0$ and falls off at high values of E_1. If E_1' is the value of E_1 at which the gain G_1 has fallen to $0.7G_1$ then equation 1.517 gives an equation for E_1' as:-

$$\sin BE_1'(1 + 0.7G_1) = C.0.7G_1E_1' \qquad 1.91$$

For high gain this equation becomes:-

$$\frac{\sin(BE_1'.0.7G_1)}{BE_1'.0.7G_1} = \frac{1 + G_1}{G_1} \qquad 1.92$$

(see Figure 1.12)

which as $G_1 \longrightarrow \infty$ then $E_1' \longrightarrow 0$. This could be critical if high gain and wide range were required. In practice very high gains are

Figure 1.11 The Saturation Gain Curves.

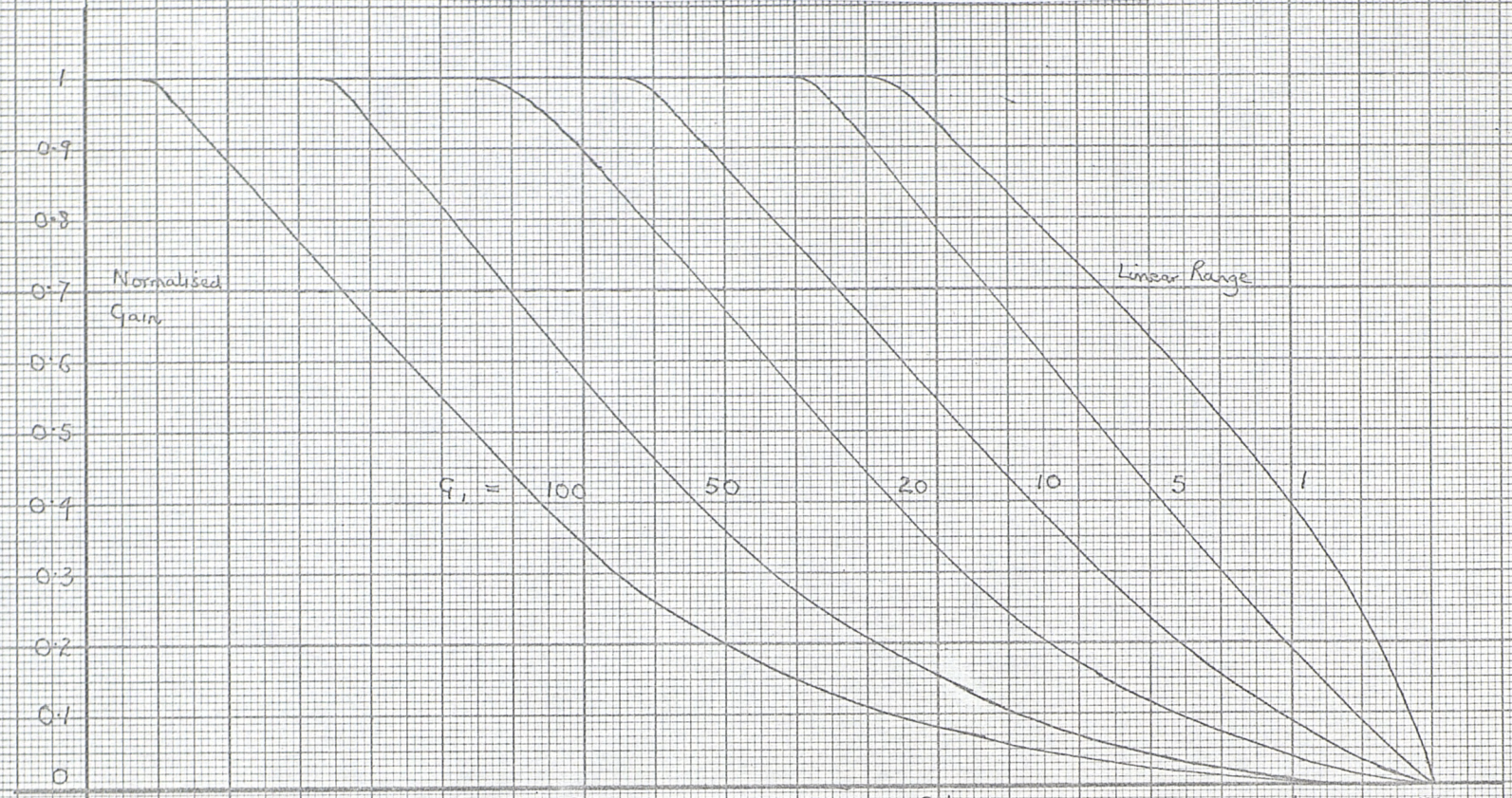

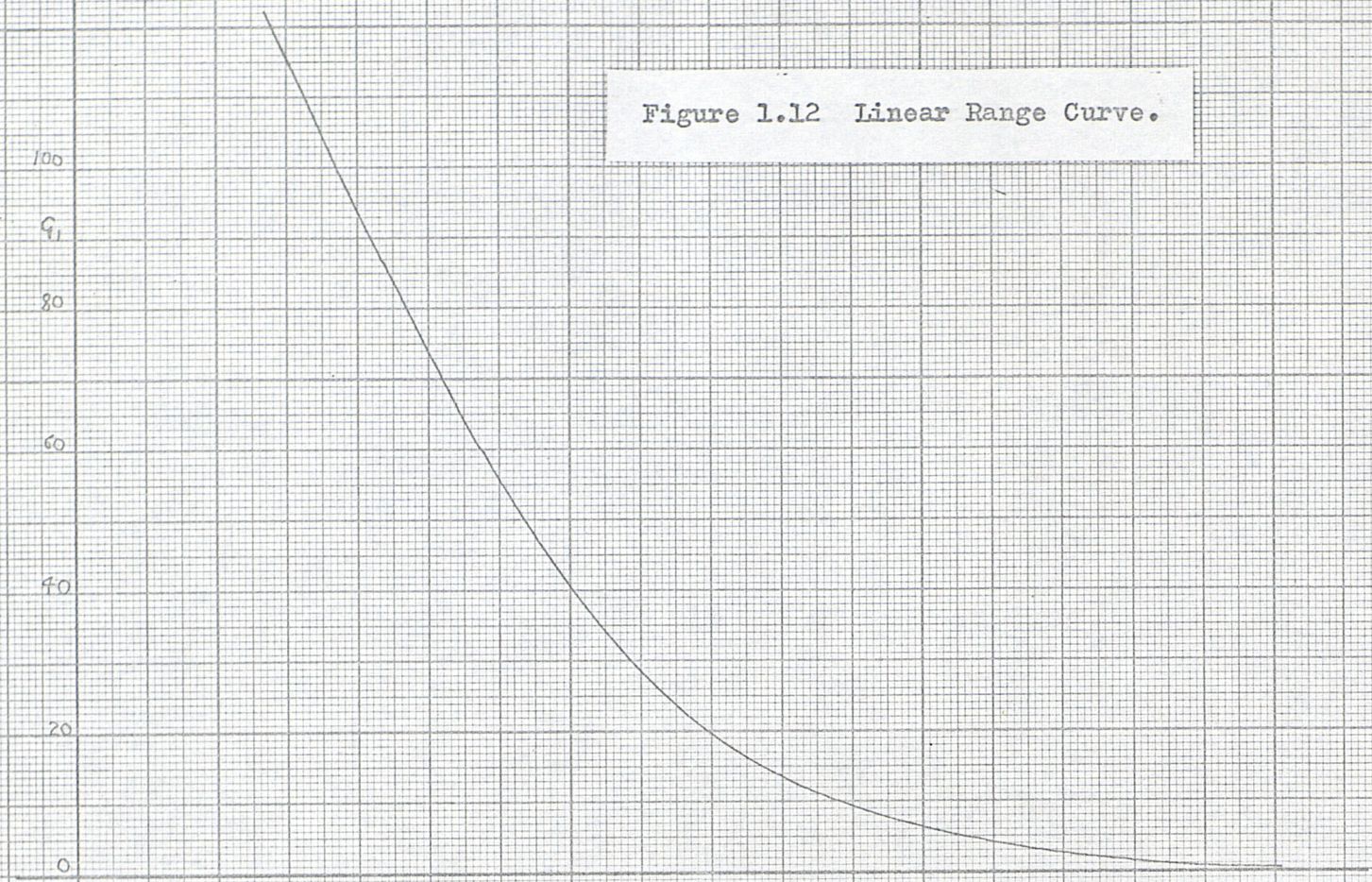

Figure 1.12 Linear Range Curve.

not achieved, mainly due to the velocity distribution effecting the value of P_m. Even if this is averaged out to the value v_o, there is a more fundamental reason why the gain rises to a maximum before oscillating rather than becoming nearly infinite before oscillating. When the gain is high the difference in the energy emitted from the beam and that emitted when oscillations just start is very small. If T_1 is the transit time of the molecules across the cavity then $T_1 = \frac{L}{v_o}$ and there will be an uncertainty in the value of this quantity, ΔT_1. Similarly if E_{osc} is the energy emitted to just start oscillations then this also will have an uncertainty, ΔE. ΔE will be a function of the uncertainties of the focusser voltage, V, the beam flux $\bar{n}$, the chamber pressure, the resonant frequency of the cavity ω_c, and the nitrogen jacket temperature. Heisenberg's Uncertainty Principle gives a minimum value of the product $\Delta E . \Delta T_1$ for each molecule as:-

$$\Delta E . \Delta T_1 \geq \hbar \qquad 1.93$$

Now if E_g is the energy emitted from the beam as $E_g \longrightarrow E_{osc}$ the gain will increase until $E_{osc} - E_g = \frac{1}{2} \Delta E$ and then the system will oscillate. Thus the smaller ΔE the higher the gain can go before oscillation starts. But from the uncertainty principle this implies that the smaller ΔT_1 the higher the maximum gain. From equation 1.37, to first order:-

$$T_1 \propto \frac{1}{T_2^3} \Delta T \qquad 1.94$$

where Δ T is the uncertainty in the measurement of T the beam temperature. Clearly as T decreases then ΔT_1 increases.

The rate of flow through the effuser leading into the focusser ($\bar{n}$) will be a function of the pressure difference δP between the source pressure P_s at the entrance to the effuser and P_c the chamber pressure at the exit. The value of T decreases as the gas is expanded through this effuser. From all this it can be seen that a smaller value of δP would produce a higher value of the maximum gain.

The next effect to be considered will be the effect caused by increasing E_1 to very large values. If the system remains coherent, theoretically, the molecules could be stimulated to make a large number of transitions in both directions. As E_1 is increased the gain falls from the value in the linear region (G) and is zero when all the molecules have done two transitions whilst in the cavity (i.e. down and up again). Beyond the value $E_1 = \frac{\pi}{B}$ the condition is similar to the linear region except that there is little overall gain. ~~And so on,~~ The gain characteristic appears like a set of similar but ever decreasing curves. The coherent nature of the maser is destroyed by molecular collisions, spontaneous emissions and collisions with the walls. This will destroy the effect just described so that for very high values of E_1 there is no further effect on the maser. Also the velocity distribution will tend to smear out the gain zeros. Once the coherent nature has been destroyed the energy levels become equally populated and so there is

no net emission or absorption, for an increase in E_1. The total energy emitted is then:-

$$P_m = \tfrac{1}{2} n h \nu_o \qquad 1.95$$

Finally, the effect of saturation on the bandwidth will be considered. In section 1.7, it was shown that the maser bandwidth was a function of the dispersion component of the emission to first order. Now this dispersion component was derived from the Kronig-Kramers relations given in equation 1.75. However, even though the form of the saturation absorption signal can easily be derived from equation 1.43, the Kronig-Kramers equations cannot be used for any case but the linear case[8]. However, from the form of equation 1.43, it can be seen that in saturation the line-shape is flattened at the centre for δ small. This would suggest that the slope of the dispersion component was reduced as the maser saturates (for small δ). Thus it follows that as the maser saturates, the bandwidth increases.

References Chapter 1

1. J.P. Gordon, H.J. Zeiger, & G.H. Townes. "The Maser ..."
   Phys. Rev. Vol. 99 No. 4 August 15 page 1264 1955

2. G. Troup, "Masers & Lasers" page 96 1962

3. J.P. Gordon. "Hyperfine structure in the Inversion Spectrum of $N^{14}H_3$".
   Phys. Rev. Vol. 99 No. 4 August 15 page 1253 1955

4. F.O. Vonbun. "Analysis of a multipole state separator and focusser for polarizable molecules"
   Jor. of Appl. Phys. Vol. 29 No. 4 April page 632 1958

5. K. Shimoda. "Characteristics of the Beam Type Maser 1"
   Jor. of the Phys. Soc. Japan. Vol. 12 No. 9 Sept. 1957 page 1007.

6. J.P. Wittke. "Molecular Amplification and Generation of Microwaves"
   Proc. I.E.R. page 291 March 1957

7. A.E. Seigman. "Microwave Solid State Masers" page 29, 1963

8. A. Abragam. "The Principles of Nuclear Magnetism"

Chapter 2

The Construction of an Ammonia Maser Amplifier

2.1 Introduction

Quite a large proportion of this part of the apparatus was built by Dr. T.H. Wilmshurst who worked on this project previously to the present author. (After referred to as T.H.W). This chapter (and chapters 3 and 6) will concentrate on the work done by the present author. Where no other record exists of the previous work, this will be given for completeness.

The first part of this chapter deals with the production of the molecular beam used in the maser. Both the system of purifying the ammonia and the system of operating the beam will be given.

The focusser design is developed from the theory and the final design that was used is described. Some of the operating problems are discussed.

Finally, the construction and temperature stabilisation of the cavity is outlined. The method used to align the cavity is also given.

2.2 The Molecular Beam

2.2 a) The Ammonia Supply.

This section of the apparatus is shown in figure 2.1 and it consisted of an ammonia cylinder, a pressure reducing valve, a reservoir cylinder, a liquid nitrogen trap and a needle valve. The pressure of ammonia in the main cylinder was about 150 lbs/in^2 (abs.). The pressure reducing valve was designed to reduce this to any preset pressure less than 45 lbs/in^2, independent of the flow rate. However, despite repeated attempts to repair it, the device normally acted as a leak valve which conveniently allowed sufficient ammonia to pass through over-night for the next day's run.

The reservoir cylinder was normally filled to about 30 lbs/in^2 (abs) and then isolated from the main cylinder by valve A (see figure 2.1). The ammonia normally contained quite a proportion of air and other impurities which reduced the efficiency of the maser. It was found necessary to purify the ammonia daily to obtain a consistent maser performance. This was achieved by a liquid nitrogen trap. The trap consisted of a german silver pipe sealed at one end and attached at the other via a pipe to the reservoir. A 'dewar' flask of liquid nitrogen was hung round thispipe. All the ammonia in the reservoir eventually froze in the pipe leaving just the air etc. in the system. This air was then pumped out by a backing pump through valve B. After this, the system was allowed to return to ambient temperature which normally took about two hours. The pressure of the purified ammonia in the reservoir was then just above

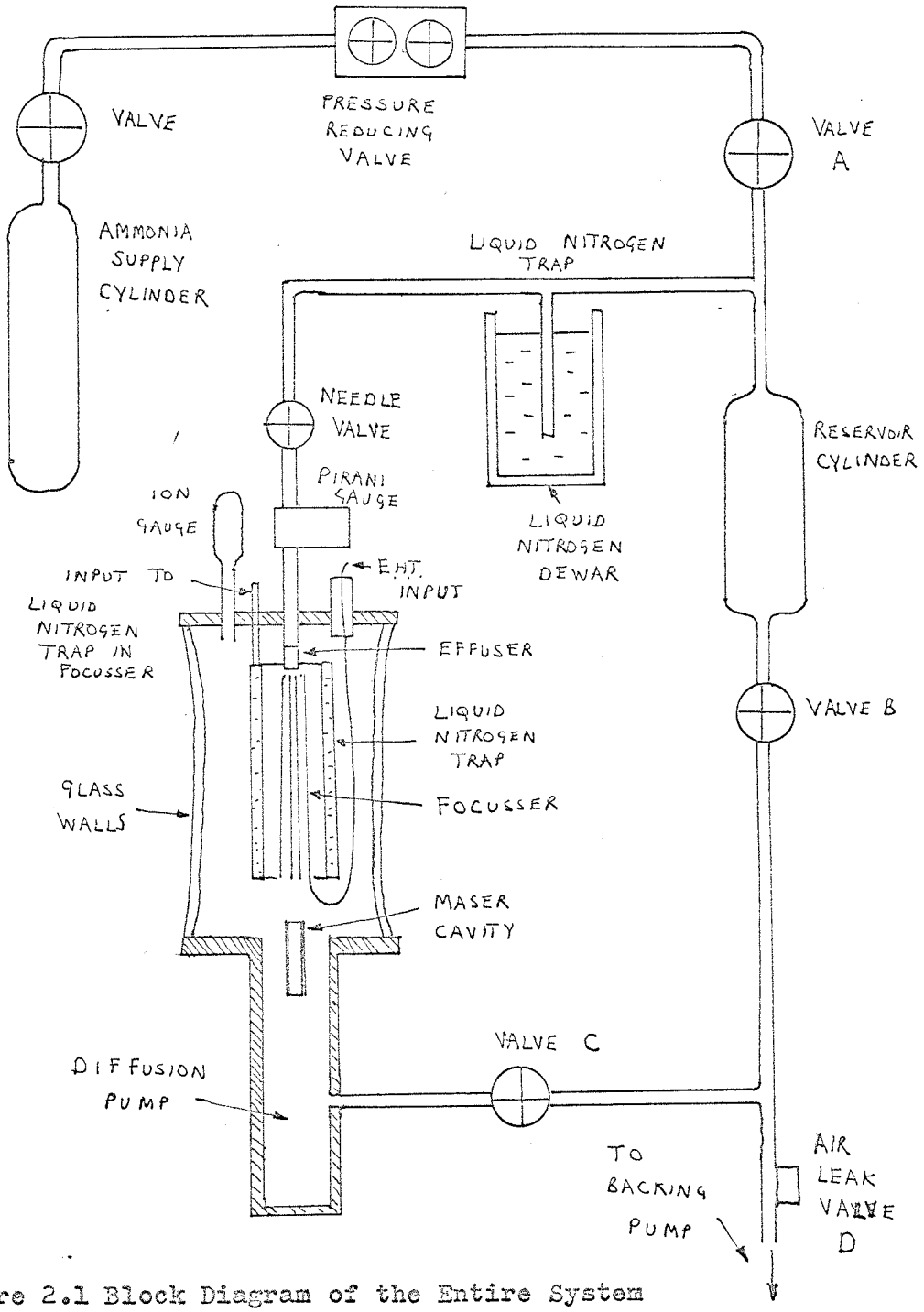

Figure 2.1 Block Diagram of the Entire System described in Chapter 2

atmospheric pressure, so that, any leaks were less likely to effect its purity. Also there was sufficient ammonia for a day's run without any noticeable decrease in the reservoir pressure. This improved the stability of the maser. The ammonia cylinder pressure and the reservoir pressure were measured by two 'steel tube' pressure gauges mounted on either side of the reducing valve.

The ammonia reservoir cylinder was connected to the maser chamber via a needle valve which reduced the pressure to about 3 Torr. Although this valve had a tendency to stick in the closed position it worked quite satisfactorily normally. The pressure beyond the needle valve (P_s the source pressure) was measured by an 'Edwards' Pirani gauge.

2.2 b) The Maser Chamber and Nitrogen Jacket.

The ammonia entered the maser chamber through an effuser (see figure 2.1). The object of the effuser was to act like a leak valve but also to produce a beam of molecules. Several types exist[1] and there is little to choose between them. One type is merely a single hole about 0.125" diameter. Another is a series of holes 1mm. diameter from 12 to 19 in number. Finally there is the 'crinkle foil' source. This is made of crinkled foil (made by passing foil through fine gear wheels) wound tightly round a core. This forms a mesh of fine tubes. This source is more transparent than the others and thus requires smaller values of P_s for the same performance of the maser. All these effusers give roughly the same angle of

divergence for the beam[2]. This divergence is also approximately proportional to P_s.

Beyond the effuser is the focusser and nitrogen jacket. The design of the focusser will be described in section 2.3. The nitrogen jacket, which was filled with liquid nitrogen, was placed all round the focusser to trap any molecules which were not focussed. The top of the jacket was placed well above the top of the focusser (see figure 2.2) so that as the nitrogen evaporated off the jacket still operated for about an hour after filling. After an hour, the maser performance was noticeably impaired. The connecting pipes leading to the nitrogen jacket were made of german silver to reduce heat flow. The 'O' ring seals were in large flanges placed round these pipes. This precaution prevented the 'O' rings freezing and leaking. All the vacuum seals in the system were of the rubber 'O' ring type and these proved adequate. The chamber pressure was measured by an ion gauge (Pye Scientific Instruments) mounted on the top of the maser (see figure 2.1) and an arrangement was made to monitor this pressure on a pen recorder. This was a little difficult as the current for 1μTorr was only 0.25 μA.

The nitrogen jacket acted as a trap for almost all the molecules coming into the focusser, if there was no voltage on the focusser. This improved the efficiency of the focusser. The nitrogen jacket also helped to maintain the chamber pressure at ~1μTorr as the vapour pressure of ammonia at 77°K (the boiling point of liquid nitrogen) is about 1μTorr. At the end of a day's run, the

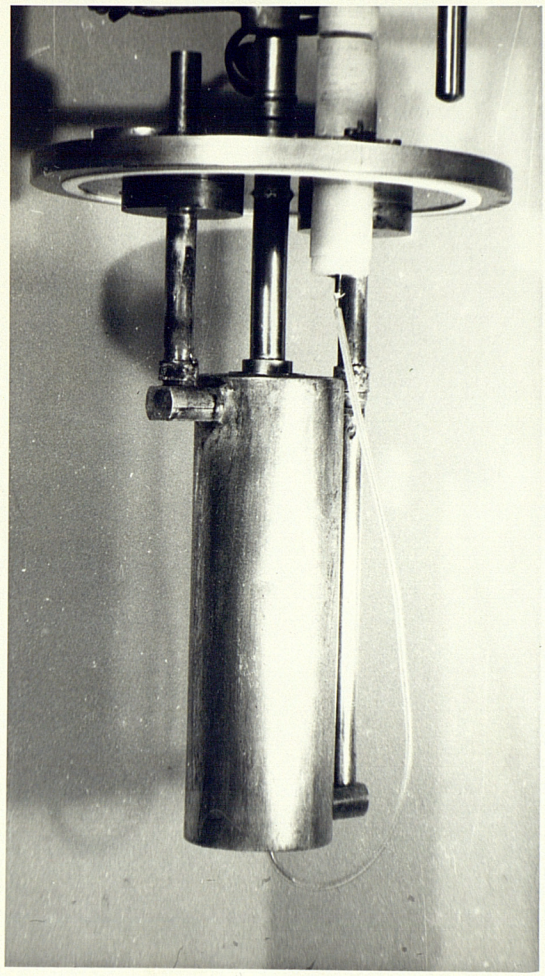

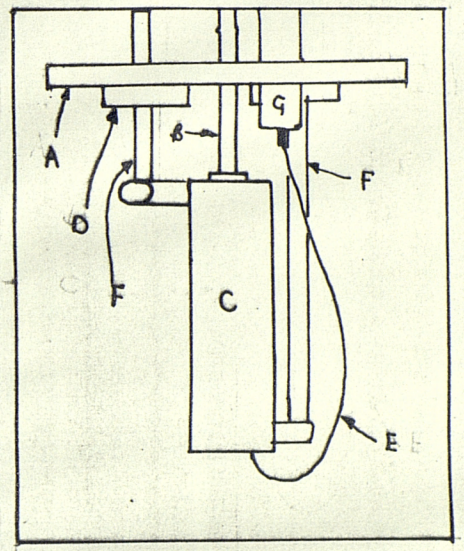

Figure 2.2 Part of the Maser Assembly. A The Top Plate of the Maser Chamber. B Ammonia Pipe supplying the Effuser. C Nitrogen Jacket surrounding the Focusser and Effuser(see figure 2.4). D Large coupling flanges to prevent freezing of 'O' rings. E Connecting wire for E.H.T. Supply to the Focusser. F Input Pipes to the Liquid Nitrogen Jacket. G P.T.F.E. block for insulating and sealing the connecting wire from the E.H.T. Supply.

jacket was emptied by sealing the outlet and allowing the resulting pressure build up to force the remaining liquid nitrogen out of the inlet where it was collected (see figure 2.2). As liquid nitrogen left open to the atmosphere collects ice particles, it was found necessary to take two precautions to prevent water collecting at the bottom of the nitrogen jacket. If this had occurred it could have burst the jacket. The first precaution was to put cotton wool in the funnel leading to the inlet pipe of the jacket. This collected any ice particles in the nitrogen from the 'dewar' flask. The second precaution was to occasionally blow compressed air through the jacket, when the jacket was empty and at ambient temperature, which removed any water that had been trapped.

The maser chamber consisted of a large hollow glass cylinder (made by Quickfit) placed between two round steel lids. The vacuum seal was made by two 'O' rings which were in round grooves in the lids. The glass allowed easy inspection for finding arcing faults on the maser.

2.2. c) The Evacuating System.

The evacuating system consisted of a conventional oil diffusion pump and an appropriate backing pump (both made by Edwards). The diffusion pump was 2" diameter which was smaller than those used in previous maser work. However it proved adequate for the region of the characteristic in which the majority of the work on the maser was done. A pressure of about 1μTorr was maintained under normal

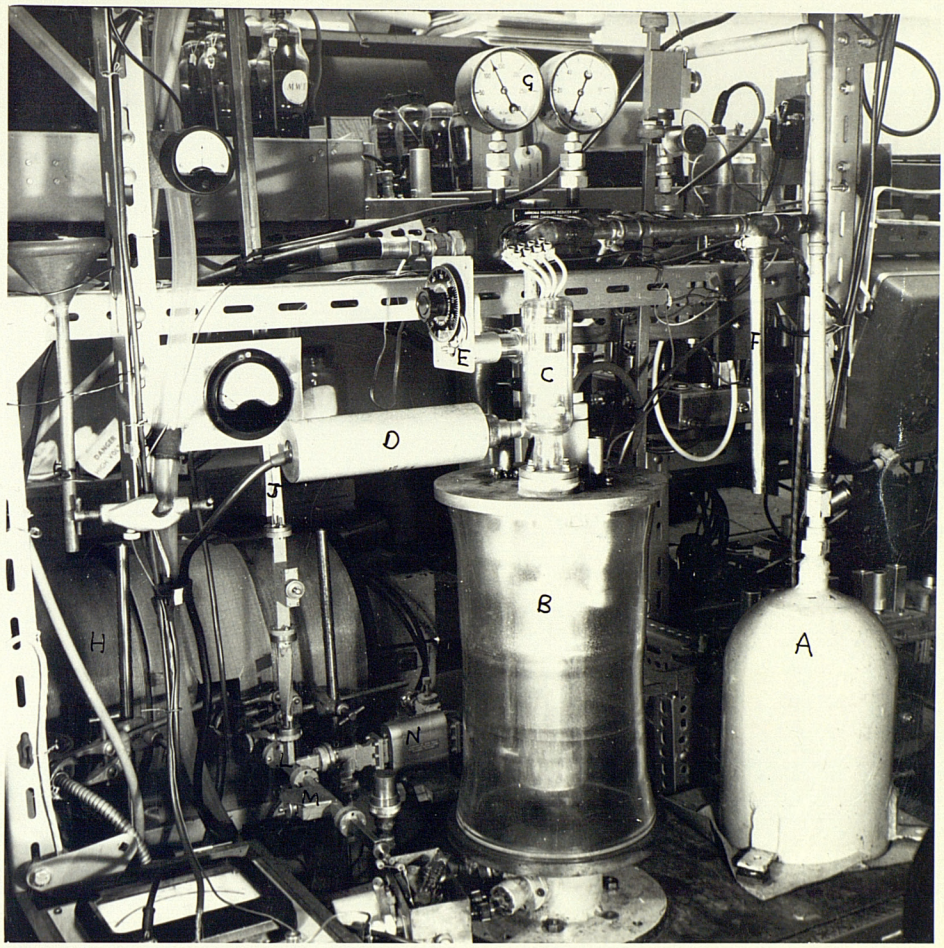

Figure 2.3 Photograph of part of the System. See figure 2.1 for:- A Ammonia Reservoir Cylinder, B Maser Chamber C Ion Gauge, D Pirani Gauge, E Needle Valve, F Liquid Nitrogen Trap, G Pressure Reducing Valve. See Chapter 5 onwards for:- H The Magnet, J The K Band Harmonic Suppressor, L The K Band Magic Tee, M The Matching Arm of the E.S.R. Bridge, N The Circulator feeding the Maser.

conditions and (this is about the limit of rubber 'O' ring seals) was considered satisfactory. Some of the diffusion pump oil was not trapped by the water jacket at the top of the pump but was collected by the maser itself. Although droplets of oil covered most parts of the maser this did not appear to impair the maser action. Throughout the work, a small intermittent leak persisted but it was considered expedient to ignore this leak rather than exhaustively hunt through all the 20 odd seals in the system. The magnitude of the leak was equivalent to a pressure change of 0.1μTorr.

The backing pump was connected to the system by a flexible pipe to reduce noise coupling and the outlet was connected to a pipe which terminated outside. At night the system was shut down as it could not withstand power cuts. This was achieved by sealing off the system at tap C (see figure 2.1) and then introducing air at the leak valve D (see figure 2.1) to prevent the oil sucking back. With this method the vacuum could be safely maintained overnight which also maintained the alignment of the maser. At the beginning of a run the backing pump quickly brought the pressure in the chamber down to 0.1 Torr again.

2.3 The Focusser

2.3 a) Design Details.

The focusser was rebuilt to improve its performance. The previous focusser was found to have poor efficiency and low breakdown voltage. One feature of the focusser is that there must be adequate space for the lower energy level molecules to get to the nitrogen jacket. A feature of the new design was that the top of the focusser was more open to allow such a space. Theory shows that the majority of the focusser action takes place in the first few centimetres of the device[6]. The breakdown voltage, in general, was only determined by the spacing between the ends of the focusser wires and the nature of the insulation between them. For this reason, some designs allow the ends to be free and the wires supported some way down the focusser. A very good design was used by Thaddeus[3]. He splayed out the focusser wires at the ends to increase the spacing and then joined them by 'pyrex' glass. This glass is an excellent insulator as it does not decompose if a discharge across it takes place. In this respect it is similar to P.T.F.E. which was used as an insulator in this present work. His design has one disadvantage in that it would be difficult to fit it into a nitrogen jacket in its present form. The design finally chosen for this present work was a compromise of existing focussers (see figure 2.2). An octupole focusser was chosen in preference to a quadrupole as the former is more rigid. The diameter of the focusser wires was 1mm. A larger number of poles gives little increase in either rigidity or efficiency.

At the top or inlet end of the focusser, the four earthed wires were terminated at the end of the diffuser. The four 'live' wires were supported by a flange placed 1.5cms. from the end of the effuser. These wires were splayed out slightly to increase spacing and were terminated 4mm. from the exit of the diffuser. The supporting flange was fixed to the diffuser by four P.T.F.E. supports which were joined to the flange by nylon screws. These supports proved adequate as long as there was no moisture on the screw threads, in which case they broke down electrically at quite low voltages. The other end (the lower end) of the focusser was terminated in a block of P.T.F.E. The purpose of this block was to hold the wires in place as some force was exerted on the wires by the electric field. One of the live wires was fed through this block to an insulated wire which was connected at the other end to special vacuum sealed P.T.F.E. connecting bush. Outside the chamber a further wire connected the focusser to the supply. This wire was arranged to be well clear of the rest of the apparatus to avoid breakdown. In practice most of the breakdown took place on the lower block of P.T.F.E. and this was reduced by several methods. The first method was to widen the entrance holes into the block, i.e. counter-sink the holes the wires were fitted into. This increased the effective path for arcing. A second method was to cut slots in the P.T.F.E. between the holes for the wires which also increased the effective path. When these modifications had been done the break-down voltage was about 26 KV. One further effect appeared to lower the breakdown voltage. This was the formation of a

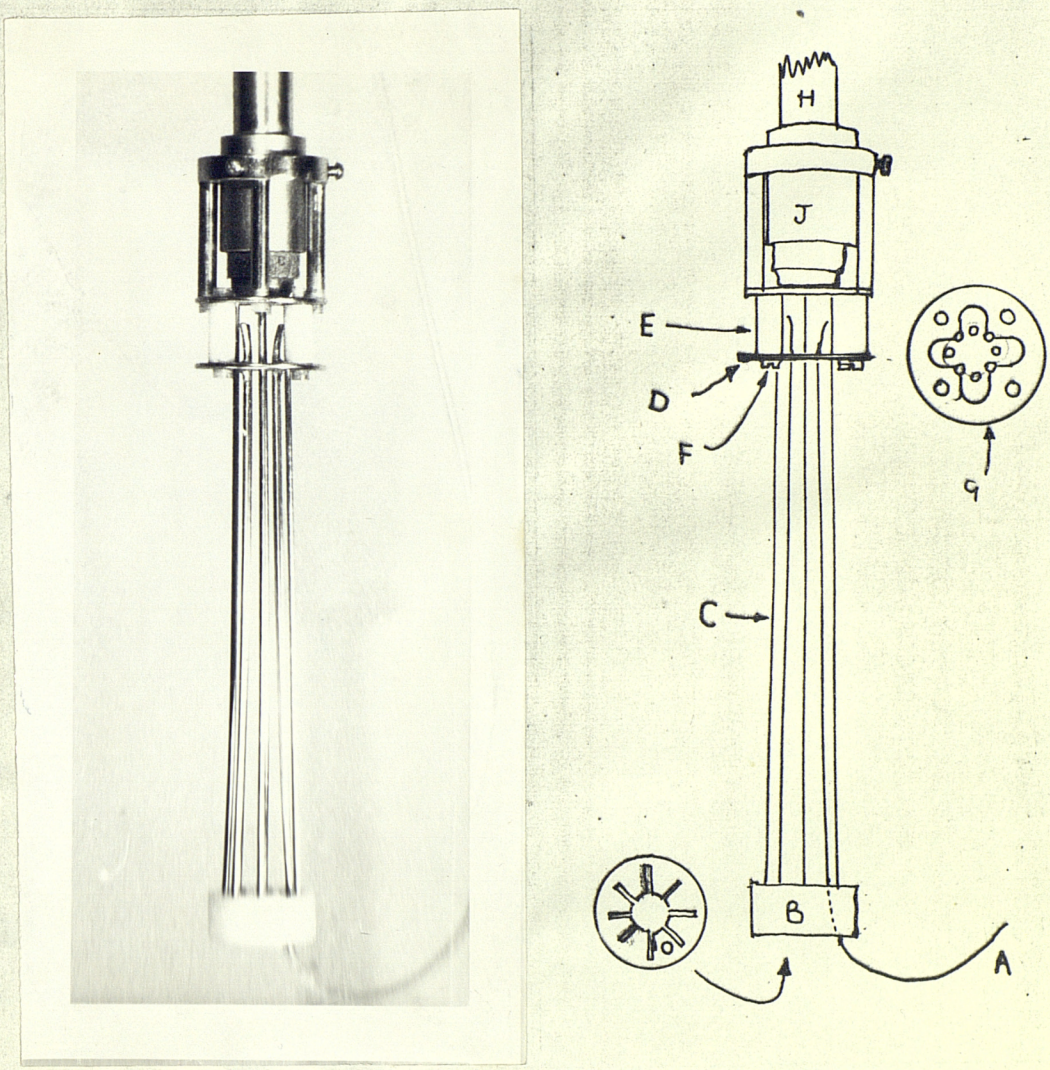

Figure 2.4 Photograph of the Focusser. A Connecting Wire to E.H.T. Supply. B,P.T.F.E. Block for holding and insulating the focusser wires. C Focusser Wires. D High Voltage Flange supported and insulated by E, P.T.F.E. Bushes, and connected by F 4 nylon screws. G Cross-section through plate D, H Ammonia Pipe feeding, J, the Effuser.

yellow-green layer on the surface of the P.T.F.E., probably due to the corrosive action of the ammonia. It was found that, as long as this was cleaned off from time to time the performance was not effected.

The design of the focusser was determined mainly by the working voltage V. From equations 1.34 and 1.37 an expression for v_c (the critical radial velocity) for the J=3, K=3 line is:-

$$v_c = \bar{\mu}\left(\frac{7}{2mh\nu_o}\right)^{\frac{1}{2}} \frac{V}{R} \qquad 2.31$$

Now for ammonia $\bar{\mu} = 4.9.10^{-30}$ coulombs. m ^{4}, $m = 2.84.10^{-26}$ Kg. For the focusser used R = 0.4 cm. Taking a value of Plank's Constant as $h = 6.625.10^{-34}$ joules sec and ν_o = 23,870 Mc/s, the expression for v_c becomes:-

$$v_c = 3.42\ V\ m/s \text{ where V is in KV} \qquad 2.32$$

The value of v_o obtained from equation 1.37 is 530 m/s. From this value and equation 2.32 it can be seen that the condition $v_c \ll v_o$ is not satisfied for V > 1KV. Thus the simple expression for the focusser efficiency η_f given in equation 1.66 does not apply, and the more complicated equation 1.68 is necessary. However, if L = 10 cms then a (used in equation 1.68) is:-

$$a = \frac{L}{R} \cdot \frac{v_c}{v_o} = 0.16\ V \text{ (using equation 2.32)}$$

Clearly, $a \geqslant 1$ for all $V \geqslant 6$ KV. The highest efficiency is in this region $a \gtrsim 1$. As the beam flux in this particular maser is smaller than that used in most designs (i.e. $\bar{n}$ is smaller) it was decided to operate in this region. The expression for η_f then becomes:-

$$\eta_f = 9 \cdot 10^{-4} (1.577 + 2\log(0.16V))$$

$$\text{for } V > 6$$

For V = 16 KV then η_f is about $\frac{1}{2}\%$.

There is an improved type of focusser which is smaller and about twice as efficient as the quadrupole which uses 'Ring or Screw' electrodes. This has been developed by G. Becker[5]. The quadrupole design was chosen as it is easier to manufacture. Vonbun[6] showed that the efficiency did not improve with increased length above a few centimetres. Thus a value of L_f the same order as L was chosen. This was in practice 12 cms. Helmer[7] showed that a focusser with parabolic wires and an inlet diameter less than the outlet diameter was more efficient. In the present focusser the outlet diameter is larger than 2R for this reason and also because this increased the breakdown voltage. Unfortunately, this did not improve the efficiency very much as the cavity inlet was also 2R.

Finally it is worth noting that only 3% of all the ammonia molecules coming out of the diffuser are in the upper energy level of the J=3, K=3 rotational state[10]. This means that $\bar{n}$ used in equation 1.64 is 3% of the total number of molecules coming through the effuser per second (At room temperature approximately). Laine[9] gives an estimate of 10^{17} molecules/sec as the rate of flow through the effuser. This rate will be a function of P_s the source pressure. If η_f is not a function of this flow rate, then the rate of flow into the cavity, n , will also be a function of P_s. This function has been found experimentally by Barnes[2].

2.3 b) The E.H.T. Supply.

The E.H.T. Supply was modified by the present author so that it gave 0 - 30 KV (The circuit used by T.H.W. had ceased to function). The circuit diagram of the supply is given in figure 2.5. The emergency on-off switch was placed near the apparatus and was used as the main switch, all the rest of the apparatus being normally 'on' continuously. This avoided switching it 'on' once the maser circuitry was stabilised as such a switching pulse was capable of unlocking a phase locked circuit. The E.H.T. could only be switched on when there was a good vacuum in the chamber (μTorr).

The E.H.T. voltage, V, was measured by draining off a small fraction of the current through a resistance of 2.5GΩ and measuring this on a 0 - 20 μA meter. This was originally supplied complete by 'Hursant' but the resistance was found to be open circuit. The resistance consisted of fifty 50MΩ resistors. Seven of these were open circuit. Once these had been replaced the system worked well, although it had a very slow response time.

The variable voltage control on the E.H.T. supply was capable of the range 10 - 30 KV. Lower voltages were achieved by lowering the H.T. voltage from the power supply. The smoothing circuit consisted of one capacitor of value 1000pF. The output impedance of the supply was about 0.22 GΩ so that the 50c/s hum was reduced by a factor of 70. The device itself had a working frequency of 1 Kc/s and this was reduced by a factor of 1,400. If the smoothing capacitance had been too large the breakdown spark would have done permanent damage to the focusser.

Figure 2.5 Circuit Diagram of the E.H.T. Supply.

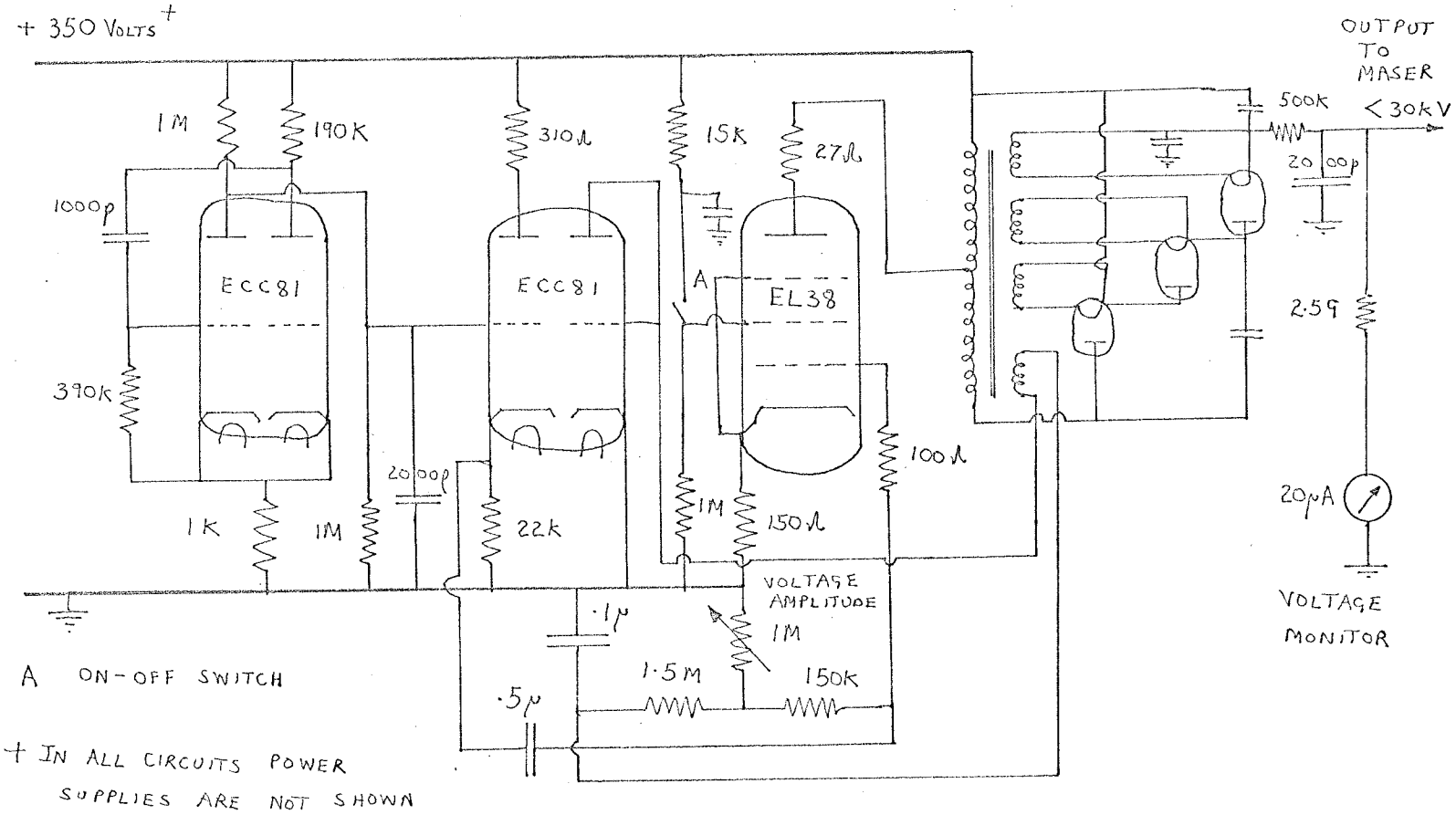

2.4 The Maser Cavity

2.4 a) Construction

The cavity was designed and built previously, and only a brief description will be included here. The mode of oscillation used was the E_{010} (TM_{010}) which had two advantages over other possible modes. The first was that the axial direction had a constant electric field and also the resonant frequency of the cavity, ω_c, was nearly independent of the length, L. This has been one of the assumptions implicit in the previous theoretical chapter. For more complex modes a solution is possible using the work done by Bonanomi[8]. The second advantage was that the electric field was approximately a half sine wave across any diameter of the cavity. Thus the field could be averaged to give the value of E used in the theory. See figure 2.6. To increase the 'Q' of the cavity, the standard practice is to put end caps on the cavity. This reduced the entrance diameter from 0.96 cms. to 0.85 cms., but this increased the 'Q' from 3,000 to about 8,000. The details of the construction of such a cavity are given in the work by Laine[9].

The length of the cavity, L, is 12 cms., and using the value of v_o = 530 m/s from section 2.3, the molecular line width $\Delta\omega_m$ can be found using the equations leading up to equation 1.83:-

$$\Delta\omega_m = 1.4 \cdot \frac{2v_o}{L} \; ; \; \Delta\nu_n = \frac{\Delta\omega_m}{2\pi} = 1.97 \text{ Kc/s} \qquad 2.41$$

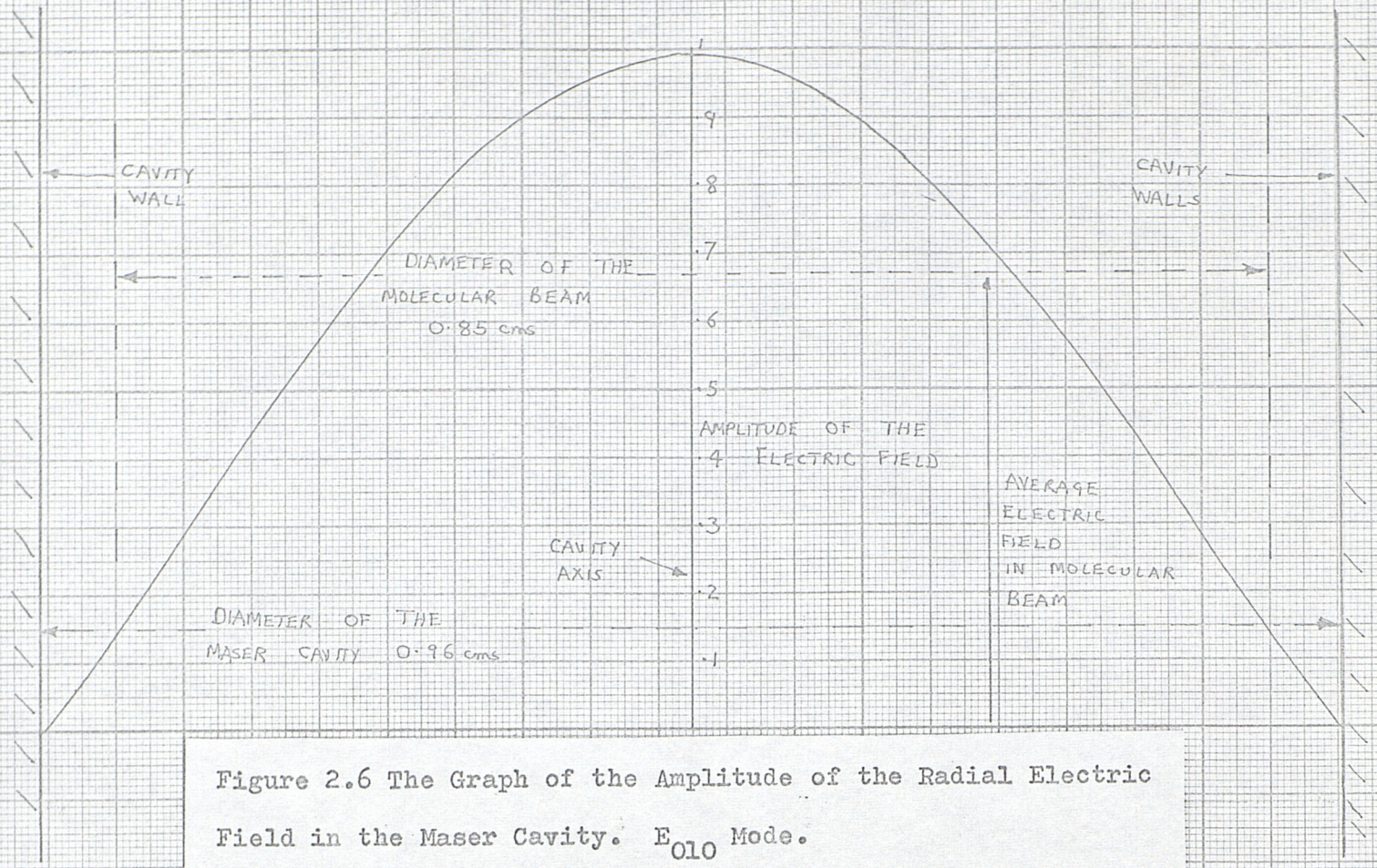

Figure 2.6 The Graph of the Amplitude of the Radial Electric Field in the Maser Cavity. E_{010} Mode.

However the bandwidth of the maser is not this value but $\Delta\nu_m$ which is given by equation 1.713

$$\Delta\nu_m = \frac{\delta_m v_o}{\pi L} = \frac{4(\alpha + 1 + \beta)v_o}{\beta\pi L}$$

$$= \frac{(\alpha + 1 + \beta)}{\beta} \cdot 5.6 \text{ Kc/s}$$

and using the definition of maser gain G:-

$$\Delta\nu_m = \frac{(\alpha - 1 - \beta)}{G} \cdot 5.6 \text{ Kc/s}$$

which as $\beta \rightarrow -(1 + \alpha)$ for high gain becomes:-

$$\Delta\nu_m = \frac{2\alpha}{(1 + \alpha)G} \cdot 5.6 \text{ Kc/s}$$

For a given value of G, the bandwidth can be increased by increasing α. This is the same as increasing the gain-bandwidth product (given in equation 1.715) for constant gain.

Now, rewriting the oscillation or high gain condition $\beta = -(1 + \alpha)$ as:-

$$A = \frac{(1 + \alpha)\,\omega_c k}{Q_o B^2} \qquad \text{(using equation 1.516)}$$

$$\text{or} \quad n = \frac{(1 + \alpha) \cdot 2k v_o^2 h}{Q_o \pi \bar{\mu}^2 L^2} = \eta_f \bar{n} \qquad 2.43$$

Although decreasing L increases the bandwidth, it can be seen that it increases the value of n required to operate the maser.

A compromise between all these various factors was achieved by making $\alpha = \frac{1}{5}$ (i.e. ~~over~~ under-coupling the cavity) and L = 12 cms. The maximum gain bandwidth that is theoretically possible is then ~~9.34~~ 2.24 Kc/s, and the voltage required on the focusser is about 16 KV.

Using tables of microwave data[11] the values of G_g (the wave-guide characteristic conductance); G_o (the cavity shunt conductance) and m (the equivalent circuit turns ratio for the coupling hole) are G_o = 2.15 m℧ and G_c = 27 m℧ and m = 200. From these values an estimate of k can be found. k is half the equivalent circuit shunt capacitance. The value found is k = $1.44.10^{-15}$ coulombs. Putting this value in expression 2.43 gives a value of $n \sim 3.7 \cdot 10^{14}$ molecules/sec. A value of $\eta_f = \frac{1}{2}\%$ was found in the section on focusser design, and using this value gives $\bar{n} \sim 7.4 \cdot 10^{16}$ molecules/sec. Thus if only 3% are present in the upper energy level then the total number of ammonia molecules required from the effuser is $\sim 2.5 \cdot 10^{18}$ molecules/sec. This compares with the figure for this flow rate estimated by Laine[9] as being of the order of 1.10^{17} molecules/sec. Laine's figure was for a smaller effuser. These figures show that to first order of magnitude the conditions for operation can be achieved.

No mention has been made so far of the effect of the distance between the focusser and the cavity. In this particular work it is 2.5 cms. Clearly this distance will reduce the effect of the focusser. Some practical work on this has been done by Laine[12] and from his work it would be a resonable estimate to say that this distance reduced η_f by a factor of 1.5. In fact, quite a large distance between the focusser and cavity is tolerable as the mean free path for this pressure is about 30 cms.

2.4 b) The Temperature Stabilising Circuit.

In some masers the cavity is connected to the nitrogen jacket of the focusser. This had two advantages. The first was that the cavity resonant frequency, ω_c (which is a function of physical size and hence of temperature) did not vary with changes in ambient temperature. The second was that the cavity was aligned in a permanent way. However, the main disadvantage was that there was an unwanted heat flow down the coupling wave guide and also there was the problem of ammonia freezing onto the cavity. So in this present system the cavity was separate from the main focusser assembly. This required a separate temperature stabiliser and some means of alignment when the maser was assembled. In this paragraph the temperature stabilisation will be outlined and the technique used for alignment is outlined in the following paragraph.

The type of temperature stabilisation was similar to that used by Laine[9]. He estimated that for a silver plated copper cavity the frequency temperature coefficient was - 0.5 Mc/s /°C. Using the value of the molecular bandwidth found in the last section a value of Q_m (the molecular 'Q' factor) can be evaluated and it is 6.10^9. For $\alpha = \frac{1}{5}$ the loaded Q of the cavity Q_L is about $6.6 \cdot 10^3$ so that equation 1.84 becomes:-

$$\omega_c - \omega_o = 6.5 \cdot 10^5 (\omega_s - \omega_o) \qquad 2.44$$

If the frequency pulling effect is to be kept less than 120 c/s (this is a reasonable estimate for the bandwidth at high gain) then the temperature must be kept within one degree centigrade.

The principle employed was to wind a bifilar heating coil round the cavity. (This was bifilar to avoid Zeeman Effects) The coil was then connected into one arm of a bridge circuit. The output of a 500 c/s selective power amplifier was connected to one side of the bridge and the other side of the bridge was connected back to the input (see figure 2.7). The action of the circuit was that of a controlled oscillator. As the system oscillated, power was dissipated in the bridge which heated the cavity. The temperature coefficients of resistance of the various parts of the bridge were arranged so that when the right temperature was reached the feedback stopped because the bridge was balanced. The power amplifier used by T.H.W. had to be rebuilt and the final circuit used maintained the cavity resonant frequency throughout the day quite satisfactorily. The actual cavity temperature was not measured but it was about 40°C. Once the system had stabilised, which took about an hour, the only heat required to maintain the cavity temperature was that lost down the coupling wave-guide. The feed-back signal was monitored on an oscilloscope so that the operation of the circuit could be easily checked. Small temperature drifts were noted as frequency pulling effects. These effects are discussed in chapter 4.

2.4 c) The Alignment of the Cavity.

The alignment of the effuser, focusser and cavity was achieved by shining a beam of light down the axis of all three and adjusting the alignment for maximum transmission. A small torch

Figure 2.7 Maser Cavity Temperature Control Circuit.

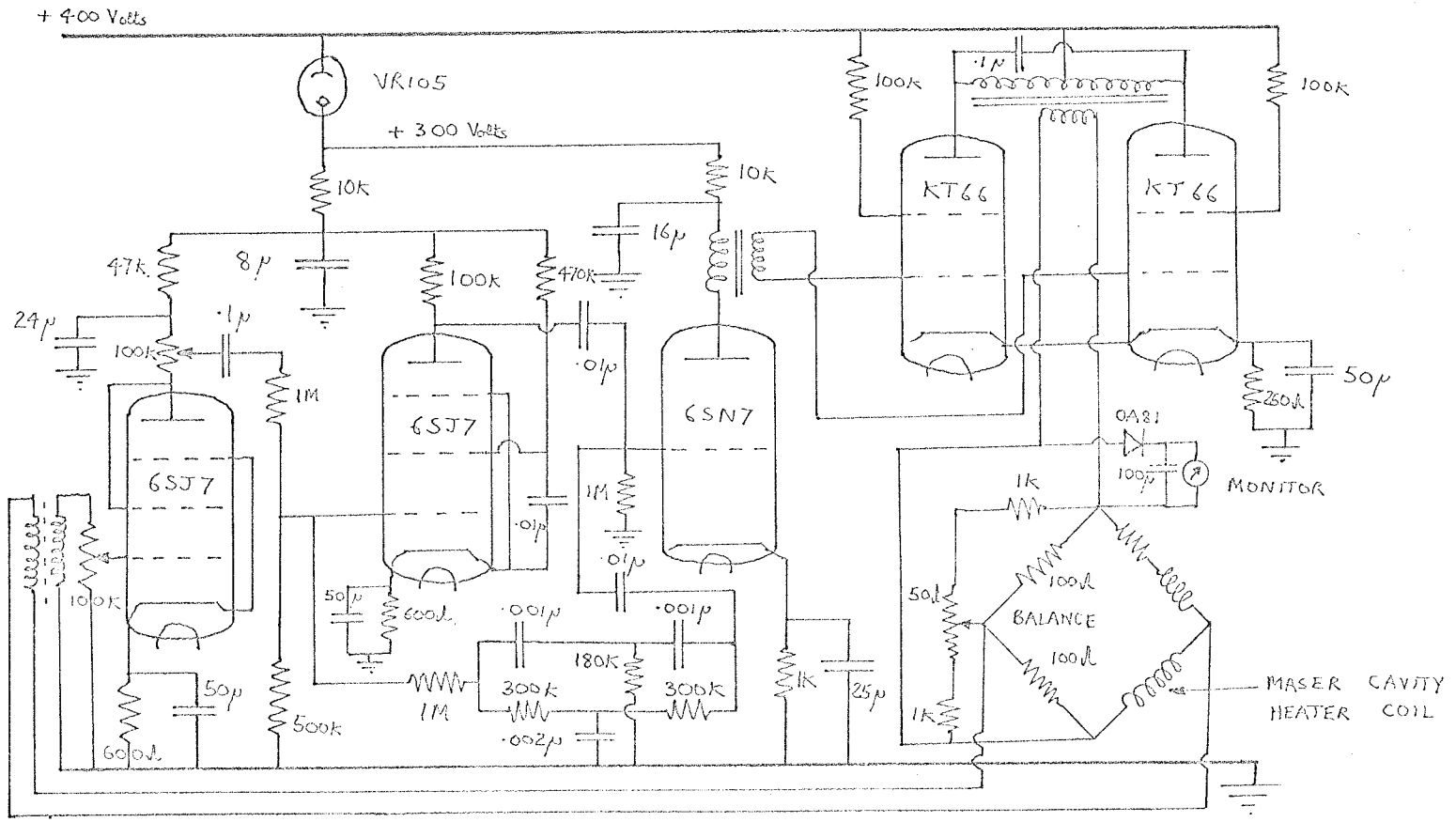

bulb, suitably connected, was pushed down the ammonia pipe into the entrance of the effuser. The diffusion pump was removed and the bulb was viewed by looking upwards through the whole maser system. First, the focusser was aligned so that it lay symmetrically round the beam of light coming through the effuser. The focusser was aligned by deflecting the lower end slightly, bending all the wires permanently. The focusser was adjusted so that the maximum light was seen in the centre. Finally, the cavity was adjusted so that the maximum light was seen in the centre as well. This was done in two ways. First, the maser chamber glass was moved across its 'O' rings slightly. Second, the maser cavity was twisted slightly about its coupling wave-guide (this was possible as there was some 'play' in the coupling ring). All this alignment procedure had to be done each time the maser was assembled. However, as long as the system was under vacuum the alignment remained fixed.

References Chapter 2

1. K. Shimoda. "Characteristics of the Beam Type Maser 2"
Jor. of Phys. Soc. Japan, Vol. 13, No. 8 August page 940 1958

2. F.S. Barnes. "Operating Characteristics of an Ammonia Beam Maser"
Proc. I.R.E. page 2088 1959

3. P. Thaddeus and L.C. Krishner. "A Maser Beam Spectrometer"
Rev. Sci. Instr. 32 page 1083 1961

4. W. Gordy, W.V. Smith and R.F. Trambarulo. "Microwave Spectroscopy" page 361 1953

5. G. Becker. "Focussing of Molecular Beams with Ring and Screw Electrodes"
Quantum Electronics III page 393

6. F.O. Vonbun (see reference 4 Chapter 1)

7. J.C. Helmer, B.F. Jacobius and P.A. Sturrock. "Focussing Molecular Beams of NH_3^1
Jor. of Appl. Phys., Vol. 31, No. 3 March page 458 1960

8. J. Bonanomi, J. De. Prins., J. Herrman and P. Kartaschoff. "Maser Oscillators with cavities whose modes depend on length"
Helv. Phys. Acta., Vol. 31, Page 282 1958

9. D.C. Laine. "Investigation of a Molecular Oscillator"
PhD. Thesis, Southampton University pages 17 & 106 1959

10. C.H. Townes and A.L. Schawlow. "Microwave Spectroscopy" 1955 page 311.

11. T. Moreno. "Microwave Transmission Design Data" 1948 page 219.

12. D.C. Laine and R.C. Srivastava. "The performance of an Ammonia Maser with two cavities in cascade"
Jor. Brit. I.R.E., Vol. 26, No. 2 August page 173 1963

Chapter 3

Microwave and Electrical Circuits used in the Measurements of the Ammonia Maser Amplifier Characteristics

3.1 Introduction

The comments made at the beginning of ~~Chapter~~ Section 2.1 also apply to this chapter. The object of this chapter is to describe the construction of the circuitry used in the maser measurements. As the final aim of this work was to use the maser with an E.S.R. K Band Spectrometer, the circuitry used in the measurements is the same as that used in the E.S.R. work. In Chapter 6 only the additional circuitry which was needed to operate the E.S.R. spectrometer will be described.

The first section of this chapter deals with the microwave circuits used to supply the input and to detect the output. In view of the stringent frequency requirements, an 'Equal Arm Stabiliser' was used to stabilise the klystron frequency. As both of these two devices are more stable at X Band rather than K Band, it was decided to operate them at X Band (7,956 Mc/s) and a frequency tripler was used to supply the K Band input signal (23,870 Mc/s).

The second section of this chapter deals with the detection of the output of the maser amplifier. A conventional system of a local oscillator, mixer crystal and I.F. Amplifier (30 Mc/s) was used. However, because of the requirements of the E.S.R. spectrometer, a system of sidebands was used. These sidebands were put on the main

signal by an amplitude modulator in the X Band circuit. This modulation was done at X Band, as the larger power available there, made the modulation linear.

Finally, a system for stabilising the Equal Arm Stabiliser was developed.

3.2. The Microwave Circuit

3.2 a) The X Band Klystron and Stabilised Power Supplies.

The frequency stability required from the main klystron was about 4 in 10^9 over about 5 minutes. To achieve this stability, sophisticated methods of stabilising were used. The first requirement was a really stable, low noise klystron. An E.M.I. 100mW X Band Klystron (No. R9562 with No. 25157 Plug in cavity) was chosen. The operating frequency was 7,956 Mc/s. Besides the normal stabilised power supplies a second stabilising circuit was used. These stabilised power supplies were built by T.H.W. and slightly modified by the present author. A circuit diagram is given in figure 3.1. The majority of the circuit was identical to that described by T.H.W.[1] and the innovations concern the reflector voltage modulator. Two features of the circuit will be mentioned. 6 volt car batteries were used for all the heaters to reduce 'hum' and the resonator grid was positive to 'earth' to reduce noise. For this reason a D.C. isolator was included in the X Band circuit. It was found necessary to replace some of the resistors in the reflector voltage modulator circuit with 'high stability' resistors to improve the temperature stability. The klystron was mounted on a flexible wave-guide in a non-acoustic box. This box was designed by T.H.W.[2] to reduce noise, microphonics and the effects of draughts.

Figure 3.1 Circuit Diagram of the Main Klystron Stabilised Power Supplies

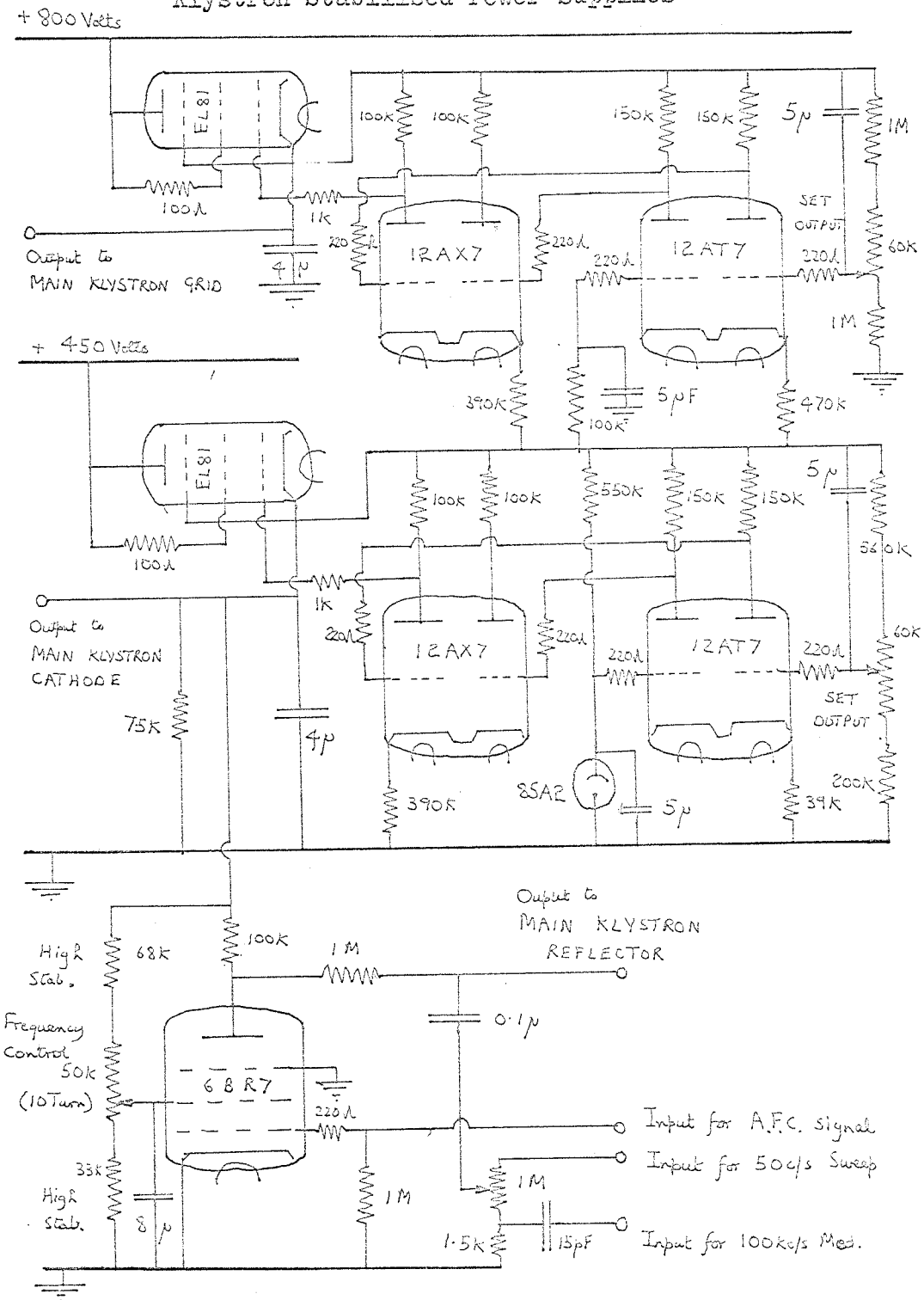

3.2 b) The Equal Arm Stabiliser.

The equal arm stabiliser was chosen as the main frequency stabiliser as it has a very fast response time and is simple in both design and operation[3]. In this particular work a modification on the stabiliser made it possible to compensate for drift by feeding a correcting signal from the maser. The stabiliser was built entirely by the author and is shown in figure 3.2. As the operation of this stabiliser is well known only the salient features of device will be described.

The operating frequency of the stabiliser is dependent on the resonant frequency of the cavity (see figure 3.2). This cavity was a cylindrical one made from Invar (to reduce the effects of thermal drift on the resonant frequency). The radius was 3.2 cms and the length was 2.71 cms and the mode was H_{011} (TE_{011}). The loaded 'Q' of the cavity was 15,000. This high 'Q' was achieved by silver plating the inside of the cavity. One of the six bolts used to hold the cavity together was fitted with a spring washer. By adjusting this bolt a fine tuning range of a few tens of kilocycles was possible. The cavity was mounted on a sponge to reduce mechanical noise (see figure 3.3).

The 45 Mc/s amplifier (see figure 3.2) had a bandwidth of 1.5 Mc/s and a gain of 70 dB. The circuit is given in figure 3.4. The working frequency of 45 Mc/s was chosen partly to give a fast response and partly so as not to interfere with the 30 Mc/s circuitry which will be described in section 3.3. The P.S.D. (Phase Sensitive Detector) was fairly conventional, except the method of coupling the

Figure 3.2 Block Diagram of the entire System described in Chapter 3

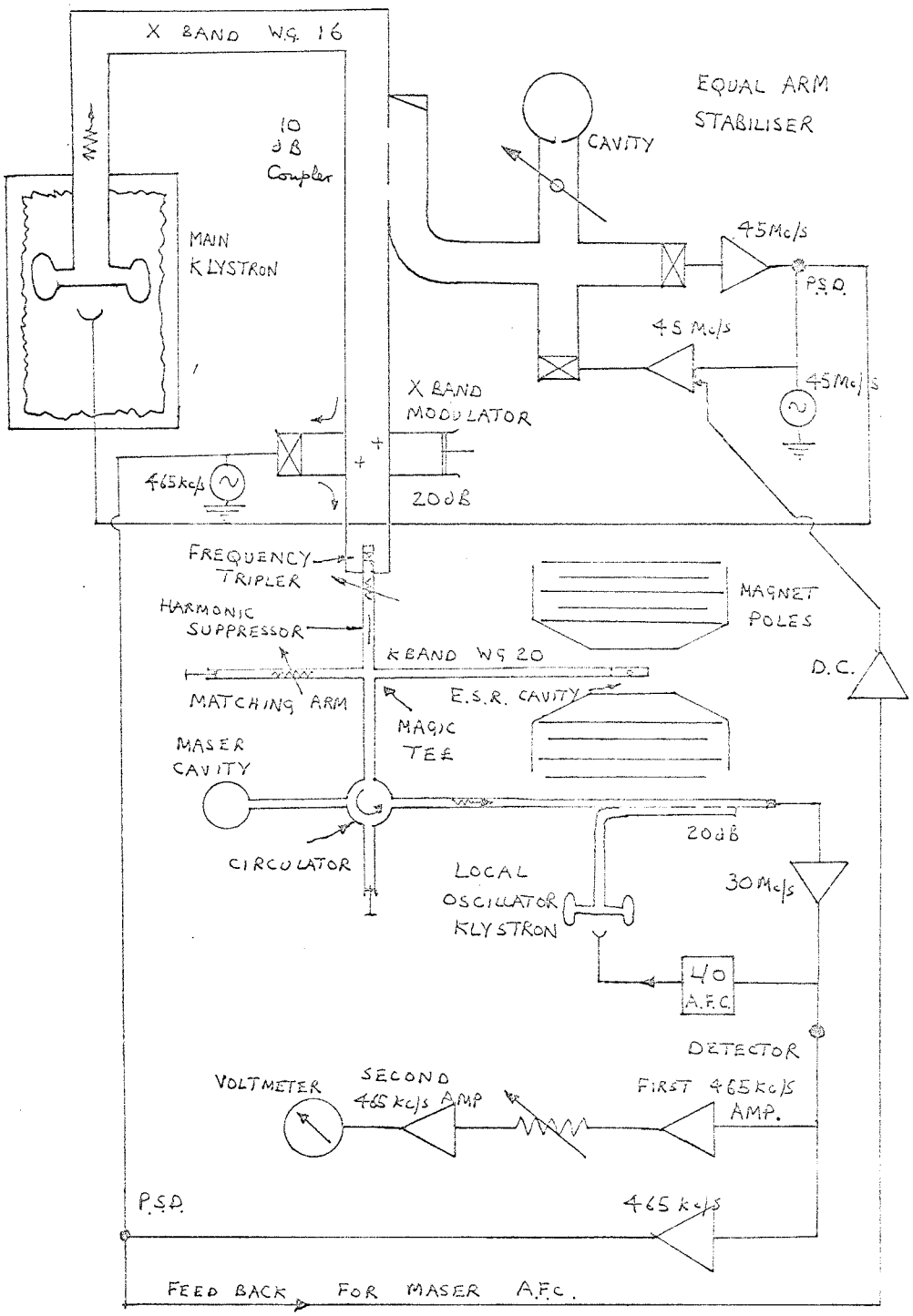

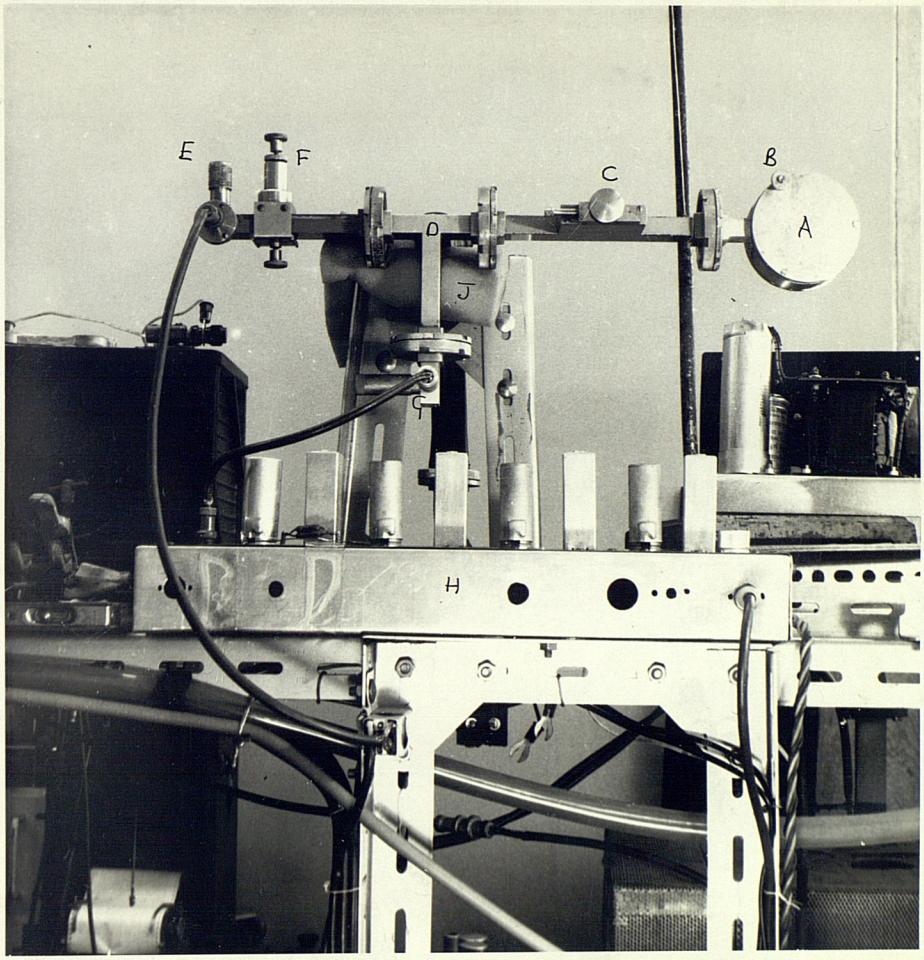

Figure 3.3 Photograph of part of the Equal Arm Stabiliser. (See figure 3.2 for block diagram) A Equal Arm Cavity. B Cavity Coarse Tuning Control (Manual). C Phase Shifter. D Magic Tee. E Switched Crystal (at 45 Mc/s) with F the crystal matching screw. G Detector Crystal with H, the 45 Mc/s Amplifier. J Anti-vibration Mounting.

two signals which avoided centre tapping a coil (see figure 3.4). The normal output of the P.S.D. is shown in figure 3.5a.

The signal required to switch the X Band crystal at 45 Mc/s was quite large and the rectified current passing through the crystal was about 30 mA. This current was monitored for reference. The 45 Mc/s signal was produced from a 5 Mc/s crystal and an amplifier tuned to the ninth harmonic. A quartz oscillator was used to reduce drift. The circuit diagram is given in figure 3.4.

The operating frequency of the stabiliser is also dependent on the mean current through the switched crystal. The operating frequency could be changed about 30 Kc/s / mA at K Band. The effect of this drift in this mean current can be eliminated by means of a drift correcting signal from the maser. Details of how this signal is produced are given in section 3.3. In previous systems this signal has been taken through a transducer (piezo-electric crystal) onto the walls of the cavity[2]. However this method required quite high voltages to drive the transducer. A second method would be to feed this correcting signal onto the crystal direct. However this would require quite a high current. The method finally chosen was to put the correcting signal on to the grid of the output valve feeding the crystal. In figure 3.5b the effect of putting a sinusoidal sweep onto this grid is shown. (The mean position is shown in figure 3.5a) As the device normally operates where the central linear portion of the characteristic cuts the horizontal

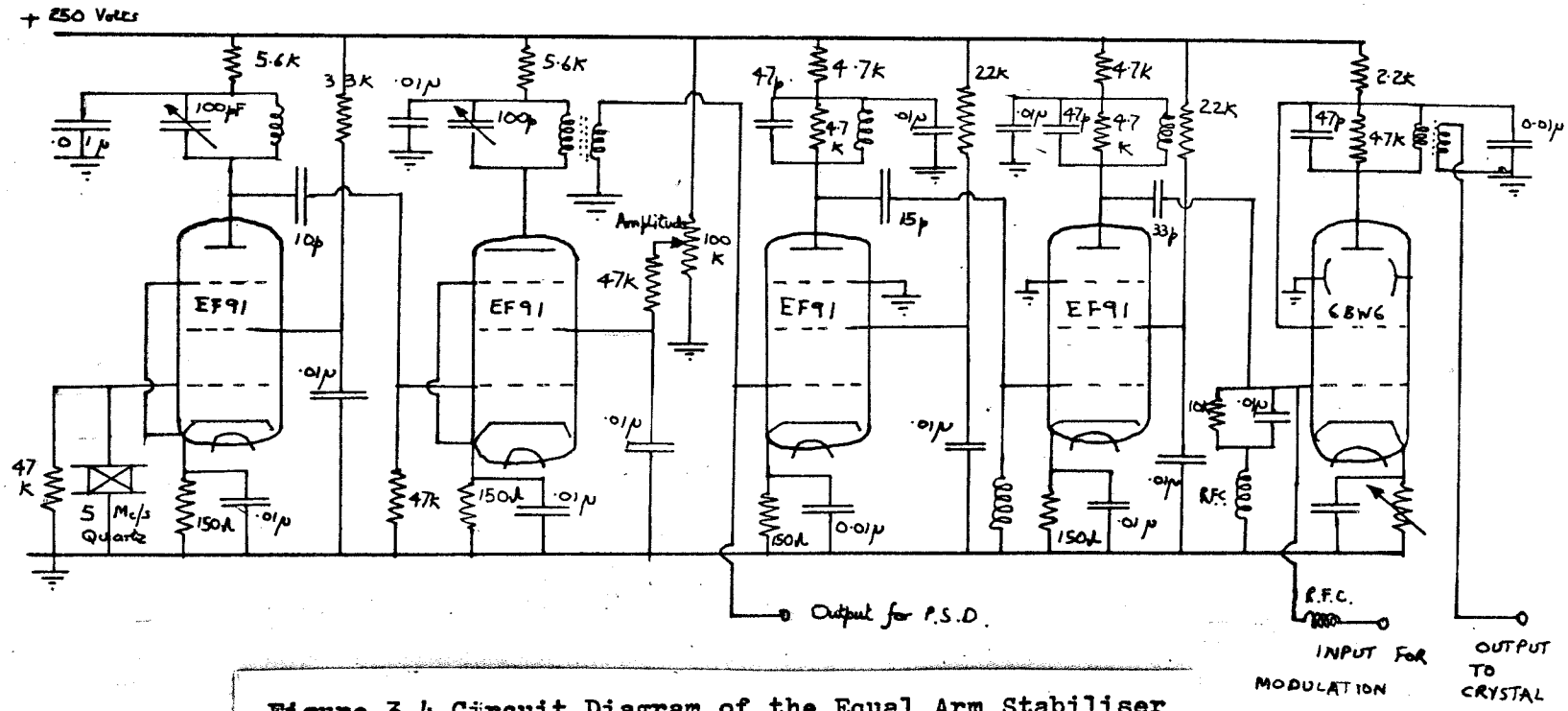

Figure 3.4 Circuit Diagram of the Equal Arm Stabiliser

Part 1 The 45 Mc/s Oscillator and Power Amplifier feeding the switched crystal.

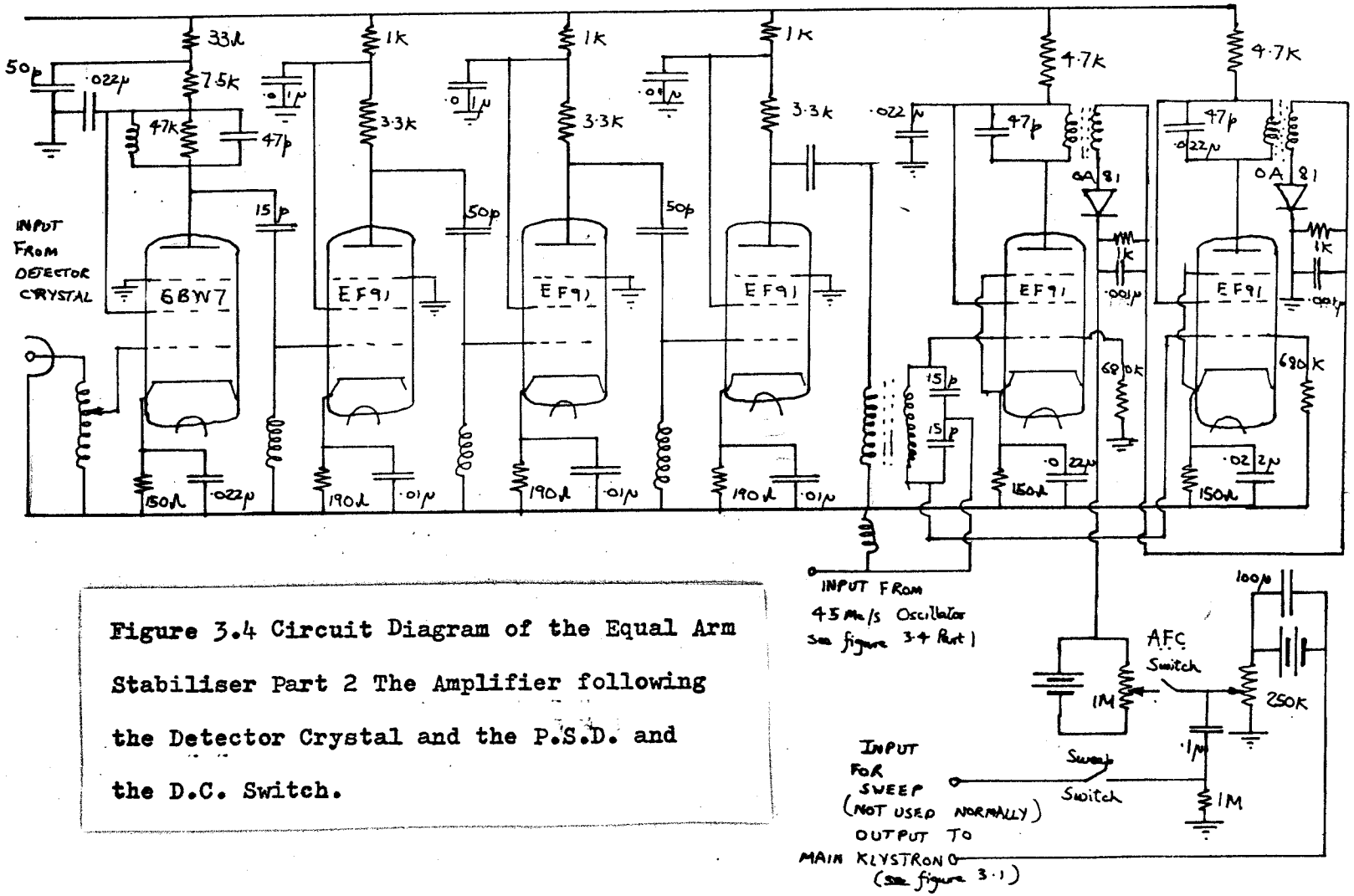

Figure 3.4 Circuit Diagram of the Equal Arm Stabiliser Part 2 The Amplifier following the Detector Crystal and the P.S.D. and the D.C. Switch.

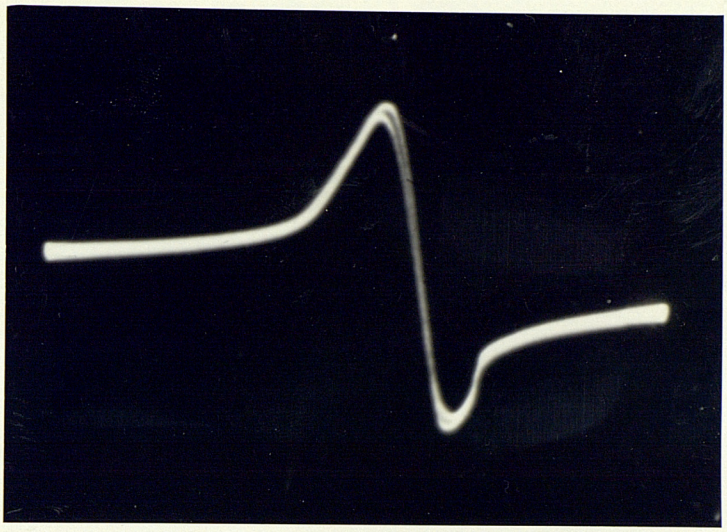

Figure 3.5a) Photograph showing the Output of the Equal Arm Stabiliser against frequency (see figure 3.4 Part 2 for the output point)

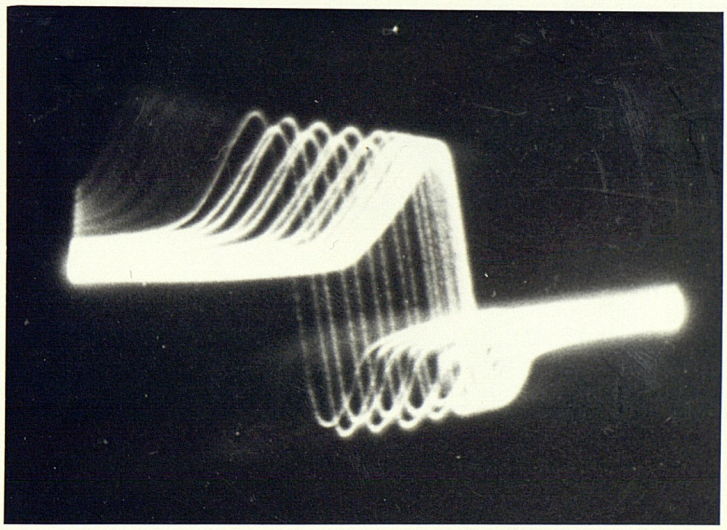

Figure 3.5b) Photograph showing the same output as above but also with a sinusoidal sweep modulating the Stabiliser. (See figure 3.4 part 1 for the modulating point)

frequency axis, it can be seen that the effect of the sinusoidal sweep is to change the operating frequency sinusoidally.

Finally a D.C. switch, see figure 3.4, was designed and built to 'lock on' the stabiliser. This switch incorporated two batteries to adjust the output level of the P.S.D. to the input level of the klystron reflector voltage modulator.

3.2.c) The X Band 465 Kc/s Modulator.

The reason why this modulator was required is given in the next section of this Chapter. The object of the modulator was to produce a linear amplitude modulation of the X Band signal at 465 Kc/s. The modulator is shown in figure 3.2. The requirement for a linear modulator is that there must be sufficient power dissipated in the crystal to cause the crystal to operate in the 'linear' region of its characteristic. This was achieved by means of an 8 dB coupler which provided about 10 mW. The crystal was matched to a 465 Kc/s oscillator via a calibrated attenuator. The variable short circuit, see figure 3.2, had to be adjusted so that the crystal was matched to the guide, otherwise some unwanted frequency modulation was generated as well.

3.2 d) The Frequency Tripler and Harmonic Suppressor.

The frequency tripler used by T.H.W. had an ordinary 1N26 K Band Crystal in it. This tripler had an efficiency of about 1%. However, the crystal had only a short life under normal operating

conditions, and the output of the device was somewhat unstable. It was decided to replace this by a tripler made by Microwave Associates. This tripler was 3% efficient and gave about 2 mW over 70 Mc/s for an input of 90 mW from the X Band Klystron. This device was tuned by the manufacturers to the ammonia transition frequency, but was found to drift during the work. A wave-guide transformer had to be made to put this tripler in circuit. A wave-guide 16 → 15 quarter-wave transformer[4] was designed and built to do this.

Like most harmonic generators, there was also an output of unwanted harmonics. These were eliminated by about a metre of reduced height wave-guide which was made by T.H.W. Although harmonics would seriously affect the operation of the spectrometer, there was no effect observed. (See figure 3.2)

Although the X Band signal has a 465 Kc/s modulation on it, the output of the tripler also consisted of a carrier and two 465 Kc/s sidebands. The effect of the higher order sidebands (930 Kc/s, 1,395 Kc/s etc.) will be discussed in the next section of this chapter.

3.2 e) The K Band Circuit.

The K Band circuit is shown in figure 3.2. The circuit consisted of the E.S.R. (Electron Spin Resonance) cavity and matching arm, a circulator and maser cavity, and a detecting system. However, for the first part of the work, the E.S.R. cavity and matching arm were not in circuit as only the maser was being investigated. The

E.S.R. part of the circuit will be described in Chapter 6.

In the previous section, the supply to the K Band circuit was outlined. This supply normally gave an output of 2 mW. In the K Band circuit before the E.S.R. part of the circuit were two attenuators (one of which was calibrated and was made by Midcentury Microwave Gear). The total attenuation possible was 80 dB. When the K Band circuit was used to measure the maser characteristics only 10^{-7} Watts were required. The reason for this level is given in section 3.3.

The circulator was a four port isolator made by Microwave Associates and tuned by them to the Ammonia Frequency. Owing to the geometrical configuration of the arms the circulator was used in an unconventional way. This is shown in figure 3.2. However, as there is an isolator following the circulator (made by F.X.R. Inc.), the circuit is equivalent to the conventional one.

The cavity has been described in section 2.4. The maser cavity arm was sealed into the vacuum system and also a mica window was put inside the wave-guide to maintain the vacuum seal.

The detecting system consisted of a conventional local oscillator and mixer crystal. The local oscillator klystron eventually used was an Elliot 12RK3 No. 58. A considerable amount of time was wasted trying to use an old 2K33A Klystron which was constantly fading out. The Elliot Klystron gave 200 mW in the first mode and 100 mW in the second. As only 100 mW were required the klystron was operated in this second mode. This also had the

advantage that a smaller reflector - cathode voltage was required. The local oscillator was coupled into the signal via a 20 dB directional coupler. (See figure 3.2) The mixer crystal used was an IN26 (supplied by Microwave Associates) and it was found that by selection, quite good noise performance could be obtained. Noise figures are given in Chapter 4. The crystal was operated under normal operating conditions of 1 mW incident local oscillator power.

3.3. The Electrical Circuit

3.3 a) The 30 Mc/s I.F. Amplifier.

Following the mixer crystal described in the previous section is an I.F. Amplifier. The operating frequency was chosen at 30 Mc/s as this frequency has been shown by T.H.W[1]., to be the best for a minimum noise factor. The amplifier was also designed so that there was sufficient gain to drive the detector at the output into the linear portion of its characteristic, when the input signal power to the mixer was 10^{-7} Watts. The amplifier and detector are shown in figure 3.2 and their circuit diagram is given in figure 3 6.

The amplifier, built by T.H.W., was found by the author to have several faults in the low noise stage at the input. This section was rebuilt by the author using a more conventional low-noise circuit (see figure 3.6). The noise figure of the amplifier was measured using a matched noise tube and it was found to be 1.59 or 2 dB. This is typical for this type of amplifier. The bandwidth of the amplifier was 2 Mc/s so that the 465 Kc/s sidebands were also amplified.

3.3 b) The Local Oscillator A.F.C.

The local oscillator A.F.C. (Automatic Frequency Control) was a system used to maintain the frequency of the local oscillator klystron 30 Mc/s away from the frequency of the K Band signal. The system used a small part of the output of the 30 Mc/s amplifier which

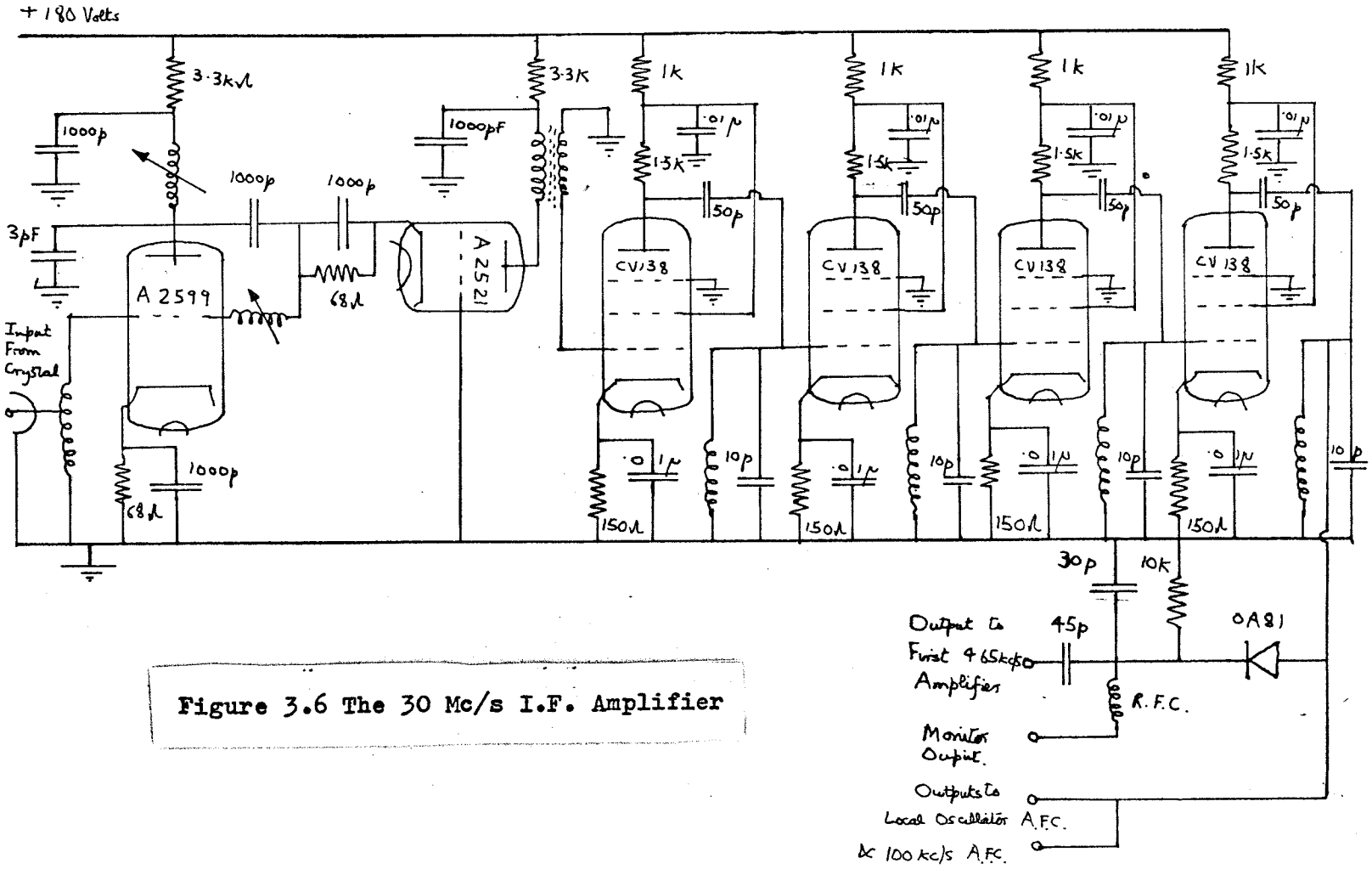

Figure 3.6 The 30 Mc/s I.F. Amplifier

was fed to a discriminator circuit. This discriminator gave out a suitable signal to correct the drift in the klystron frequency.

The entire system was built by the author and worked satisfactorily only when a new stable local oscillator klystron was used. Only some of the features of the system will be outlined here. A small fraction of the output of the 30 Mc/s amplifier was taken so as to avoid any unwanted feed-back effects. The drift correcting signal produced by the discriminator had to be D.C. coupled to the reflector of the local oscillator klystron. Unfortunately, this reflector was normally about 2.4 Kv negative to earth potential. The 'D.C. jump' was achieved before the discriminator using an isolating R.F. transformer. In order to reduce the amount of amplification required in the D.C. amplifier following the discriminator (see figure 3.7) most of the amplification was done in the R.F. stages. However, to achieve such high gain without oscillation the signal frequency had to be changed to 10 Mc/s using a 40 Mc/s local oscillator. In the 10 Mc/s amplifier a limiting stage was used to improve the signal to noise ratio of the system. Under normal conditions, the circuit worked whatever the amplitude of the output from the I.F. amplifier. This was a big advantage when setting up the various circuits. Another advantage of the frequency changing stage was that by tuning the local oscillator frequency (by tuning the coil) the I.F. frequency could be adjusted so that the I.F. amplifier worked on the best part of the characteristic (i.e. gave the maximum output). When the system was locked to one of the 465 Kc/s sideband frequencies the

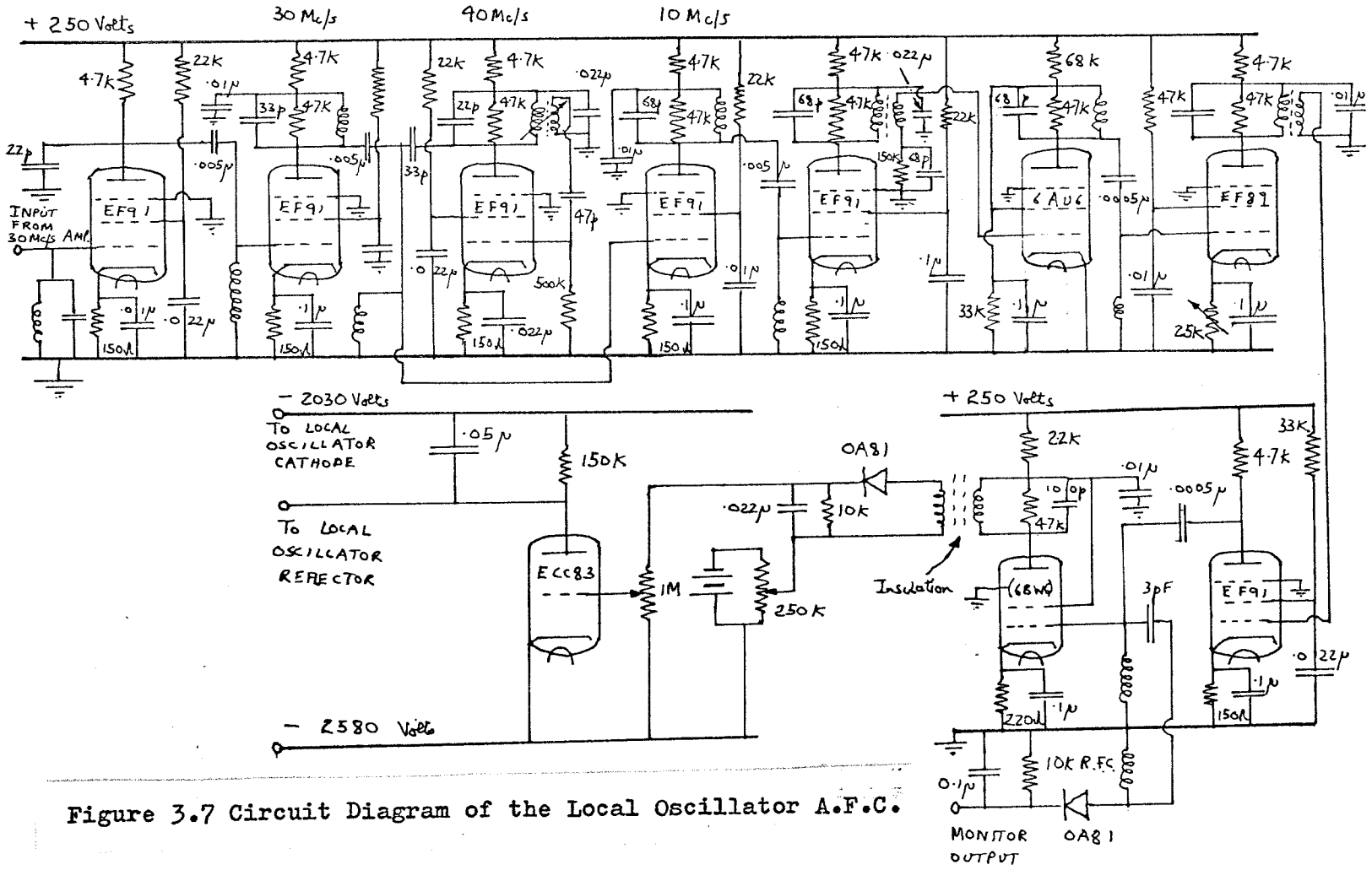

Figure 3.7 Circuit Diagram of the Local Oscillator A.F.C.

local oscillator could be used so that the system gave the maximum output at the sideband frequency. However, this was usually a very small adjustment.

Finally, the D.C. amplification was achieved by one valve which was supplied by the klystron's own power supply. A D.C. switch was also designed and built to 'lock in' the A.F.C. It was found that of the two possible 30 Mc/s sidebands only one gave the correct signal for the A.F.C. This is explained in Appendix 1. Also in Appendix 1 is the relevant theory of this type of A.F.C. A circuit diagram is given in figure 3.7.

3.3 c) The 465 Kc/s Detection System and P.S.D.

The input power to the maser is normally about 10^{-12} Watts[5]. The main K Band signal could be used for the measurements of the maser characteristics but the output would be inconveniently small to detect. Assuming a gain of about 20 dB the output power would be only 10^{-10} Watts. The A.F.C. system described in the previous section would not be feasible as the signal to noise ratio would be too small. So it was decided to tune the main klystron so that one of the 465 Kc/s sidebands was at the maser frequency. In figure 3.8 the sidebands are shown on the diagram of the ammonia J=3, K=3 hyperfine structure. If any of the other sidebands were at the frequency of one of the hyperfine components it would depopulate the upper energy level of the component. This may decrease the main maser action. It can be seen from figure 3.8 that nearly all the sidebands are well clear

Figure 3.8 Hyperfine Structure and the 465 Kc/s Sidebands.

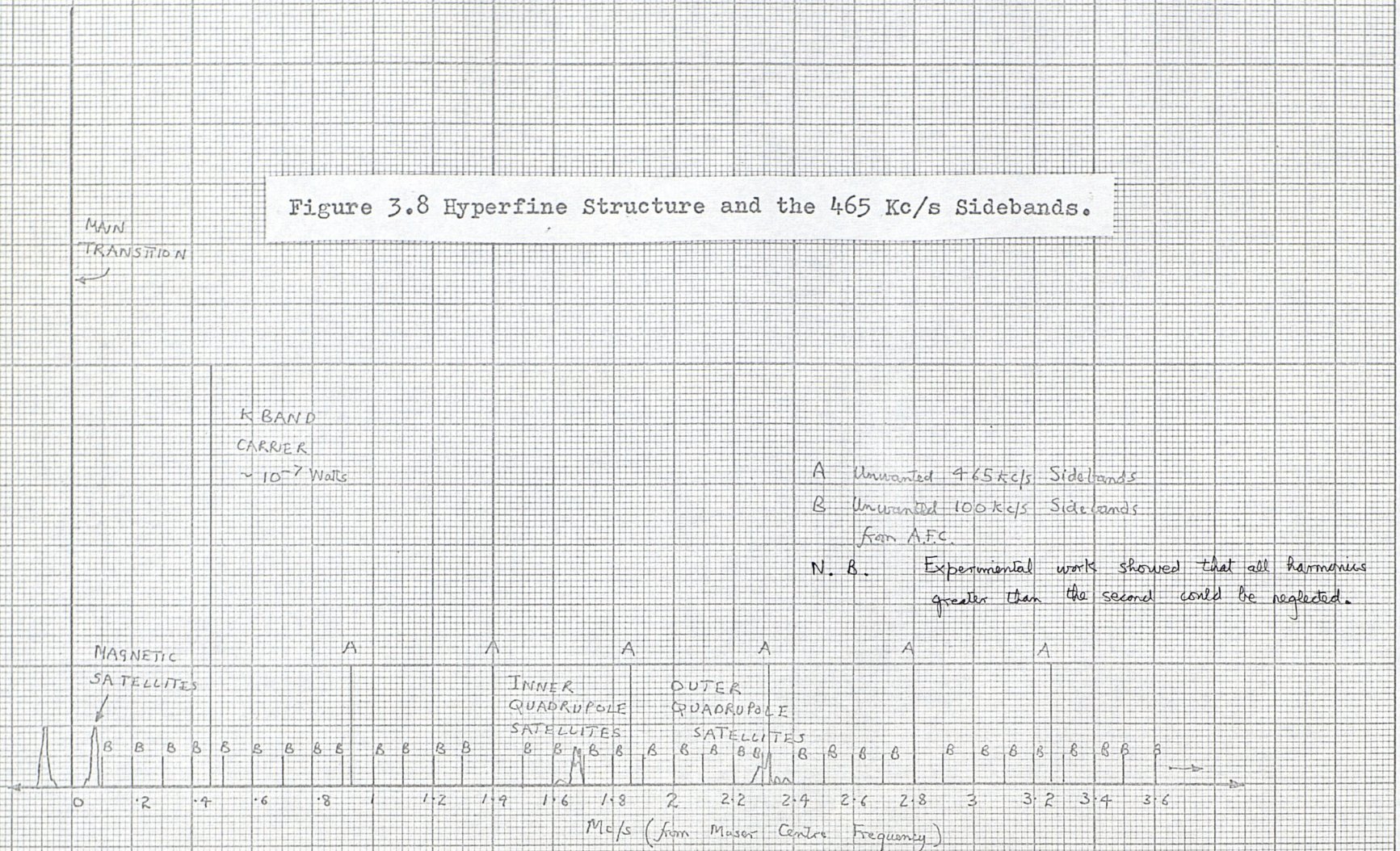

of hyperfine components so that their effect can be neglected. The carrier is also well clear but as it is normally 10^{-7} Watts it can affect the maser action even though it is displaced from the maser centre frequency. However the equation 1.69 shows that the maser response to signals at large deviations δ is governed by:-

$$P_m = \frac{AB^2E^2}{2\delta^2} \qquad \left(= AB^2E^2 \text{ when } \delta = 0 \right)$$

$$\delta \neq 0$$

which for $\delta = 3{,}300$ (i.e. for the 465 Kc/s sideband) the rejection factor of the maser is $2.2 \cdot 10^7$. Thus the carrier power of 10^{-7} Watts is effectively only 10^{-14} Watts at the maser frequency. Several tests were made to ensure that the carrier had no measurable effects on the maser. The carrier power of 10^{-7} Watts was conveniently large to detect easily by the method described in the previous sections. The output of the 30 Mc/s amplifier, after detection, consisted of two separate signals. There was a large D.C. signal (normally about 2 volts) which was produced by the 10^{-7} Watts carrier and a much smaller signal at 465 Kc/s which was produced by the maser output. This 465 Kc/s signal was then amplified in a selective amplifier. One of the outputs of this amplifier was matched to a calibrated attenuator. The output of this attenuator was matched to a further amplifier the output of which was passed onto a voltmeter. Great care was taken to ensure that at no time these amplifiers saturated. This attenuator was used to measure the maser gain and the method is given in the next chapter. The circuit is shown in figure 3.9.

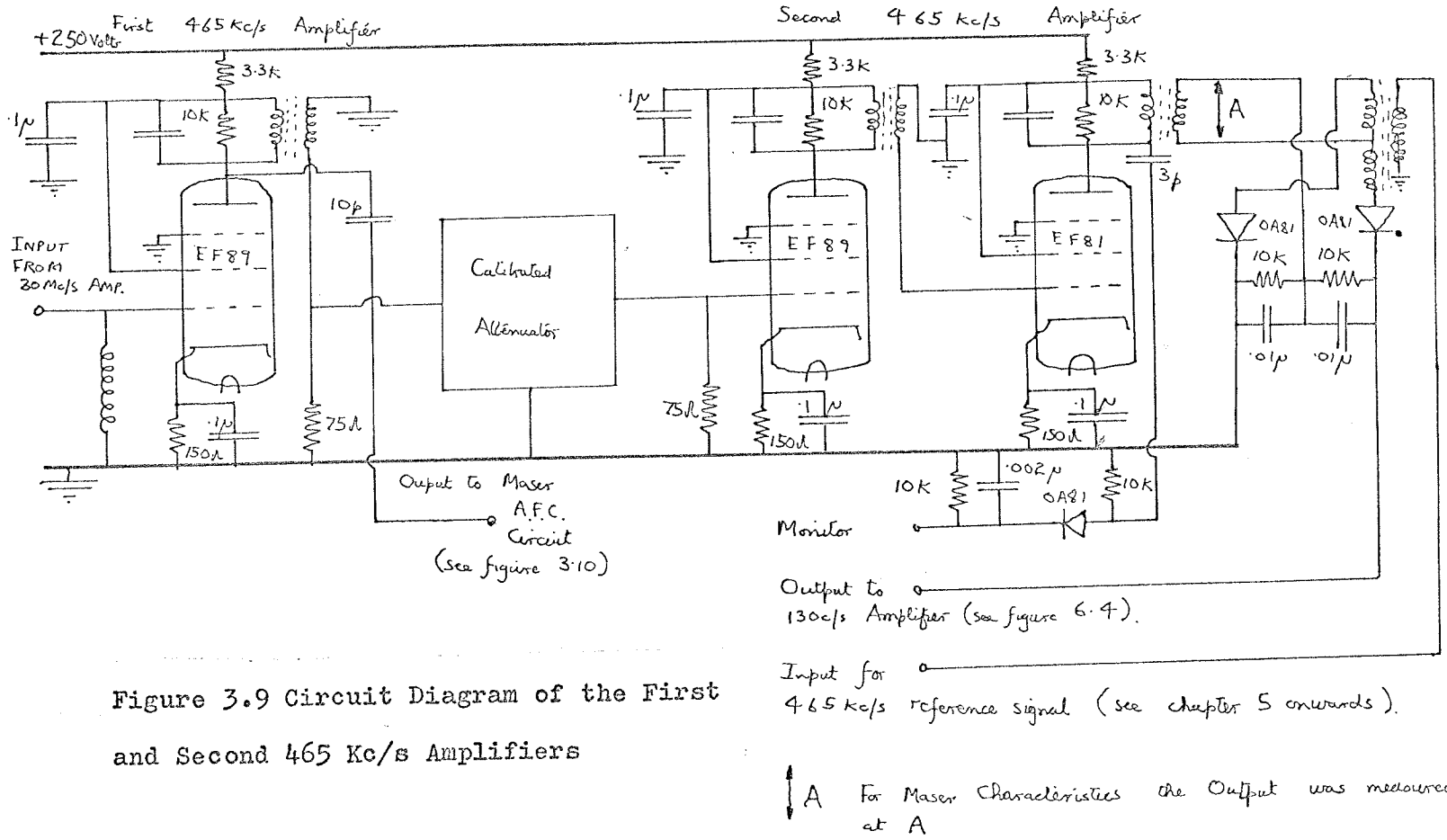

Figure 3.9 Circuit Diagram of the First and Second 465 Kc/s Amplifiers

The other output of the first 465 Kc/s amplifier was used as an A.F.C. (Automatic Frequency Control) signal. The output was further amplified in a third amplifier and then detected in a P.S.D. (Phase Sensitive Detector). As before, care was taken to prevent this amplifier and P.S.D. ever becoming saturated. The reason for this will be given in Chapter 5. Finally the output of the P.S.D. was further amplified in a D.C. amplifier which was allowed to saturate as this improved the signal to noise ratio of the system. The output of this amplifier was passed through a low-pass filter (the required characteristics of which were found experimentally) and then via a D.C. switch back to the Equal Arm Stabiliser. The method of connecting this drift correcting signal into the Stabiliser was described in section 3.2 b) in this chapter. The gain required to achieve satisfactory operation is derived in Appendix 1. Provision was also made to feedback a sinusoidal sweep to the Equal Arm Stabiliser so that the maser characteristics could be displayed on an oscilloscope. This could only be done when the drift correcting signal was not connected. In this case the drift correction was done by means of a manual system. This part is shown in figure 3.10.

Finally the maser could be made to oscillate quite easily, and when this happened the maser and the carrier signal mixed to give an output at the 465 Kc/s amplifier. This output, when displayed by sweeping the frequency, appeared as the response of the 465 Kc/s amplifier. The bandwidth of the 465 Kc/s amplifier was about 10 Kc/s

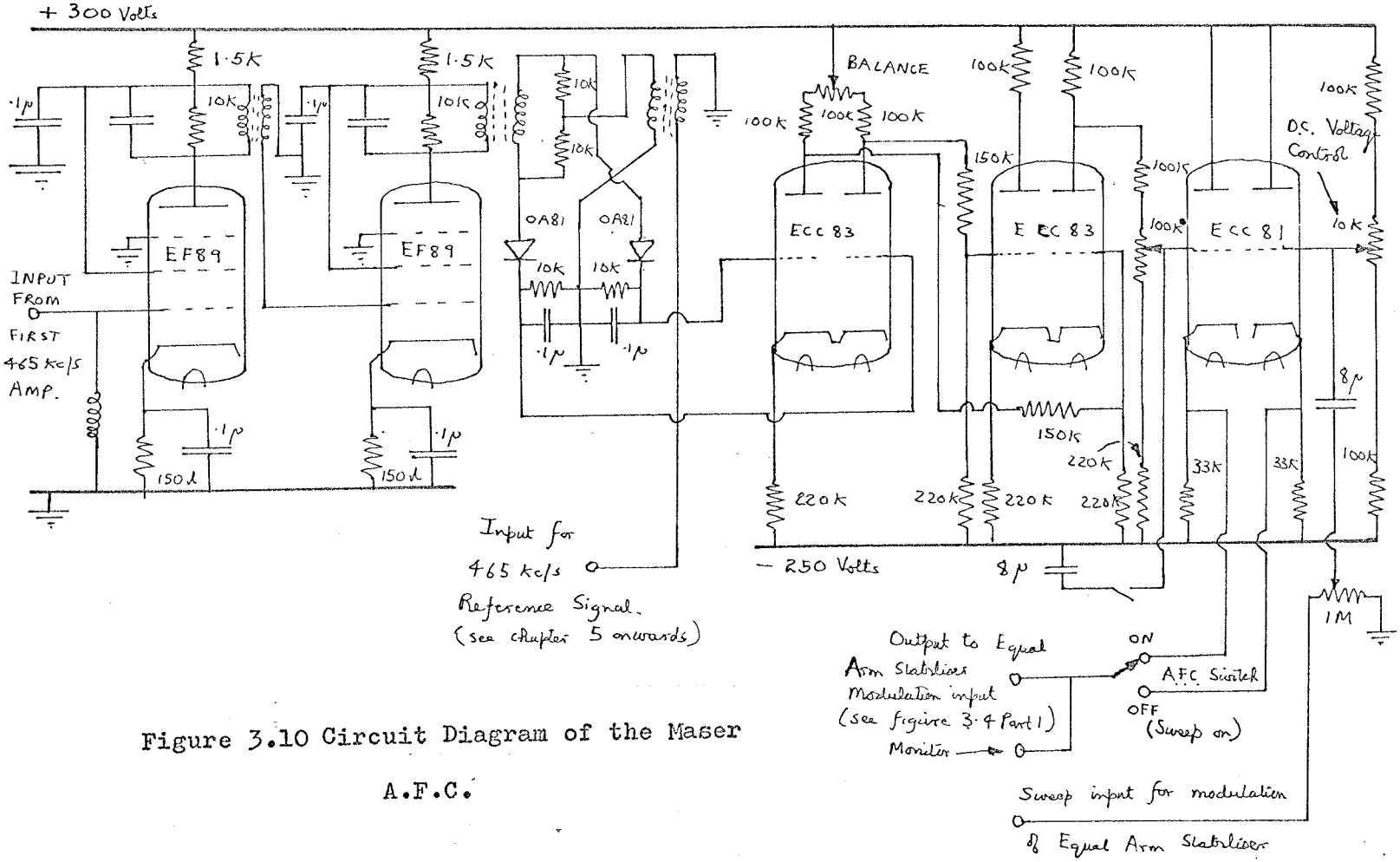

Figure 3.10 Circuit Diagram of the Maser A.F.C.

and was larger than the bandwidth of the maser. (All three amplifiers had the same bandwidth) This had the advantage in that when the maser oscillated the output could easily be distinguished from the amplifier output. When the maser both amplified and oscillated this could also be differentiated. This is shown in figure 3.11.

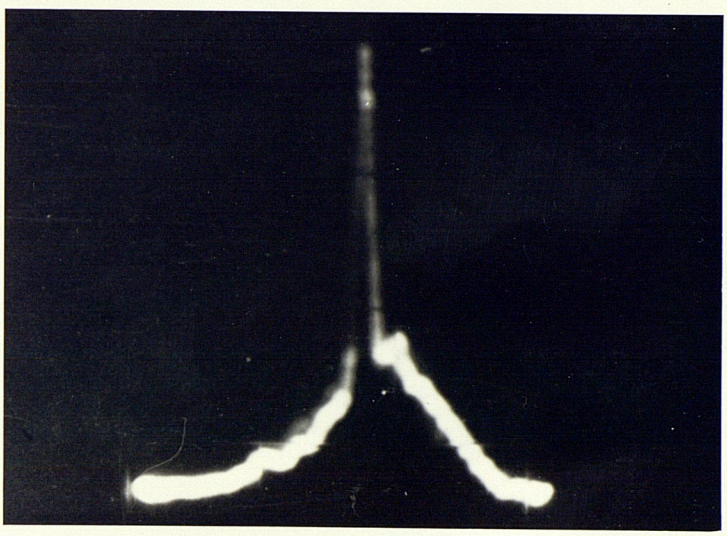

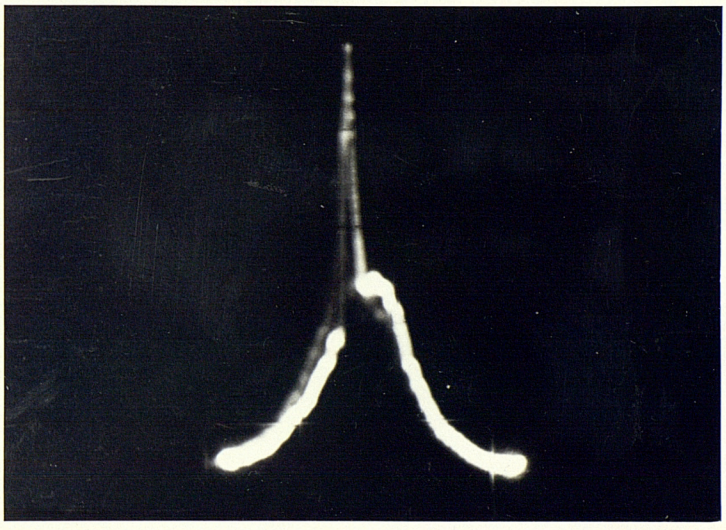

Figure 3.11. Two Photographs of the Maser Oscillating and Amplifying. Photographs show the output of the second 465 Kc/s amplifier against frequency. Frequency sweep is 23Kc/s. Lower photograph is for a higher focusser voltage. The 'spike' is the amplifier characteristic.

References Chapter 3

1. T.H. Wilmshurst. "Noise and Sensitivity Studies in E.S.R." Ph.D., Thesis Southampton pages 134 & 163. 1960

2. W.A. Gambling and T.H. Wilmshurst. "Application of the Ammonia Maser Amplifier to E.S.R. Spectroscopy" Quantum Electronics III. page 403

3. W.G. Tuller and W.C. Galloway and F.P. Zaffarano. "Recent Development in Frequency Stabilisation of Microwave Oscillations" Proc. I.R.E., 36, p 794 ~~page~~ 1948

4. L.G. Huxley. "A Survey of the Principles and Practice of Wave Guides" page 195.

5. J.P. Gordon, H.J. Zeiger and C.H. Townes. "The Maser ..." Phys. Rev. Vol. 99, August 15 page 1226 1955

Appendix 1

A.F.C. Systems.

The object of this appendix is to derive the relevant theory for the general A.F.C. system and then outline the method of measuring the stability. In any frequency source there is usually a controlling voltage (v_{in}) which can be used to adjust the frequency of the output (f_o - note that symbols used in this appendix are an independent set from those used in the rest of the thesis). For example a klystron can be controlled by the reflector voltage. See figure A 1.1. All changes in the output frequency can be referred to the input voltage. A change of δv at the input would produce a change in frequency δf at the output. A transfer function T can be defined for the frequency source as:-

$$\delta f = T. \delta v \qquad \text{A 1.1}$$

Now this change in frequency can be reduced by feedback as shown in figure A 1.2. The feedback transducer produces a voltage proportional to the frequency deviation. Let the frequency deviation with feedback be Δf. If G is the transfer function of the transducer then:-

$$\Delta f = T (\delta v - G \Delta f - \Delta v)$$

using equation A 1.1

and it follows that:-

$$\Delta f = \frac{T (\delta v - \Delta v)}{1 + GT} \qquad \text{A 1.2}$$

Δv in equation A 1.2 is a small D.C. voltage also fedback from the frequency transducer. This is often present and it has

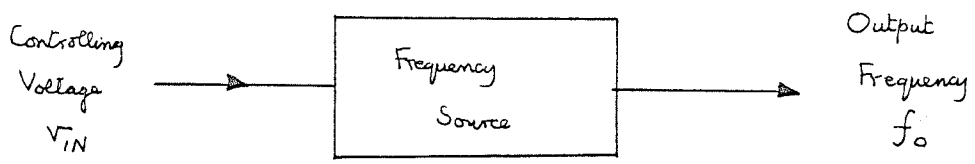

Figure A 1.1 The System without feedback.

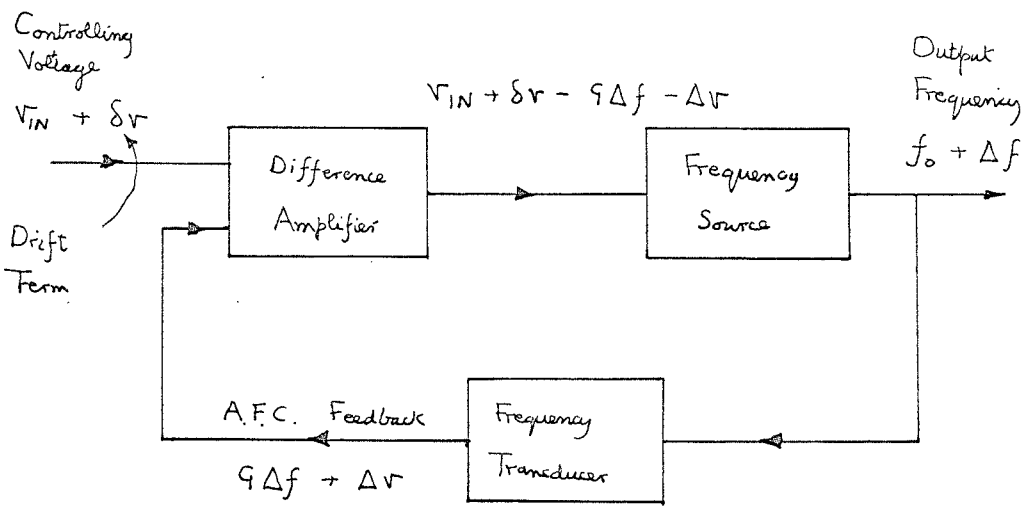

Figure A 1.2 The System with A.F.C. Feedback.

been included in the theory to show the effect of such a voltage. The stability of the system can be defined as the improvement in drift caused by the feedback. This is the ratio of the two frequency deviations given by equations A 1.1 and A 1.2. This ratio is S where:-

$$S = \frac{\delta v}{(\delta v - \Delta v)} \cdot (1 + GT)$$

The stability can be made independent of drift by adjusting the system so that $\Delta v = 0$., the stability is then:-

$$S = 1 + GT$$

$$= GT \text{ for } S > 1 \qquad \text{A 1.3}$$

To measure the value of S the A.F.C. system has to be disconnected at the output of the frequency transducer. By introducing a known change in the input voltage δv an output voltage v_{out} can be measured at the output of the frequency transducer. The stability can readily be shown to be:-

$$S = \frac{v_{out}}{\delta v} \qquad \text{A 1.4}$$

The response time of the A.F.C. is usually quite slow and is made so by a long time constant circuit at the output of the frequency transducer. This means that the value of S decreases with increasing frequency of δv. In certain circuits, the time constant can introduce a phase shift equal to π, with $S > 1$. In this case the A.F.C. oscillates at the frequency at which these conditions occur. The normal practice used, to provide high D.C. loop gain, is to make a large difference between the main time constant in the circuit and any other time constant in the circuit.

Chapter 4

The Characteristics of the Ammonia Maser Amplifier.

4.1 Introduction

The first object of this chapter is to present the experimentally observed characteristics of the ammonia maser amplifier. In this amplifier there are four main variables, P_s the source pressure, V the focusser voltage, ω_c the resonant frequency of the cavity and P_o the input power to the maser. There are two dependent variables $\Delta\nu_m$ the maser bandwidth, and G the midband gain. As far as possible the variation of all six variables has been examined. In addition two second order effects caused by variations in P_c the maser chamber pressure, and the amount of liquid nitrogen in the focusser will be discussed. Where possible, the practical characteristics will be compared with the theoretical ones. Also in this chapter the hyperfine structure which is resolved in the 'high gain' condition will be discussed.

The second object of this chapter is to examine these characteristics to find the optimum working conditions for the maser amplifier. Also the performance of the amplifier when working under A.F.C. conditions is investigated. These investigations cover both noise and stability (although these are obviously related).

4.2. Determination of the Operating Point. The Midband Gain Characteristics.

4.2 a) The Pressure Characteristic (The Graph of Source Pressure against Chamber Pressure).

One of the main factors determining the optimum working point of the maser is the pressure characteristic. As the source pressure is increased a larger amount of ammonia enters the maser chamber. Up to a point the evacuating system can cope with the flow of ammonia and maintain the chamber pressure of about 1μ Torr. However, as the amount of ammonia is increased the chamber pressure rises. As the chamber pressure rises the mean free path of the ammonia molecule decreases and the number of collisions between molecules increases. This also has the effect of increasing the relaxation of the upper energy level of the transition of the molecules leaving the focusser. For normal chamber pressures this relaxation effect can be neglected. However, when the pressure rises, the relaxation effect reduces the focusser efficiency.

The graph of chamber pressure against source pressure (P_c against P_s) shows the point where this relaxation effect is likely to become significant. The measurement was done with the liquid nitrogen trap in the focusser filled. The sensitivity of the 'Pye Scientific Instruments' Ion gauge was increased by using a 'Cambridge' spot galvanometer which had a full scale deflection of 10 μA. The pressure characteristic is shown in figure 4.1. It can be seen from the graph that above about P_s = 3 Torr the chamber pressure begins to rise.

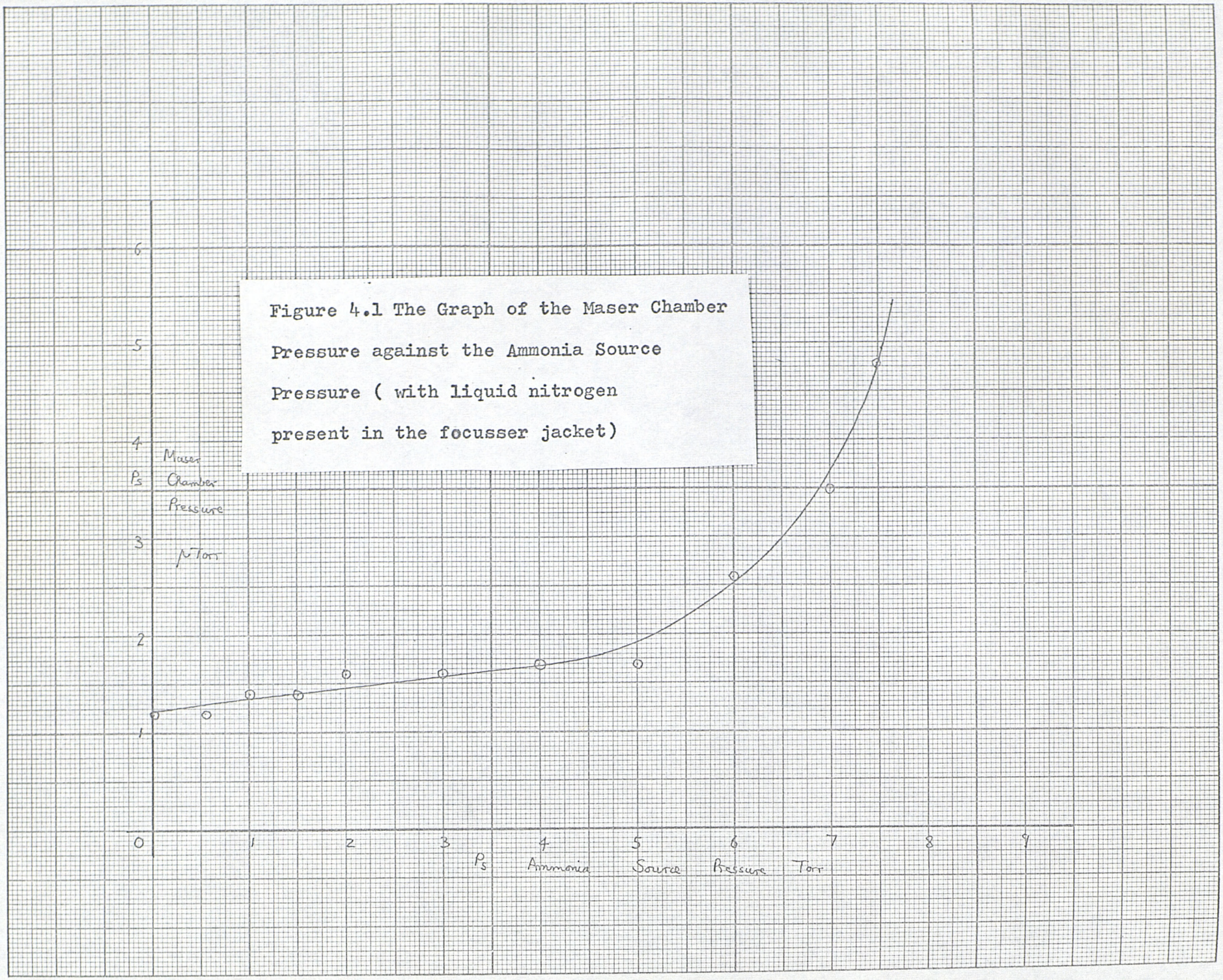

Figure 4.1 The Graph of the Maser Chamber Pressure against the Ammonia Source Pressure (with liquid nitrogen present in the focusser jacket)

4.2 b) Determination of the Operating Point from the Oscillation Characteristics.

The optimum operating point can be determined quite easily from the oscillation characteristics. The optimum operating point could be determined from the amplifier characteristics but this is a more difficult proposition as the maser amplifier has got to be operated in an unsaturated condition throughout the measurement. Once the optimum operating point was found the saturation characteristics were measured at that point (see section 4.2 d)).

The method of using the oscillation characteristics was as follows. With no input signal at the maser frequency, i.e. the 465 Kc/s sidebands removed, the maser was made to oscillate by increasing the focusser voltage. For fixed values of focusser voltage, the source pressure P_s was varied and the amplitude of oscillation was measured by a voltmeter (Marconi Vacuum Tube) at the output of the second 465 Kc/s amplifier. Section 3.3c explains this measurement. The various characteristics for fixed values of focusser voltage (V) are shown in figure 4.2. As expected, the amplitude initially increases with increasing pressure but eventually decreases to zero as the relaxation (mentioned in the previous section) rate increases. If A_{max} is the maximum amplitude occurring at a pressure Ps_{max} then further graphs of A_{max} against V and Ps_{max} against V can be plotted. The operating point is given in figure 4.3 where $A_{max} = 0$. The optimum operating point is V = 16.5 Kv and $P_s = 2.25$ Torr. The oscillation characteristics were first found by Barnes[1].

Figure 4.2 The Graph of Maser Oscillator Output against Ammonia Source Pressure (for various focusser voltages)

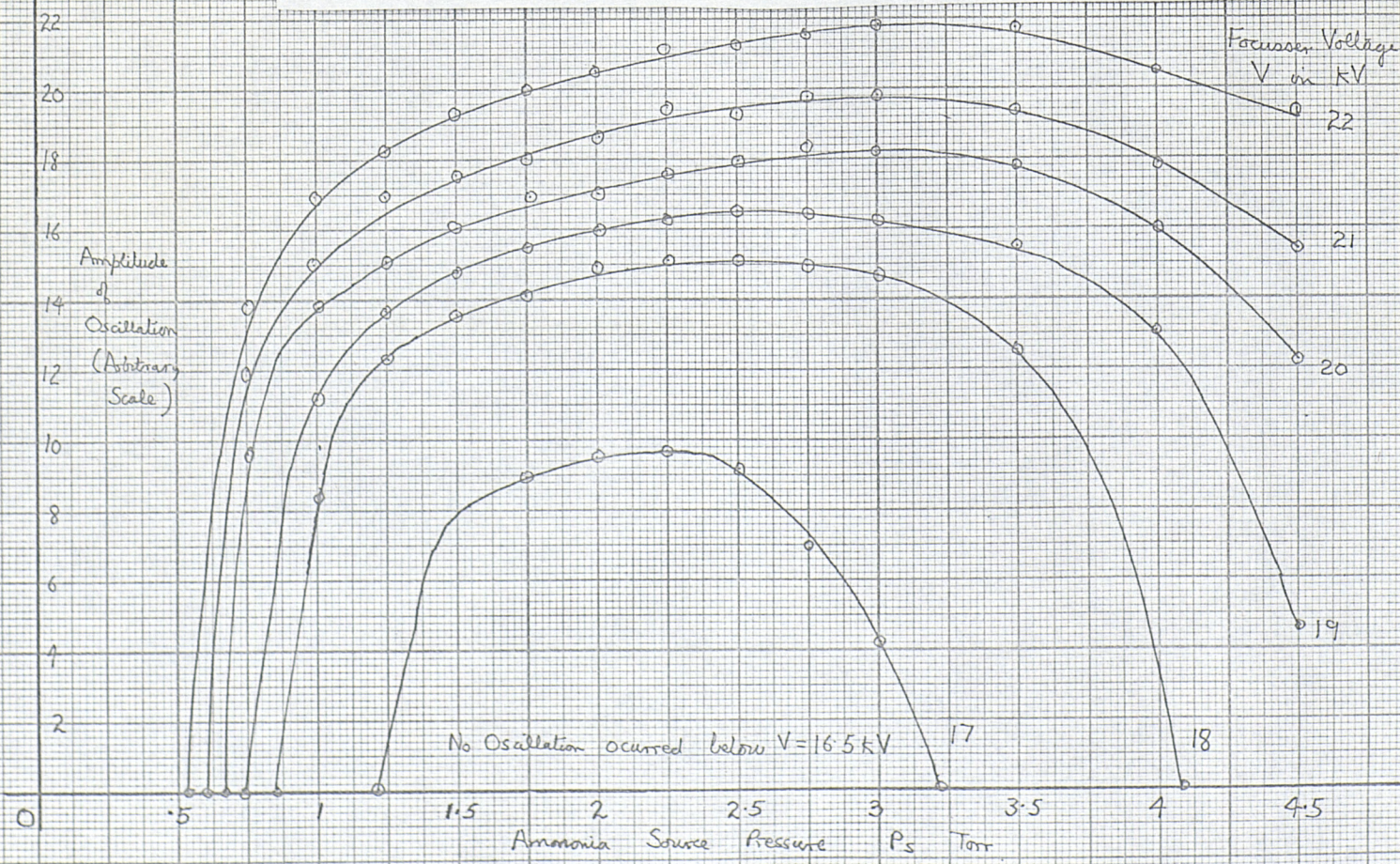

Figure 4.3 The Graphs of A_{max} and P_{smax} against V

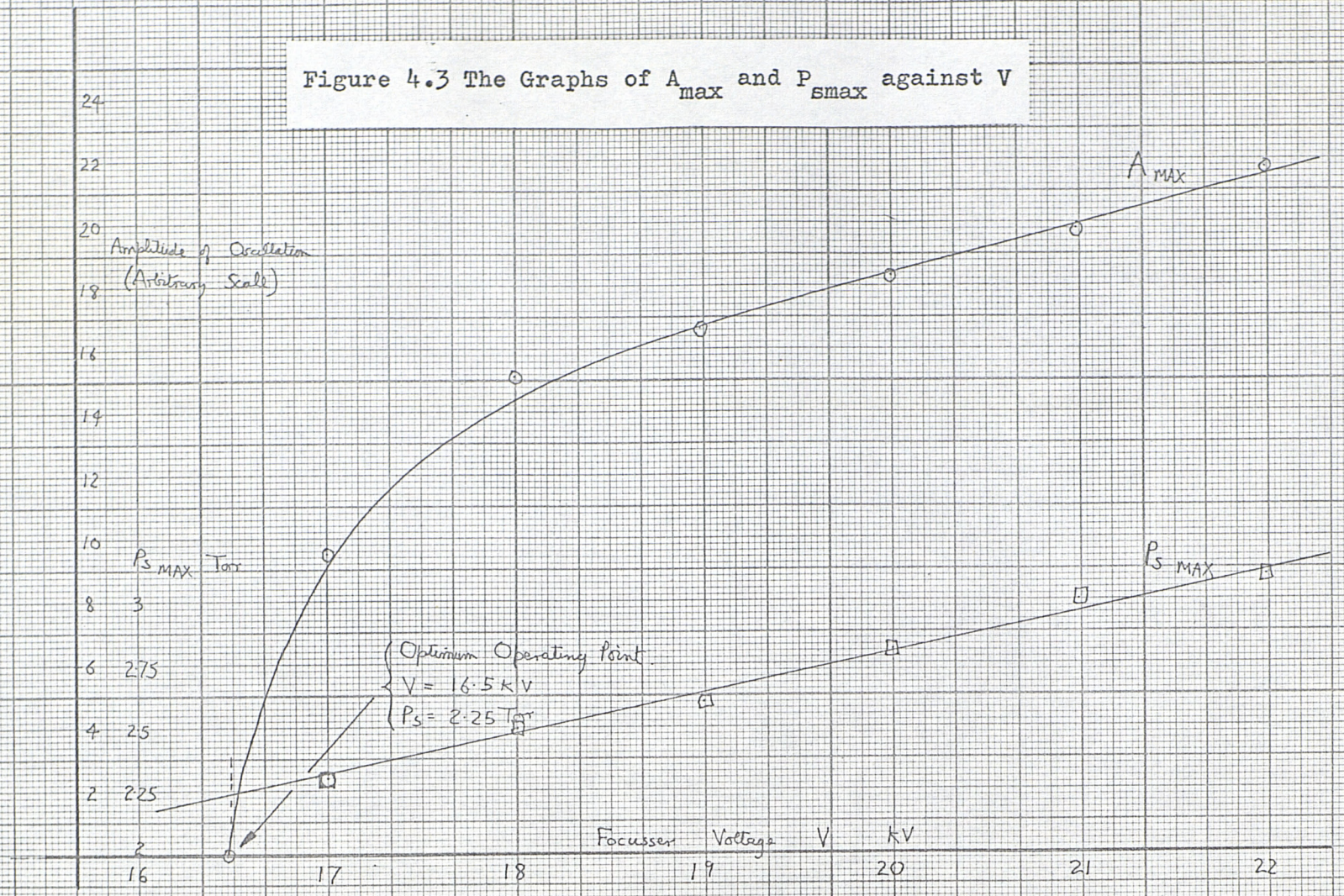

4.2 c) Measurement of Gain.

The Gain was measured by the following method. The input signal to the X Band Modulator could be varied by a calibrated attenuator (let the value of the attenuator be A_{in}). The output of the second 465 Kc/s amplifier (see section 3.3) could also be varied by a calibrated attenuator at the input to the amplifier, (let the value of this attenuator be A_{out}). A Marconi Vacuum Tube Voltmeter was used to measure the output of the 465 Kc/s amplifier. With the maser off, the entire system was checked for linearity by increasing A_{in} in steps and finding the value of A_{out} required for a constant signal output voltage. However, the measurement was not quite so simple as the voltmeter gave a reading of both the signal and noise levels. These could be differentiated by switching the signal on and off. It was found that the relationship between A_{in} and A_{out} was directly linear. When the maser was switched on, the attenuator A_{out} was then adjusted to give the same constant signal output voltage. The change in reading of A_{out} is equal to the apparent (or available) gain G'. The relationship between G' and G is obtained as follows:-

From equation 1.55 $G = \dfrac{\alpha - 1 - \beta}{\alpha + 1 + \beta}$

Let the amplitude of the two 465 Kc/s sidebands entering the maser be S_1 and S_2. Using equation 1.54 the output of the 465 Kc/s amplifier, with maser off, is proportional to:-

$$(S_1 + S_2)\frac{(\alpha - 1)}{(\alpha + 1)} = (S_1 + S_2)\frac{2}{3} \quad \text{if} \quad \alpha = \frac{1}{5} \qquad 4.21$$

With the maser on the output is proportional to:-

$$S_1 \frac{(\alpha - 1)}{(\alpha + 1)} + S_2 \frac{(\alpha - 1 - \beta)}{(\alpha + 1 + \beta)}$$

assuming the maser is tuned to the S_2 sideband. This can be simplified to:-

$$\frac{2}{3} S_1 + GS_2 \qquad 4.22$$

The apparent or available gain is given by the ratio of the expressions 4.21 and 4.22. Thus:-

$$G' = \frac{\frac{2}{3} S_1 + GS_2}{\frac{2}{3} (S_1 + S_2)}$$

and if $S_1 = S_2$, which is normally the case:-

$$G' = \frac{1}{2} + \frac{3}{4} G$$

which if $G > 1$ becomes:-

$$G' = \frac{3}{4} G$$

In dB $\quad G = G' + 2.5$ dB $\qquad 4.23$

In the work on the maser characteristics the gain is given as G throughout. However, in the later work on E.S.R. the apparent gain G' is used.

4.2 d) The Midband Gain Characteristics.

The first set of gain characteristics measured were the saturation characteristics. These characteristics were all measured at a source pressure of 2.25 Torr and a focusser voltage of up to 16.5 Kv. (See the previous section for the evaluation of these optimum

operating conditions) The characteristics are shown in figure 4.4. They have also been replotted for comparison with the theoretical predictions (shown in figure 1.11) in figure 4.5. The input power was adjusted by using the attenuator before the modulator (see section 3 b)) and was calibrated using the conversion factor found in Appendix 2.

Owing to slight drift of the maser throughout the plotting of these characteristics, the values of focusser voltage have been adjusted. This correction is described in section 4.4.

The lower limits of the graph are dictated by the inherent noise of the system. The upper limit is governed by the fact that modulator was non-linear for higher input powers. Although the apparent gain (G') was measured, the graphs show the maser gain G.

The second set of characteristics measured shows the variation of gain G with both P_s and V. In order to avoid confusion, a low input power was used to insure that at no time the maser was saturated. The shape of the second set of characteristics (see figure 4.6b) can be explained in terms of the focusser equation. If n_o is the number of molecules in the upper energy state which just make the cavity oscillate then from equation 2.33:-

$$\bar{n}_o = \eta_f n_o = n_o 1.6 \cdot 10^{-3}(1.577 + 2.\log\ 0.16\ V\ )$$

where V is in Kv.

$\bar{n}_o$ is the number of molecules flowing through the effuser. (Both numbers are per second) $\bar{n}$ is proportional to the pressure difference across the effuser, which if P_c is constant, is also proportional to P_s.

Figure 4.4 The Mid-Band Gain Saturation Characteristics

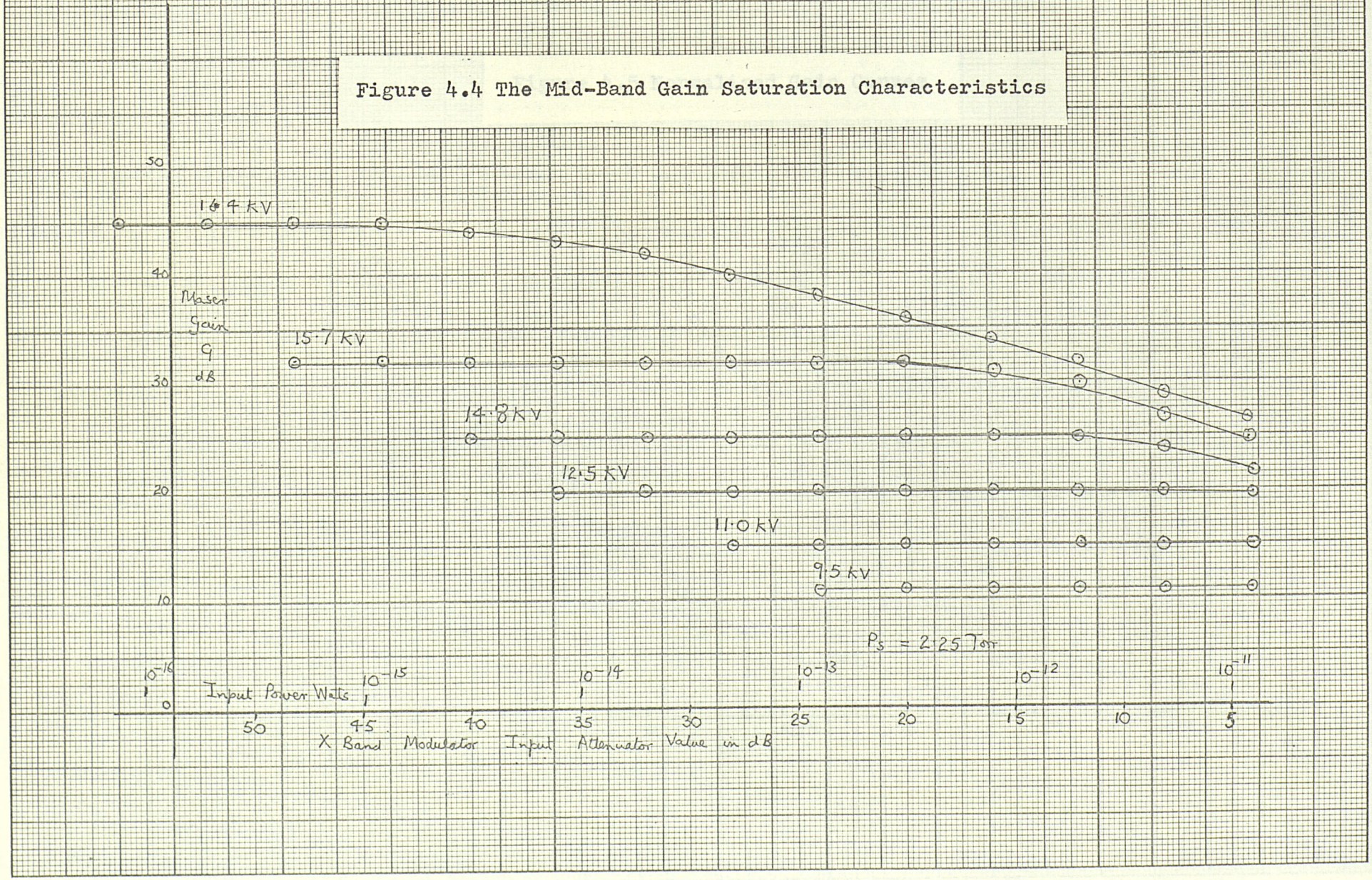

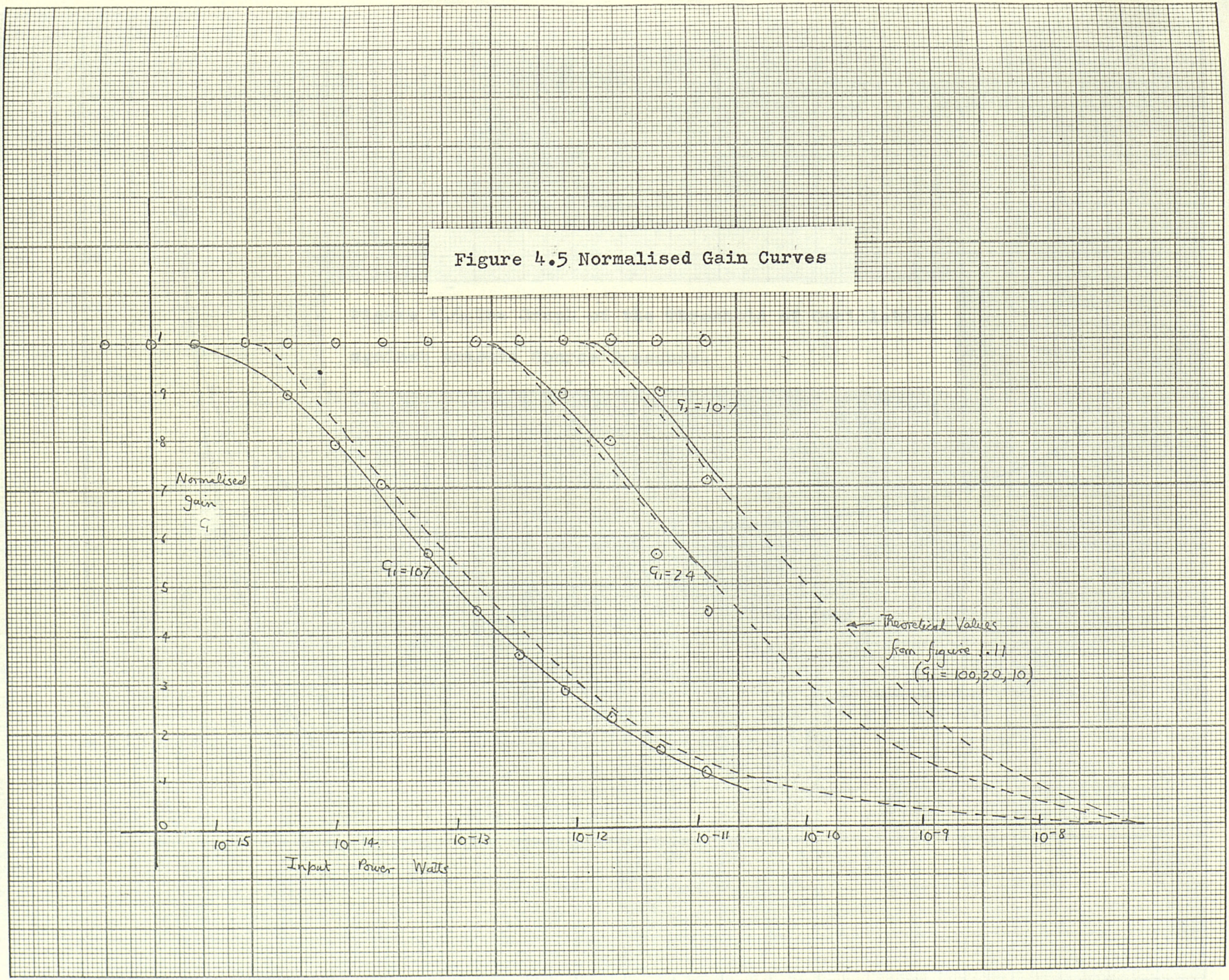

Figure 4.5 Normalised Gain Curves

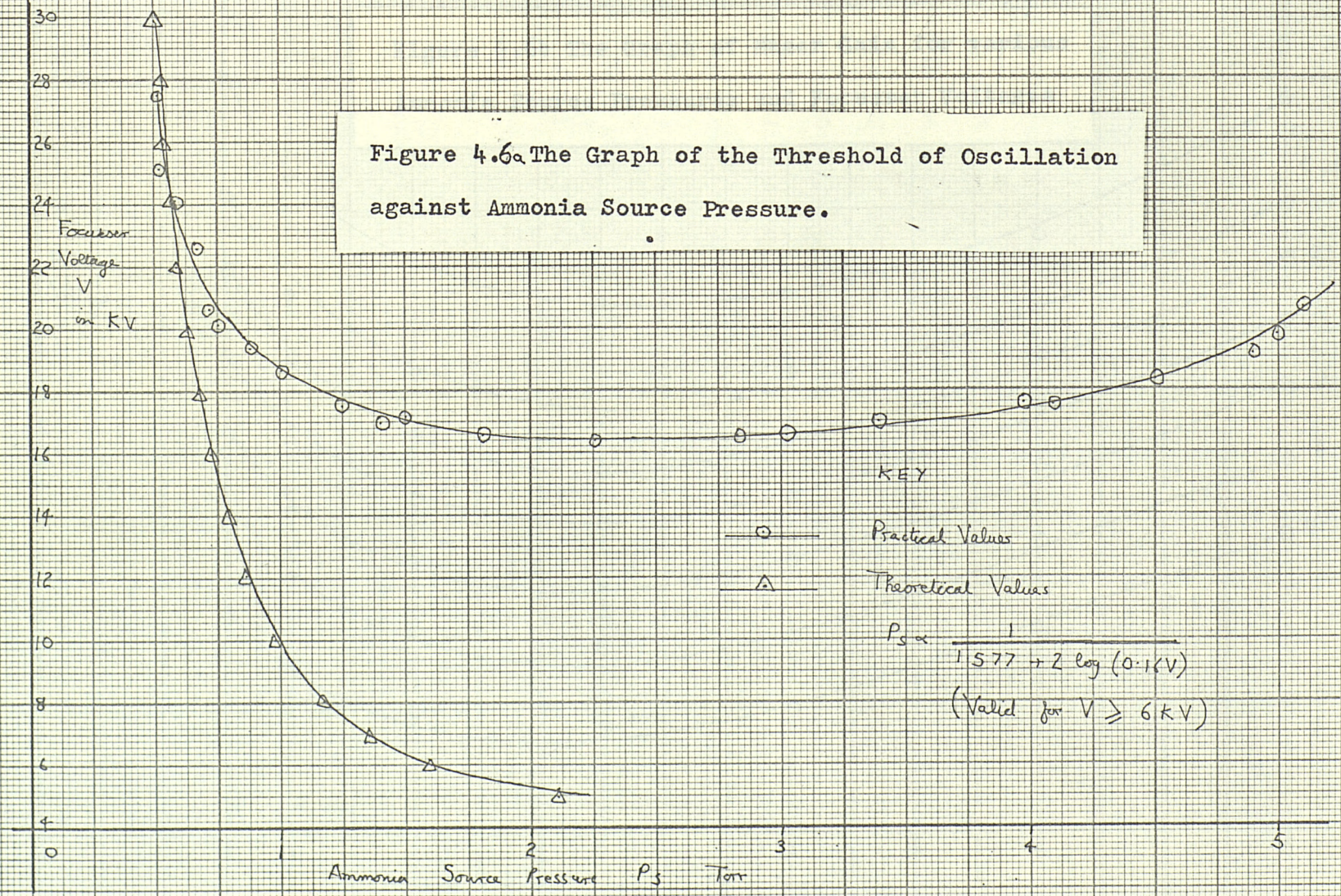

Figure 4.6a The Graph of the Threshold of Oscillation against Ammonia Source Pressure.

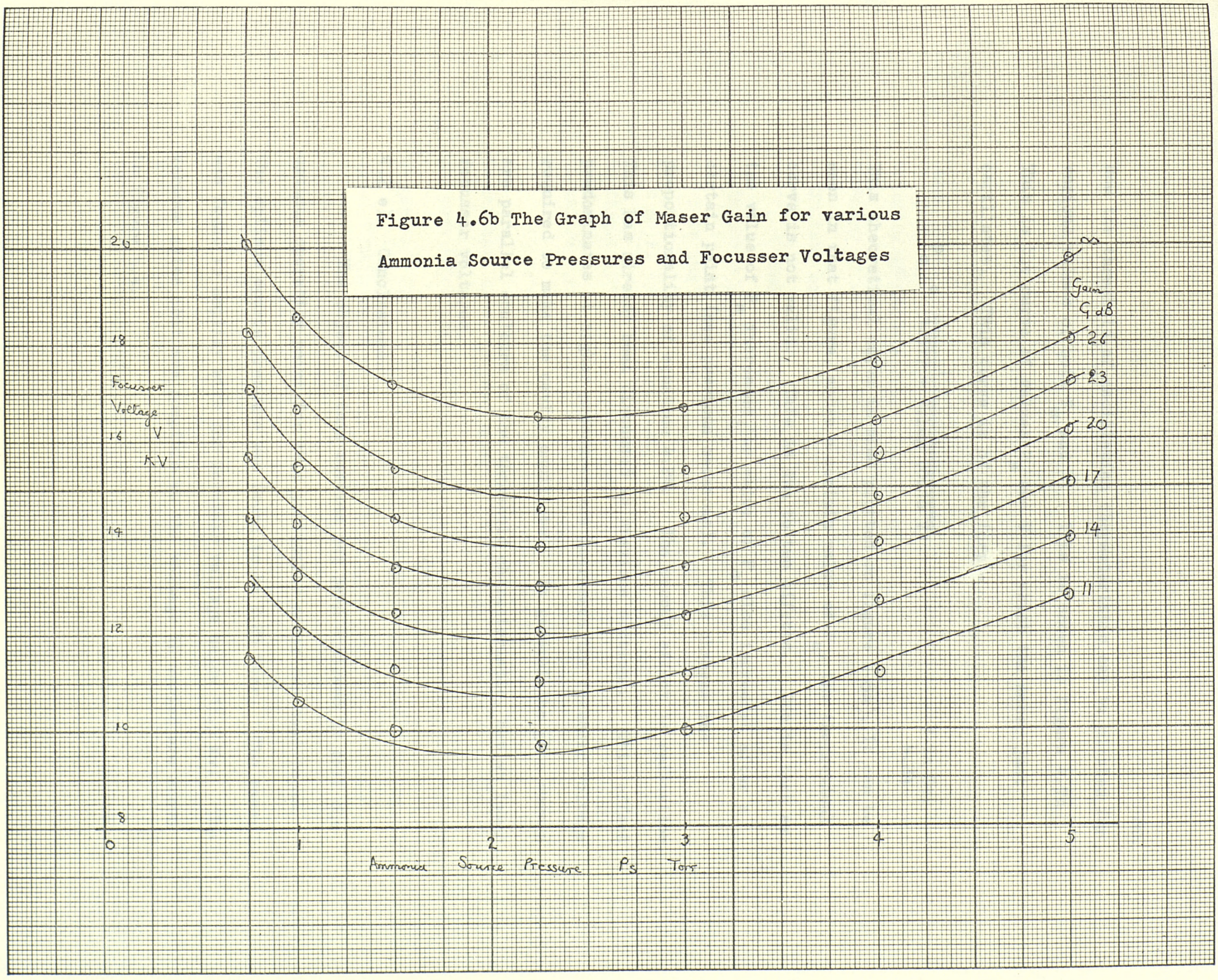

Figure 4.6b The Graph of Maser Gain for various Ammonia Source Pressures and Focusser Voltages

Now the threshold of oscillation characteristic can be plotted for various values of both P_s and V. This is shown in figure 4.6a). This is the curve of values P_s and V for which the maser just oscillates. This curve is of the form:-

$$P_s \propto \frac{1}{1.577 + 2.\log (0.16\ V)} \qquad \text{V in Kv.} \qquad 4.24$$

This theoretical curve is also plotted on figure 4.6a). It can be seen in that figure, above a certain value of P_s, the theoretical curve is not valid. This is due to two effects. One is that as the value of P_s increases, the value of P_c also increases after a certain point (see previous sections). This changes the proportionality of equation 4.24. The second effect is relaxation. This has already been discussed in previous sections. This effect predominates at higher pressures and increases the focusser voltage required to make the cavity oscillate. In general the gain curves are parallel contours of the threshold characteristic, but at lower focusser voltages.

4.2 e) Conclusions.

The object of this section has been achieved in that the optimum operating point for this particular maser has been found. The optimum source pressure was found to be 2.25 Torr. The maser was found to amplify with the focusser voltage below 16.5 Kv. The various gains that are possible as the voltage is varied are shown in figure 4.4.

Two sections of the theory, which were developed in the first chapter, have been verified partly, as well. The first theory concerns the saturation characteristics. Comparing figure 1.11 with figure 4.5 it can be seen that for the few points available there is reasonable agreement between the theory and practice. The majority of the readings in this chapter were repeatable with an accuracy of about 10%. It was unfortunate that not more points could have been plotted.

The second theory concerns the focusser characteristic. In section 1.6 it was shown that an equation existed for both the region $V > 6$ Kv and $V < 6$ Kv. In the work by Laine[2], the relationship $P_s \propto \frac{1}{V^2}$ is shown to agree with practice for the region $V < 6$ Kv. In figure 4.7 it can be seen that the more complex proportionality (equation 4.24) agrees with the practical result in the region $V > 6$ Kv.

In all this work the relaxation effect (neglected in chapter 1) has been shown to predominate at high source pressures. Shimoda[3] has postulated that the relaxation is caused by collisions within the focusser. This is to be expected as there is a greater gas density there. This means that as far as the cavity goes, there is no relaxation effect at all. This is why the theory for the cavity developed in chapter 1 can be used to predict the practical performance of the maser.

Finally, figure 4.5 shows the power levels in the maser. For example an input of 10^{-12} Watts would just saturate the maser when the unsaturated midband gain (G) is 32 dB. These figures agree with those of other masers[1].

4.3. Line Shape and Bandwidth Characteristics.

4.3 a) Observed Hyperfine Structure.

In section 1.2 the hyperfine structure of the J = 3, K = 3 rotational line of the ammonia molecule was discussed. The main line of that hyperfine structure is used in the present maser. However, the main line (or transition) also consists of three hyperfine lines. Most of the hyperfine structure has been found experimentally. The first and most extensive work was done by Gordon[4]. Later, more accurate experimental work was done by Bonanomi[5]. The spectrometer used by Gordon did not have sufficient resolution to show the three hyperfine lines in the main transition. The work done by Bonanomi used the main transition as a reference frequency and so was not able to resolve structure either. It was possible with the present apparatus to resolve the structure by artificially increasing the resolution. In this section the method and results will be outlined.

The method used to resolve the structure was to increase the gain of the amplifier which decreased the bandwidth. (The gain bandwidth for the maser was found to be 9 Kc/s in section 2.4) As the bandwidth decreased the resolution of the spectrometer (for the maser amplifier is just this) increased. At the end of section 1.8 the hyperfine structure of the main transition was given in detail. Bonanomi[6] found the centre frequency of the main line to be 23,870,129,420 c/s $\pm$ 50 c/s. Shimoda[7] found the hyperfine lines theoretically to be:-

	Power Ratio	Voltage Ratio	Frequency Deviation
c_2	0.0470	0.217	+ 1 Kc/s
c_3	1	1	- 1.25 Kc/s
c_4	0.9174	0.959	+ 0.42 Kc/s.

The practical output is shown in figure 4.7. This spectrum was obtained by sweeping the equal arm stabiliser with a 0.1 c/s sinusoidal sweep, and sweeping the X axis of the oscilloscope with the same sweep. The sweep was calibrated in frequency by putting 3 Kc/s sidebands onto the 465 Kc/s signal going into the X Band modulator. These sidebands also produced spectra which are spaced 3 Kc/s either side of the main spectrum. This is shown in figure 4.7. The amplitudes of the various components have to be adjusted as they are effectively amplified a variable amount. This has the disadvantage in that the smaller line c_2 is not resolved by this method. The centre of the spectrum was found by increasing the input signal strength so as to saturate the maser. In the saturated condition the hyperfine structure is not resolved. Roughly, the maximum height gave the centre of the spectrum. The practical results are:-

	Power Ratio	Voltage Ratio	Frequency Deviation
c_2	-	-	-
c_3	1	1	- 1.2 Kc/s
c_4	0.8	0.9	+ 0.3 Kc/s

These results show quite a degree of correlation with the theoretical predictions, both in amplitude and frequency.

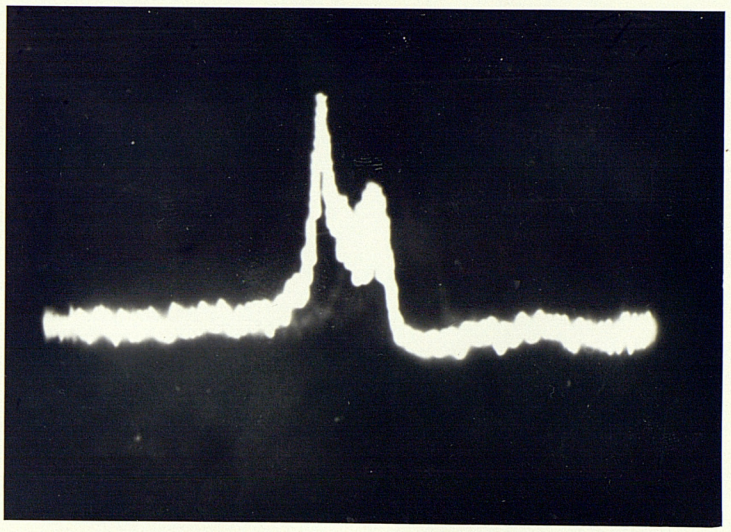

Figure 4.7 Hyperfine Structure of the Main Line of the J = 3, K = 3, Transition of Ammonia.

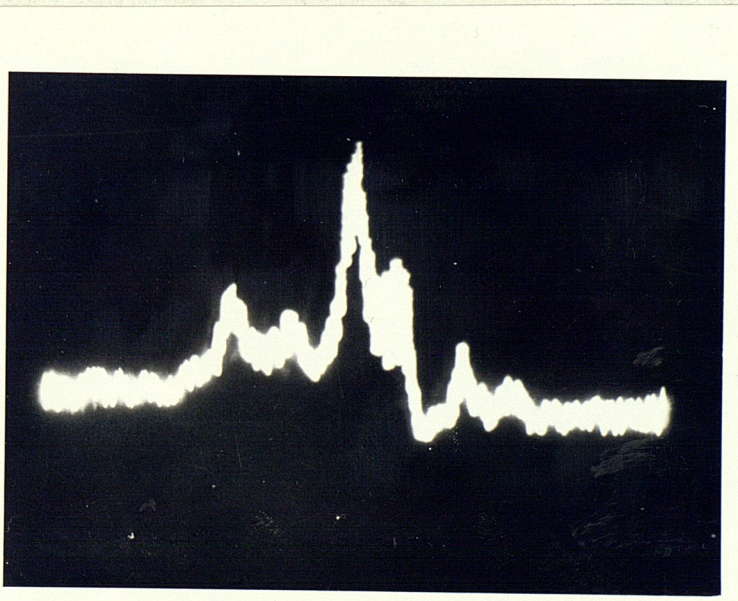

Figure 4.8 Hyperfine Structure, as above, with two 3 Kc/s side-bands used for frequency calibration.

Figure 4.8 Analysis of the Hyperfine Structure

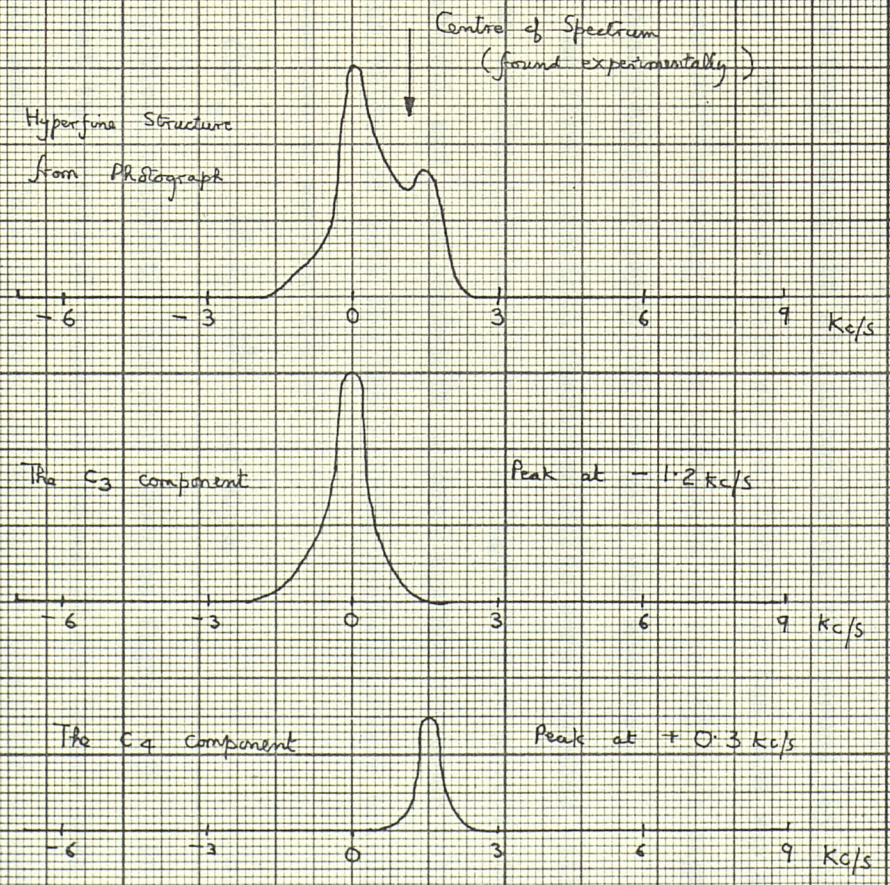

Ratio of Amplitudes 1:2

Gain of Amplifier 30 dB

∴ Voltage Ratio of Lines without distortion 0·9 : 1

P_S = 2·25 Torr

4.3 b) Bandwidth Characteristics and the Equivalent Circuit.

The maser amplifier is not a simple amplifier in that it does not have a constant gain.bandwidth product. In section 2.4, it was shown that the theoretical maximum gain.bandwidth product was 9.34 Kc/s. The measurement of the bandwidth was achieved in a similar way to the measurement of the hyperfine structure in the previous section. A slow sweep (0.1 c/s sinusoidal) was put on the equal arm stabiliser and the output of the maser was displayed on a long persistence oscilloscope (Solartron Type AD 557). The bandwidth was measured between the '3 dB' points in the usual way. The '3 dB' points were found using the attenuator before the second 465 Kc/s amplifier. The frequency axis was calibrated in the same way as in the previous section using 3 Kc/s sidebands on the 465 Kc/s signal. For each measurement of bandwidth the gain was measured.

The first bandwidth characteristics were measured with the maser in an unsaturated condition. In figure 4.9 is plotted the gain, bandwidth and gain.bandwidth product against focusser voltage. For various values of gain the theoretical bandwidthswere calculated from an equation in section 2.4:-

$$\Delta\nu_m = \frac{(\alpha - 1 - \beta)}{G} \cdot 5.6 \text{ Kc/s} \qquad 4.31$$

These theoretical bandwidths are also shown on figure 4.9. It can be seen that the practical values of bandwidth are larger than the theoretical ones. This increase is due to the hyperfine structure. The graph also shows that the bandwidth does not tend to zero as the

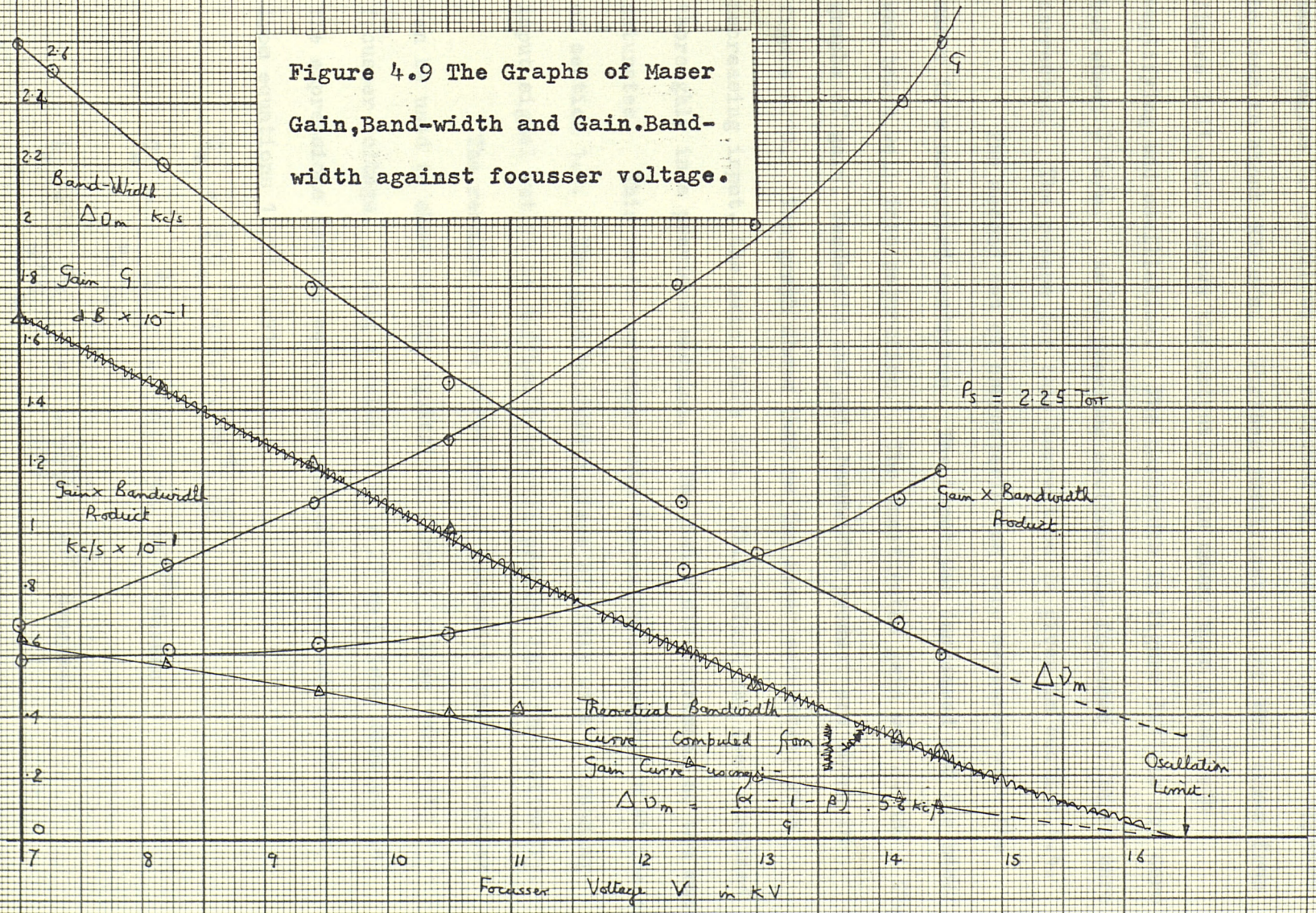

Figure 4.9 The Graphs of Maser Gain, Band-width and Gain.Band-width against focusser voltage.

maser begins to oscillate as predicted by equation 4.31. It appears to tend to about 300 c/s. Further justification for this comes from figure 3.11 which shows the output of the maser when it is both amplifying and oscillating. The bandwidth in figure 3.11 is not zero but about $\frac{1}{2}$ Kc/s. As in previous sections the focusser voltages were corrected. The reason for this correction is given in section 4.4.

The second set of characteristics were measured with the maser in a saturated condition. The input was increased and the maser was taken well into saturation. The unsaturated gain was 24 dB. The graphs of gain, bandwidth and gain.bandwidth product are shown in figure 4.10. The graph shows that as the maser saturates, with increasing input, the gain falls off. This effect has been examined thoroughly in a previous section. The bandwidth increases as the maser saturates. This is in agreement with theoretical prediction at the end of section 1.9. The gain bandwidth rises slightly with increasing input signal but it is difficult to even predict this theoretically.

The results in the first set of bandwidth characteristics can be used to show how the equivalent circuit values vary with focusser voltage. Using a value of G_c = 27 m$\mho$ (see section 2.4) the expressions for the equivalent circuit values can be obtained from equations 1.718, 1.719:-

$$G_m = \beta G_c = \beta . 2.7 \cdot 10^{-8} \mho$$

$$C_m = \frac{G_m}{\omega_o Q_m} = |\beta| \cdot 5 \cdot 10^{-29} \text{ Farads}$$

$$L_m = \frac{Q_m}{\omega_o G_m} = \cdot \frac{1.48}{|\beta|} \cdot 10^{6} \text{ Henries.}$$

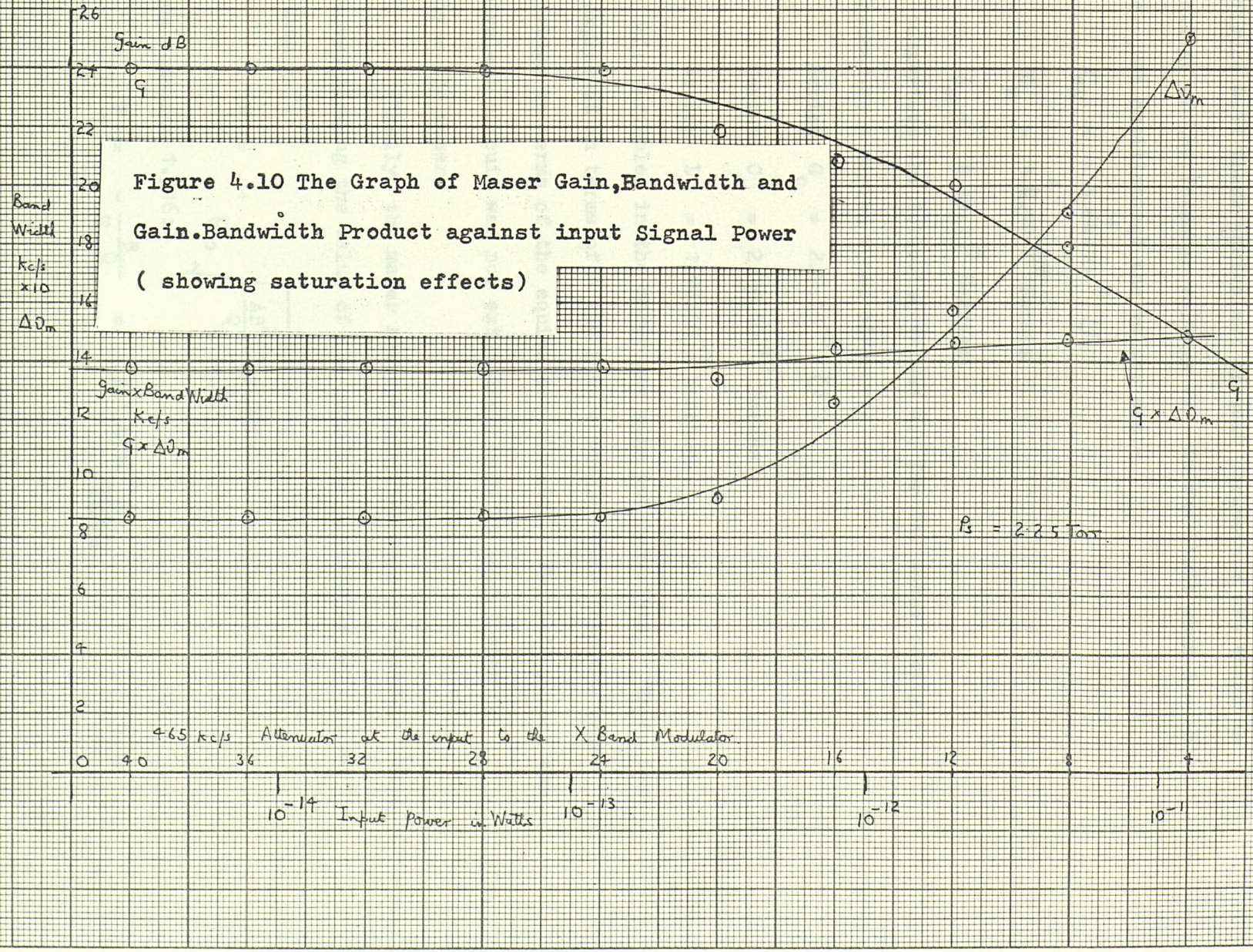

Figure 4.10 The Graph of Maser Gain, Bandwidth and Gain.Bandwidth Product against input Signal Power (showing saturation effects)

In figure 4.11 these equivalent circuit parameters are shown as functions of the focusser voltage V. In the limit when $\beta = -1.2$ (i.e. just oscillating) the values are:-

$$G_m = -3.24 \times 10^{-8}\ V$$

$$C_m = 6 \times 10^{-28} \text{ Farads}$$

$$L_m = 1.23 \times 10^{6} \text{ Henries.}$$

For comparison the following values are for the maser cavity expressed as a series tuned circuit:-

$$\text{Series } G_c = 2.7 \times 10^{-8}\ V$$

$$\text{Series } C_c = 2.25 \times 10^{-22} \text{ Farads}$$

$$\text{Series } L_c = 1.98 \times 10^{-1} \text{ Henries.}$$

The main variables in the maser are gain and bandwidth. These can be expressed in terms of α and β in a simpler form than the same variables in terms of the equivalent circuit. For this reason the equivalent circuit was not extensively used in this thesis to analyse the maser.

Finally, the maser susceptibilities were evaluated. This involved finding the value of the amplitude F which is derived in section 1.7.

$$F = + \frac{1}{\epsilon_o} \sqrt{\frac{AB^2(1+\alpha)}{Q_o\, \omega_o\, k}}$$

Using equation 1.516:-

$$F = -\frac{\beta}{\omega_o Q_o} = -\beta\ 1.4 \times 10^{7} \frac{m}{\text{Farad}} \qquad 4.32$$

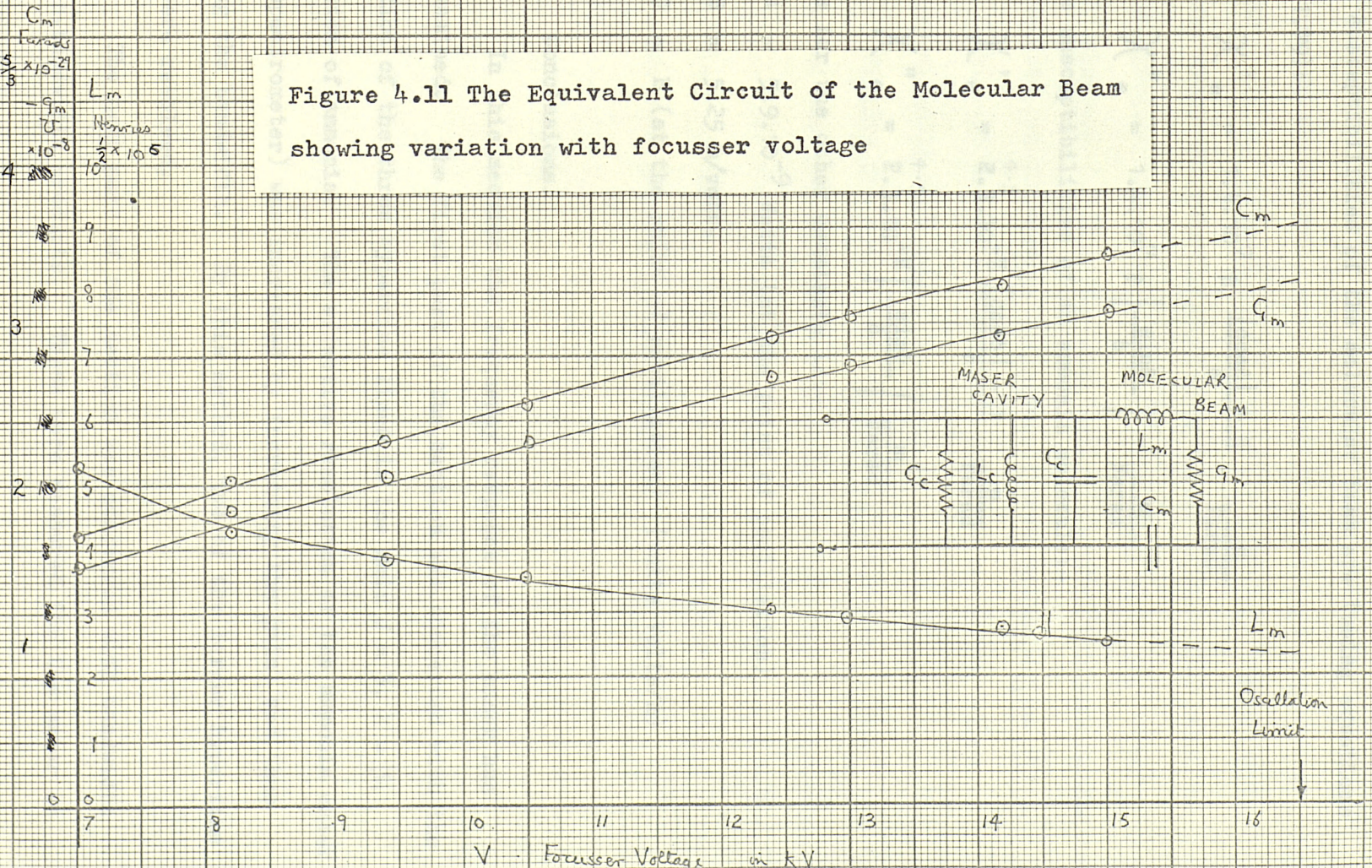

Figure 4.11 The Equivalent Circuit of the Molecular Beam showing variation with focusser voltage

So the susceptibilities of the molecular beam are (using equations 1.78, 1.79):-

$$\chi'_e = 1.4.10^7 \beta \frac{|\cos\delta| - 1}{\delta} \quad \frac{m}{Farad}$$

$$\chi''_e = 1.4.10^7 \beta \left| \frac{\sin\delta}{\delta} \right| \quad \frac{m}{Farad}$$

And the susceptibilities of an ammonia molecule:-

$$\chi'_e = 2.3.10^{-8} \frac{|\cos\delta| - 1}{\delta} \quad \frac{m}{Farad}$$

$$\chi''_e = 2.3.10^{-8} \left| \frac{\sin\delta}{\delta} \right| \quad \frac{m}{Farad}$$

A value for the other constants is:-

A = $5.9.10^{-9}$ Watts (at the point of oscillation)

B = 5.25 m/volt.

C = B (at the point of oscillation) (units Volts/m)

4.3 c) Conclusions.

In this section the frequency response of the maser has been examined. The first part of the section was concerned with the resolution of the three hyperfine lines in the main J = 3, K = 3, transition of ammonia. The effective resolution of the ammonia maser (as a spectrometer) was increased by increasing the gain, and thus lowering the bandwidth. By this method, two of the larger hyperfine lines were resolved.

The next part of the section was concerned with bandwidth and gain.bandwidth products. These were measured for the maser in

both the saturated and unsaturated conditions. In the unsaturated condition typical figures were a bandwidth of 700 c/s for a gain of 24 dB. It was found that the hyperfine structure increased the bandwidth above the value predicted by theory. Also the gain. bandwidth product increased with gain as predicted by the theory. Typical value was 1.2 Kc/s for high gain. In the saturated condition the bandwidth was increased. Typical figures would be from 700 c/s to 2.5 Kc/s. It was also found that the gain.bandwidth product increased slightly with gain.

Finally the equivalent circuit was evaluated. The variation of the component values with focusser voltage is shown in figure 4.11. In view of the simplicity of the variables α β δ etc., the equivalent circuit was not used in this thesis extensively. Finally, the molecular susceptibilities were evaluated.

4.4. Stability

4.4 a) Definition of Stability.

When the maser output was examined for noise, there were two types present. There was an amplitude noise modulation and a frequency noise modulation. Both these types were caused by two different categories of apparatus. The first category includes all the apparatus which produced thermal noise, shot noise and flicker noise etc. This would include for example the K Band detecting crystal. This category will be considered in the next section. The second category included all the apparatus which produced intermittent fluctuations or drift. This category would include for example the equal arm stabiliser and the thermal tuning of the maser cavity. Any fluctuations or drift can be referred to as instability. These categories are not 'water-tight' but are useful in analysing the various causes of noise and instability.

4.4 b) Frequency Stability of the Main Klystron with and without the Equal Arm Stabiliser.

In order to achieve the required frequency stability to use the maser amplifier, some extensive measurements were necessary to be able to show that the circuitry was capable of this. The frequency drifts of the main klystron with and without the equal arm stabiliser were some of the measurements required. The details of these measurements are given in this section.

The frequency drift of the main klystron without the

stabiliser was measured over about two hours at intervals of five minutes. The frequency drift was measured relative to the ammonia line frequency. If the frequency of the main klystron was swept sinusoidally (by applying an alternating voltage to the reflector) the output of the 30 Mc/s I.F. amplifier could be displayed on an oscilloscope. At the point on the display where the klystron frequency was equal to the ammonia line a 'marker pip' appeared which was due to the saturated maser amplifier. The drift was measured by measuring the slow movement of this marker pip across the oscilloscope trace every five minutes. This measurement was done using the D.C. control which had previously been calibrated in Mc/s by using an X Band frequency meter (Mid-Century Microwave Gear). The average drift over two hours was 19 Kc/s a minute at K Band. This drift is quite small compared with other klystrons.

The Equal Arm Stabiliser was then 'locked on' and a similar measurement was made.

The output of the maser was displayed from the second 465 Kc/s amplifier using 465 Kc/s sidebands as normal. The Equal Arm Stabiliser was swept with a slow sinusoidal signal. The trace on the oscilloscope was calibrated in frequency using 3 Kc/s sidebands on the 465 Kc/s in the way described in a previous section in this chapter. The D.C. voltage control feeding the equal arm stabiliser (see figure 3.10) was also calibrated in frequency by the same method. The drift was measured every minute and this was done by measuring the amount the maser characteristic had moved across the trace. The drift

was measured over a period of 16 minutes. The average drift was 1.5 Kc/s a minute. This showed an improvement in stability of a factor of 13. This factor includes drift in the D.C. amplifiers supplying the gain in the A.F.C. circuit before the equal arm stabiliser (see figure 3.10). The equal arm stabiliser also improved the amplitude modulation noise of the output of the main klystron.

When the maser A.F.C. was 'locked on' the system remained 'locked' for periods of up to two hours. This suggests that the majority of the drift in the equal arm stabiliser was caused by the crystal drift (the crystal being switched at 45 Mc/s see figure 3.6) rather than drift in the invar cavity. As the application for the maser only required operation over a period of about 15 minutes it was decided that the entire system had an adequate frequency stability.

4.4 c) The Effects of Thermal Drift of the Maser Cavity.

The theory of frequency pulling of the maser oscillator by the maser cavity was discussed in section 1.8. This theory was used to predict the change in β as the cavity resonant frequency changed (equation 1.87). This effect was first measured by plotting a threshold of oscillation characteristic for $\Delta\omega$ against focusser voltage. This is a graph of $\Delta\omega$ against the focusser voltage required to just cause the cavity to oscillate. $\Delta\omega$ was measured as follows. In the previous section a method was described whereby the D.C. control of the main klystron could be calibrated in frequency. If the frequency of the main klystron was swept sinusoidally (by switching off the

equal arm stabiliser and applying an alternating signal to the reflector) the output of the 30 Mc/s I.F. amplifier could be displayed on an oscilloscope. The output showed the response curve of the maser cavity with a 'marker pip' produced by the maser. The centre frequency of the cavity (i.e. $\frac{\omega_c}{2\pi}$) was given by the lowest point of the trace. The frequency difference between this point and the marker pip was measured by the D.C. control of the main klystron's reflector voltage. This frequency difference is $\frac{\Delta\omega}{2\pi}$. The graph of the focusser voltage required for oscillation against $\Delta\omega$ is shown in figure 4.12. The incremental change in cavity temperature is also shown in figure 4.12. (The calibration is given in section 2.4) A theoretical curve, for comparison, can be obtained from the graph in figure 4.12. This is obtained from equation 1.87 as follows. The threshold of oscillation is the condition $\beta_\delta = \delta$. [1.2] Hence from equation 1.87:-

$$\beta = \delta \left| \frac{\frac{2}{(1+\alpha)\Delta\omega_c}}{\sin\left\{\frac{2}{(1+\alpha)\Delta\omega_c}\right\}} \right| \qquad 4.41$$

For the various practical values of $\Delta\omega$ measured, a value of β can be calculated using equation 4.41. A graph of β against focusser voltage can be plotted. Also on this graph are the values of β found in section 4.3 (see figure 4.13). This graph is shown in figure 4.13. The graph is a smooth curve which suggests that the theory used is a valid explanation of the phenomenon.

Figure 4.12 The Graph of the Focusser Voltage required to just make the Maser oscillate against $\Delta\omega$.

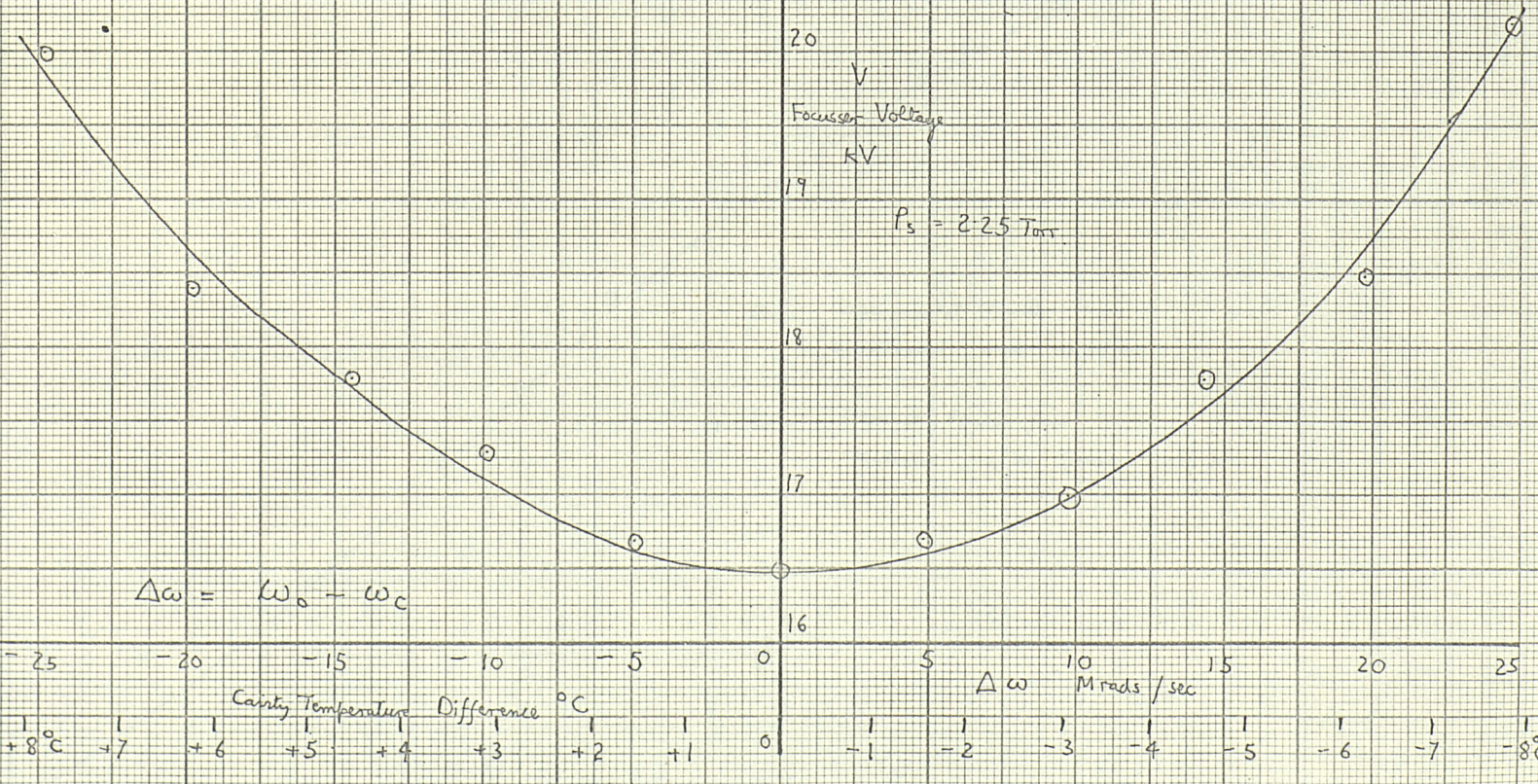

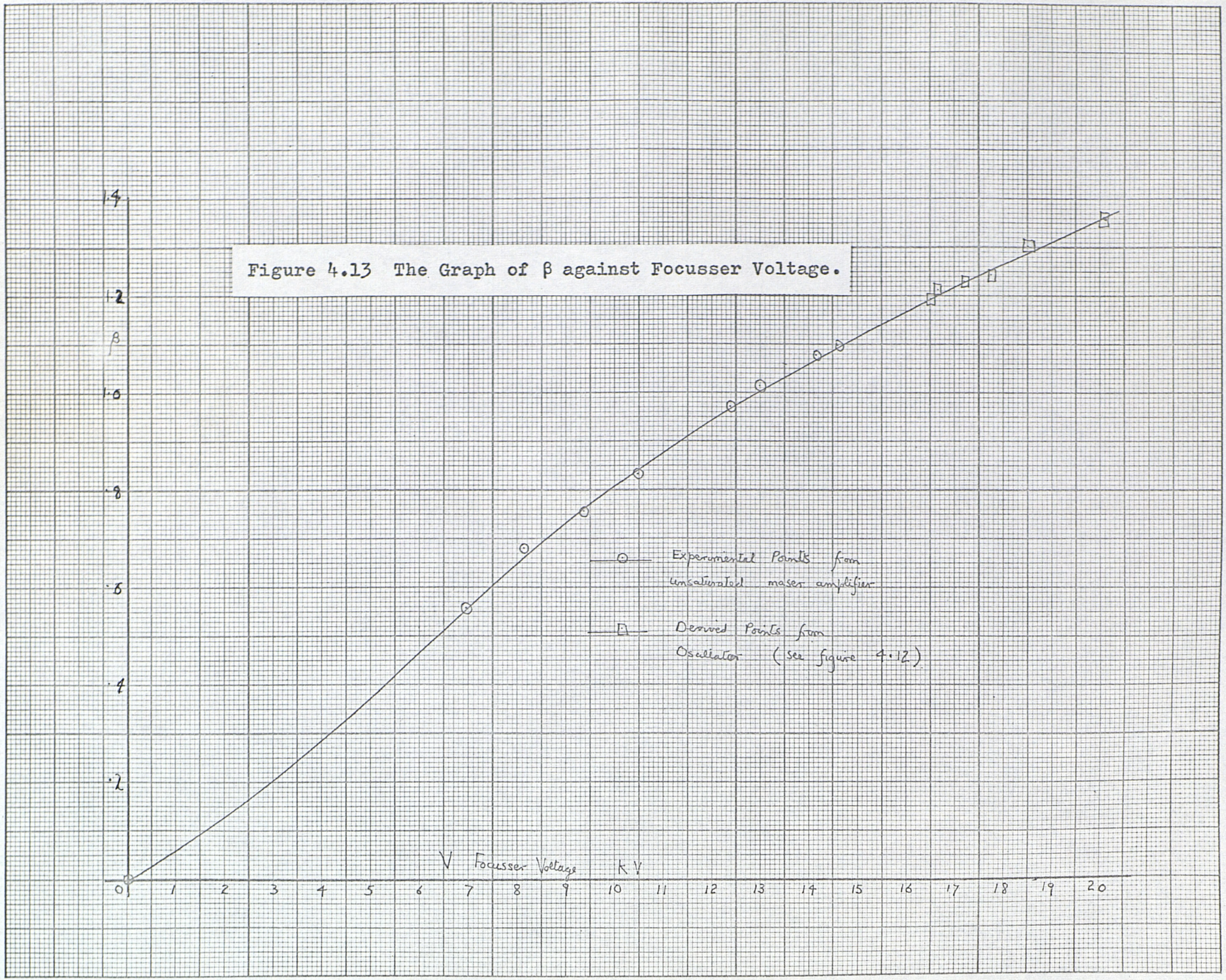
Figure 4.13 The Graph of β against Focusser Voltage.
1.4
1.2
β
1.0
.8
.6
.4
.2
0
1
2
3
4
5
6
7
8
9
10
11
12
13
14
15
16
17
18
19
20
V Focusser Voltage KV
Experimental Points from unsaturated maser amplifier
Derived Points from Oscillator (see figure 4.12)

This frequency pulling effect changes the gain as well as the threshold point. Just as in figure 4.6 the gain contours of the maser are parallel to the threshold characteristic so the contours would be parallel with the threshold characteristic shown in figure 4.12. During the day, the cavity temperature drifted slightly. However, this could be corrected as follows. Let V_{osc}, V_g, $V_{g\omega}$ be the focusser voltages required to give maser threshold of oscillation, maser gain G when $\Delta\omega = 0$, and maser gain G when $\Delta\omega \neq 0$ respectively. Using the fact that the gain contours are parallel, a correction formula for the focusser voltage is:-

$$V_g = V_{g\omega} \cdot \frac{16.5 \text{ Kv}}{V_{osc}} \qquad 4.42$$

where $V_{osc} = 16.5$ Kv when $\Delta\omega = 0$. The drift in the maser cavity could be corrected from time to time by measuring V_{osc} and applying the correction to the focusser voltage. Most of the characteristics shown in this chapter have had the focusser voltage corrected. The correction was a good one as it did not change the value of the gain actually measured. Any variation from day to day in the ammonia purity was also ~~corrected~~ eliminated by this correction formula. These variations were of second order.

4.4 d) Gain Stability.

In this section the various causes of random fluctuation in the gain of the maser will be examined. In the previous section the drift of the maser cavity and the day to day changes in the ammonia

purity were discussed. In this section the effects of changes in chamber pressure P_c, and focusser voltage V, and liquid nitrogen content in the focusser, and source pressure P_s.

The vacuum system for the maser was not perfect and throughout the work there was a small intermittent leak. This leak caused a series of sharp 'dips' or 'spikes' in the maser output. Their duration was about a second (being the recovery time of the diffusion pump) and their repetition rate varied from two a minute to one every four minutes. When this leak was initially observed, it was occurring in two places. One was in the rubber seal between the diffusion pump and the maser chamber. This was cured by removing some dust which appeared to have broken the seal. Figure 4.14 shows the effect of both leaks on the chamber pressure and the maser output. It can be seen that there is a definite correlation between the 'spikes'. The other graph in figure 4.14 shows the output when one of the leaks had been removed. Although the remaining leak affected any E.S.R. spectrum amplified by the maser it was decided not to spend months finding it as the spectrum need be only run through once again to eliminate the effect. In any case the spikes were quite distinctive and could easily be accounted for.

Several tests were made to see if the focusser voltage drifted sufficiently to affect the maser gain. There was no apparent drift due to this cause. From figure 4.6 it can be seen that the change in focusser voltage per dB of gain at G = 20 dB is about 300 volts/dB. As noise from other sources at G = 20 dB is about 1 dB in

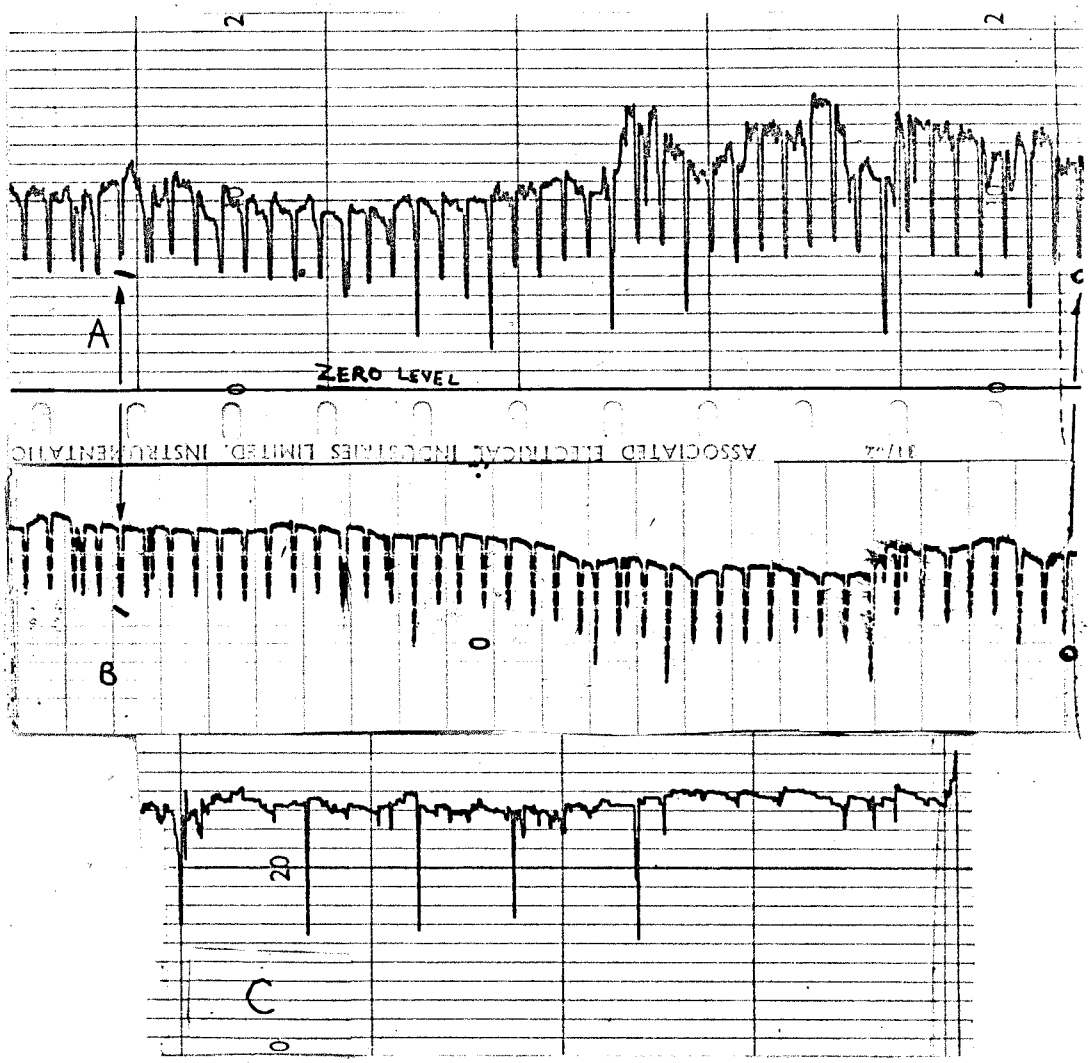

Figure 4.14 The effect of intermittent leaks in the maser chamber on the maser output. A shows the maser output against time and B shows the maser chamber pressure against time during the same period as A. C shows the maser output after several of the leaks had been eliminated.

magnitude the focusser voltage would have to change by 300 volts in order to have any noticeable effect. This meant that the stability of the E.H.T. supply was < 1%.

The quantity of the liquid nitrogen in the focusser did not appear to effect the maser gain except for a short time after the jacket had been refilled. During this period, about two minutes, the gain increased about 2 or 3 dB and then returned to the original value. If ever the quantity of nitrogen became too low in the jacket, then the gain decreased rapidly.

Finally, the changes in source pressure were examined to see if they had any effect on the maser gain. They appeared to have no effect at all. This can be explained by figure 4.6 by the gain contours. As all the gain contours are parallel with the source pressure axis for P_s = 2.25 Torr, the rate of change of maser gain with source pressure is zero.

In general, as long as the noise due to instability was less than the noise due to thermal effects etc., the system was operating satisfactorily.

4.5. Noise Performance

4.5 a) The Measurement of Overall Noise Figure without the Maser.

The overall noise figure describes the complete noise performance of the detecting system. The improvement in noise figure due to the maser gain cannot be evaluated until this overall noise figure has been found. Before the description of the measurement is outlined, some theoretical explanation of which of the many noise figures was measured, will be given. The normal definition of overall noise figure F_o is:-

$$F_o = \frac{\text{Noise power at the output}}{\text{Noise power at the output due to the source alone}}$$

$$= \frac{2G_d\ K\ T\ B + N_d}{G_d\ K\ T\ B} \qquad 4.51$$

where G_d is the overall gain of the detecting system including the conversion loss of the K Band crystal. K is Boltzmann's constant. T is the absolute temperature of the noise source, and B is the bandwidth of the detecting system. N_d is the noise power at the output due to the detecting system alone. N_d includes any noise from the local oscillator. The factor of two in the numerator is due to 'second channel noise'. In most systems of local oscillator and I.F. amplifier there are always unused second channels which contribute noise to the systems.

The noise figure was measured by placing a noise tube at the input to the detecting system. The noise tube was made by Mid-Century Microwave Gear. The noise tube was designed so that when it was

switched off it supplied a noise power of K.T.B. to the detecting system and $(N_e + 1)$ K T B when switched on. N_e is the excess noise figure of the noise tube. The noise output from the detecting system was measured at the output of 30 Mc/s amplifier. This avoided any complications caused by non-linearities in detecting crystals. Any noise contributed by the rest of the circuit can quite reasonably be ignored as the majority of the noise comes from the input stage of the detecting system. This fact was easily verified by measuring the noise output at the output of the second 465 Kc/s amplifier with the 30 Mc/s amplifier off. The noise was measured by a valve voltmeter (Marconi Vacuum Tube Voltmeter). With the noise tube off the output voltage was V_{n1}. When the noise tube was switched on the output voltage was V_{n2}. Now with the noise tube off:-

$$V_{n1}^2 \quad \alpha \quad (2G_d \text{ KTB} + N_d)$$

and with the noise tube on:-

$$V_{n2}^2 \quad \alpha \quad (2G_d \text{ KTB} + 2N_e G_d \text{ KTB} + N_d)$$

if $\frac{V_{n1}}{V_{n2}} = \sigma$ then:-

$$F_o = \frac{2N_e}{\sigma^2 - 1} \qquad 4.52$$

In practice $N_e = 39.1$ and $\sigma = 1.75$ so that $F_o = 38$ or 15.8 dB. Using the Friis[8] formula for overall noise figure:-

$$F_o = F_x + \frac{F_a - 1}{G_x} \qquad 4.53$$

where F_x is the noise figure of the K Band crystal and F_a is the

noise figure of the 30 Mc/s amplifier. G_x is the conversion gain of the crystal. The noise figure of the I.F. amplifier was measured and found to be 1.59 (or 2 dB) (see section 3.3). The makers of the K Band crystal (Microwave Associates) quoted a conversion loss of 7 dB. Using this figure in equation 4.53 gives a crystal noise figure of 33.2 or 15.2 dB. The makers also quoted an overall noise figure of 13 dB. Converting this figure to the system at present (which has second channel noise) the figure becomes 16 dB. This shows that the noise performance is within the normal range of K Band crystals.

4.5 b) Improvement of the Noise Figure by the Maser.

The Maser amplifier contributes a negligible amount of noise to the system. This is because the spontaneous emission ~~caused by collisions in the cavity~~ can largely be neglected. The only noise in the maser is from the thermal noise in the cavity walls. If the K Band circuit had been operated at $4^{o}K$ then the noise figure of the maser would have been significant. The noise temperature of the ammonia maser is normally reckoned to be about $10^{o}K$ [9]. As the system is all at ambient temperature, the thermal noise from the waveguide and cavity etc., is greater than the noise from the molecular beam. The improvement to overall noise figure F_o (see previous section for definition and evaluation of F_o) is a function of the maser gain G'. This function is obtained from the Friis[8] formula:-

$$F_{om} = 1 + \frac{F_o - 1}{G'} \qquad 4.54$$

Where F_{om} is the overall noise figure with the maser operating. In

practice for a maser gain of say, 20 dB, the value of F_{om} would be 1.37. So the improvement in overall noise figure is a factor of 28. However, a more useful measurement of the improvement is obtained when the output signal to noise ratio is considered. If S_n is the signal to noise voltage ratio when the maser is off and S_{nm} when the maser is on, then:-

$$\frac{S_{nm}}{S_n} = \sqrt{\frac{F_o}{F_{om}}} \qquad 4.55$$

Figure 4.15 shows the improvement in signal to noise voltage ratio for various maser gains. The maximum improvement, for very large maser gain, is 6.05 or 15.65 dB. Also in this figure are shown the maximum input power for linear gain and the bandwidth for various maser gains. This figure summarises the main results of this chapter.

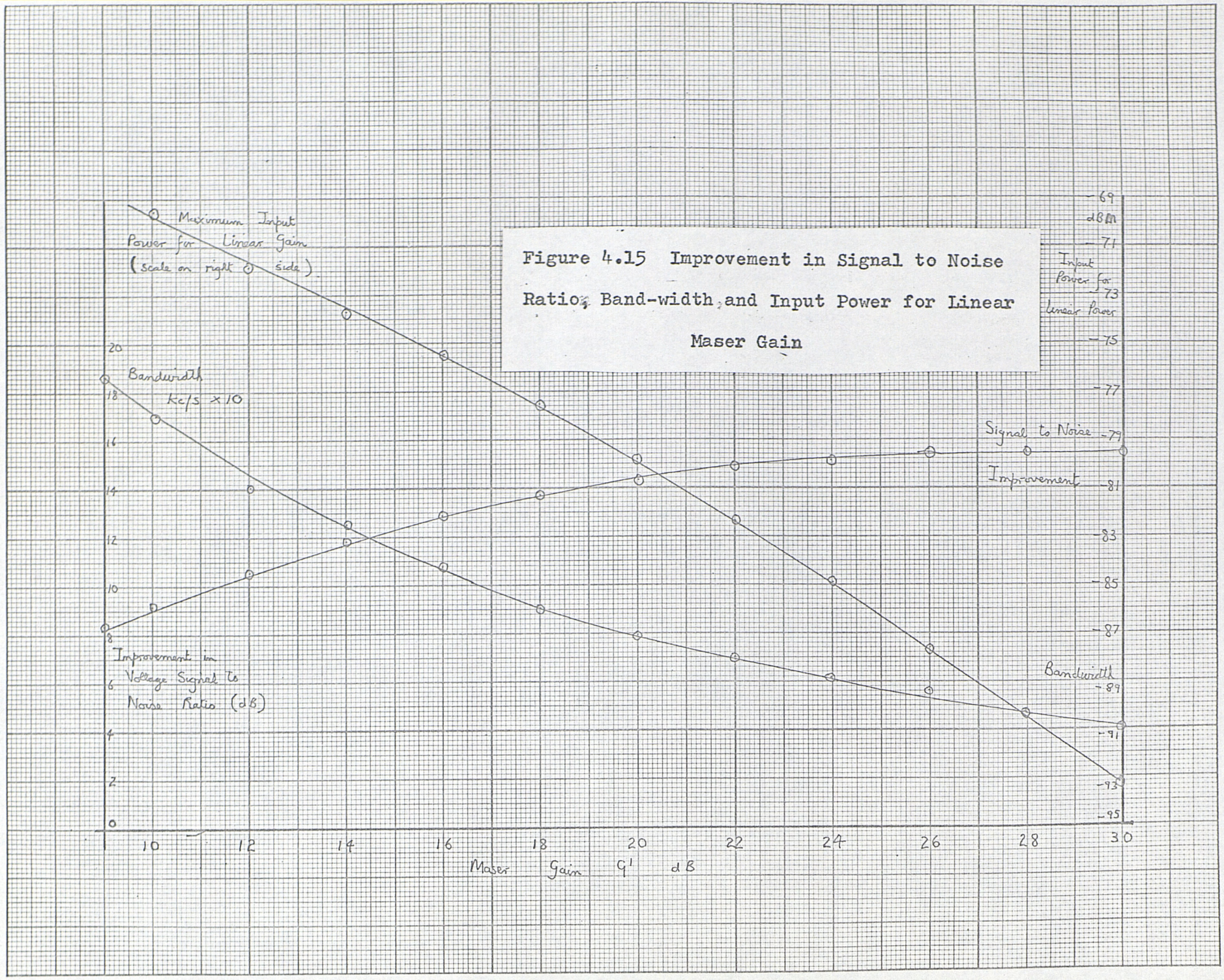

Figure 4.15 Improvement in Signal to Noise Ratio, Band-width, and Input Power for Linear Maser Gain

References Chapter 4

1. F.S. Barnes. "Operating Characteristics of an Ammonia Beam Maser (Oscillator)". Proc. I.R.E., p. 2085, Dec. 1959

2. D.C. Laine. "Investigation of a molecular Oscillator". Ph.D. Thesis, Southampton. page 91 1959

3. K. Shimoda. "Characteristics of the Beam Type Maser II". Jor. of Phys. Soc., Japan. Vol. 13, No. 8, Aug. page 941 1958

4. J.P. Gordon. "Hyperfine Structure in the Inversion Spectrum of $N^{14}H_3$ by a New High-Resolution Microwave Spectrometer". Phys. Rev. Vol. 99, No. 4, August 15 page 1253 1955

5. J. Bonanomi, J. De Prins, J. Herrman and P. Kartaschoff, "Inversion of the NH_3 Magnetic Satellites". Helv. Phys. Acta., Vol. 30, p. 290 1957

6. J. Bonanomi, J. De Prins, J. Herrman and P. Kartaschoff, "Determination of the inversion frequency of Ammonia". Helv. Phys. Acta., Vol. 29, p. 451 1956

7. K. Shimoda. "Characteristics of the Beam Type Maser I". Jor. of Phys. Soc., Japan. Vol. 12, No. 9, Sep. p. 1012. 1957

8. H.F. Friis. "Noise Figure of Several Amplifier Stages connected in Cascade". Proc. I.R.E., Vol. 32, p. 419 1944

9. J.P. Gordon, H.J. Zeiger, C.H. Townes. "The Maser ....." Phys. Rev., Vol. 99, No. 4, August 15 page 1273 1955

Appendix 2

Power Calibration.

The input power to the maser is too small for most power meters to detect, assuming a suitable carrier rejection filter was available. Most power meters at present have an ultimate sensitivity of about 10^{-9} Watts. The only calibrating point available in the maser characteristics is the high gain or verge of oscillation point. It has been found in section 2.4 that at this point about $3.7 \cdot 10^{14}$ molecules a second are entering the cavity in the upper energy level. The available energy from such a set of molecules is about $5.9 \cdot 10^{-9}$ Watts. Thus the maximum power available from the amplifier in the high gain condition is $5.9 \cdot 10^{-9}$ Watts. This maximum power is released when E_m is a maximum. Now numerical calculations for graphs in figure 1.11 showed that the maximum value of E_m was a constant for high gain. The value was $BE_m = 0.95$. This figure was also obtained from figure 1.7 as it is the maximum value of E_m at the point where $\frac{B}{C} = 1$. This leads to a conversion factor for all scales in the form BE_m or BE_1. They are:-

$$\text{Power in Watts} = 6.6\,(BE_1)^2 \cdot 10^{-9}$$

$$BE_1 = 1.23\,(\text{Power in Watts})^{\frac{1}{2}} \cdot 10^{4}$$

These conversion factors have been used to calibrate the input power and the output power of the maser.

Chapter 5

Basic Theory of the K Band E.S.R. Spectrometer

5.1. Introduction

The Basic theory of the E.S.R. Spectrometer is well known and in this chapter it will only be briefly outlined. The main purpose of the theoretical analysis will be to show how the sensitivity of the E.S.R. Spectrometer changes with operating frequency. The definition of sensitivity, that is used, is the normal one of the number of spins per gauss line width that give a signal to noise ratio of unity at the output of the spectrometer. This definition will be considered in terms of the 'double modulation' spectrometer and some modification of the definition will be derived in terms of modulation depth.

The maser amplifier improves the sensitivity by a factor of about 5 and this improvement will be found. The operation of the E.S.R. spectrometer and the maser together required special techniques. A brief theory of the detection of the E.S.R. signal and the three other A.F.C. signals will be given. From this theory the various conditions for optimum sensitivity are derived.

5.2. Electron Spin Resonance Spectroscopy

E.S.R. (Electron Spin Resonance) spectroscopy is a technique for detecting the presence of unpaired electrons in a substance. The technique can provide information about the number of unpaired electrons present in a sample of the substance and some details of the coupling of the electrons to the neighbouring atoms and electrons. The substances which have unpaired electrons can be divided into three groups:-

1) Substances with unpaired electrons in their normal chemical bonds, e.g. paramagnetic salts.
2) Substances in which the normal chemical bonding has been modified so that an unpaired electron is left associated with the system - called free radicals
3) Substances in which the unpaired electrons have been produced by irradiation damage - called radicals produced by irradiation.

When a sample of the substance is placed in a D.C. magnetic field the electronic energy levels are split according to the Zeeman splitting equation. At a temperature T, there will be a population difference between these levels determined by the Boltzmann distribtuion. If the static susceptibility per gm, χ_o, of such a set of unpaired electrons is derived theoretically using these effects the result is[1]:-

$$\chi_o = \frac{1}{3\,KT} \cdot N_o \cdot g^2 \cdot \beta_e^2\, S\,(S+1) \qquad 5.21$$

Where K is Boltzmann's constant, N_o is the number of spins per gm, g is the spectroscopic splitting factor, β_e is the Bohr magnetron for

an electron and S is the spin quantum number for the electrons. This static susceptibility can be measured practically[1] but it is easier to measure the dynamic susceptibility using E.S.R. A relation exists between them. The dynamic susceptibility is per gm χ_m and is:-

$$\chi_m = \chi_m' - j\chi_m'' \qquad 5.22$$

The method for measuring this susceptibility is to place a sample of the substance in a microwave magnetic field and a D.C. magnetic field such that these fields are perpendicular. Zeeman showed that transitions between the split levels will occur when the frequency ω of the microwave field and the amplitude of the D.C. magnetic field H_o are linked by this equation:-

$$H_o = \frac{\hbar \omega}{g \beta_e} \qquad 5.23$$

The technique for measuring these transitions is to keep ω fixed (in practice $\omega = \omega_o$, the ammonia maser centre frequency) and to sweep H_o through the condition of resonance given by equation 5.23. In a similar way to the ammonia transition, equation 5.22 shows that the resonance will have a line-wdith and an absorption and dispersion characteristic. Normally only the absorption curve is detected and the bandwidth is $\Delta \omega_e$. However, the bandwidth is measured in magnetic field as ΔH_e. The conversion is possible using equation 5.23:-

$$\Delta \omega_e = \frac{\omega_o}{H_o} \Delta H_e \qquad 5.24$$

In equation 5.23 the only unknown is 'g'. Since all the other quantities can be measured a value for 'g' can be found. The value

of 'g' can be interpreted as the amount of coupling between the electron and the surrounding atomic structure. For a free electron, $g \sim 2$. g also varies as the D.C. magnetic field is rotated in a plane perpendicular to the microwave magnetic field. g value anisotropy with this rotation can be interpreted in terms of the nature of the electronic orbit.

A simple expression links χ''_m with χ^1_o :-

$$\chi''_m = \chi_o \left(\frac{\omega_o}{\Delta \omega_e} \right) \qquad 5.25$$

$\omega = \omega_o$

For a free electron $S = \frac{1}{2}$ so that from equations 5.21, 5.24 and 5.25

$$\chi''_m = \frac{N_o (\hbar \omega_o)^2}{4 KT H_o \Delta H_e} \qquad 5.26$$

Equation 5.26 shows that if χ''_m is measured the N_o can be found. The sample is placed in a microwave cavity at the point of maximum microwave magnetic field, and the cavity is placed in a D.C. magnetic field. Bloch[2] showed that the spins precess round the D.C. magnetic field at various discrete angles and that transitions only occur when the microwave magnetic field is rotating at the precession frequency (which is ω_o). Any linearly oscillating field can be split into two components rotating in opposite directions. Thus in a normal cavity only half the available microwave field is used in the absorption.

The simplest method of describing how the measurement is made is to use an equivalent circuit for the microwave cavity. In this case a series of L_e and C_e and R_e will be used. The 'Q' factor

for the cavity is then:-

$$Q_e = \frac{\omega_o L_e}{R_e} \qquad 5.27$$

If the magnetic susceptibility is linked with the inductance (the dual of the case in section 1.7) the absorption is equivalent to a series resistance R_s of value:-[3]

$$R_s = \eta_e \chi''_m R_e Q_e \qquad 5.28$$

η_e is the filling factor and is a measure of the coupling of the cavity magnetic field to the sample. The change in the value of Q_e as a result of the absorption is:-

$$\Delta Q = Q_e^2 \eta_e \chi''_m \qquad 5.29$$

Using an expression that will be developed in a later section this change in Q can be detected as an output voltage V_e where:-

$$V_e = \sqrt{\frac{P_e R_o}{16}} \cdot \eta_e \chi''_m Q_e \qquad 5.210$$

Where R_o is the characteristic impedance of the waveguide. P_e is the power entering the system from the klystron. This expression is derived from equation 5.29 and work done by Feher[4]. The limiting factor in any detecting system is noise and the output voltage due to noise V_n is:-

$$V_n = \sqrt{KT \Delta\nu F_{om} R_o} \qquad 5.211$$

where $\Delta\nu$ is the bandwidth of the detecting system and F_{om} is the overall noise figure of the detecting system. For a signal to noise ratio of unity, the minimum detectable susceptibility which can be measured is:-

$$\chi''_{m\ min} = \frac{4}{\eta_e Q_e}\sqrt{\frac{KT\,\Delta\nu\,F_{om}}{P_e}} \qquad 5.212$$

This equation is derived from equations 5.210 and 5.211. It can be seen from this equation that several factors improve the sensitivity. An increase in both Q_e and P_e improve the sensitivity. Using equation 5.26 the minimum number of spins per gm which can be detected is:-

$$N_o = \frac{16\,H_o\,\Delta H_e}{(\hbar\omega_o)^2\,\eta_e\,Q_e}\sqrt{\frac{K^3T^3\Delta\nu\,F_{om}}{P_e}} \qquad 5.213$$

This equation can be simplified if the filling factor is expressed in terms of sample volume. The filling factor η_e is equal to the ratio of the sample volume V_s and the cavity volume V_c multiplied by a parameter F_e which depends on the field distribution in the cavity and the sample:-[4]

$$\eta_e = \frac{V_s}{V_c} \cdot F_e \qquad 5.214$$

Now if ρ_e is the density of the sample, then the mass of the sample is $\rho_e V_s$. Using equation 5.213 and equation 5.214 the minimum number of spins which can be detected for a sample size V_s is:-

$$\rho_e V_s N_o = \frac{16\,H_o\,\Delta H_e\,V_c\,\rho_e}{(\hbar\omega_o)^2\,F_e\,Q_e}\sqrt{\frac{K^3T^3\,\Delta\nu\,F_{om}}{P_e}} \qquad 5.215$$

The sensitivity S_e for a volume V_s is then:-

$$S_e = \frac{\rho_e V_s N_o}{\Delta H_e} = \frac{16\,H_o V_c\,\rho_e}{(\hbar\omega_o)^2\,F_e Q_e}\sqrt{\frac{K^3T^3\,\Delta\nu\,F_{om}}{P_e}} \qquad 5.216$$

For a free electron this becomes:-

$$S_e = \frac{8 V_c \ell_e}{\omega_o Q_e \hbar \beta_e F_e} \sqrt{\frac{K^3 T^3 \Delta\nu F_{om}}{P_e}} \qquad 5.217$$

The function F_e has been shown by Feher[4] to be about 4. Equation 5.216 can be used to show how the sensitivity S_e varies with frequency. There are two ways of considering this variation. The first is to consider a constant sample volume V_s. In any E.S.R. cavity the sample is normally put in a sample tube. The volume of the tube in the cavity is called the maximum active sample volume, V_{max}. Now the cavity volume V_c is a function of ω_o if the same mode of electromagnetic oscillation is maintained in the cavity. The function is $V_c \alpha \omega_o^{-3}$. The 'Q' factor is also a function of ω_o as the skin resistance of the cavity changes. The function is $Q_e \alpha \omega_o^{-\frac{1}{2}}$.

For constant F_e and V_s then:-

$$S_e \alpha \omega_o^{-\frac{7}{2}} \qquad 5.218$$

If the density of unpaired electrons is so low that the sample fills the sample tube $V_s = V_{max}$. If F_e is constant then V_{max} is the same function of frequency as V_c. This changes the definition of sensitivity to one of constant filling factor:-

$$S_e \alpha \omega_o^{-\frac{1}{2}} \qquad 5.219$$

Normally, the second definition is only used for low spin density specimens and high frequencies. Finally, using equation 5.217 and equation 4.54 the improvement in sensitivity with the maser is:-

$$\frac{S_e \text{ (with the maser)}}{S_e \text{ (without the maser)}} = \sqrt{\frac{F_{om}}{F_o}} = \sqrt{\frac{G + F_o - 1}{G F_o}} \qquad 5.220$$

this equation shows that the sensitivity is improved as the maser gain G increases.

All these equations form the basic theory of the sensitivity of most forms of E.S.R. Spectrometer. One further variable which has not been discussed in this section is that of modulation depth. This will be discussed in the next section.

5.3. The E.S.R. Cavity and Matching Arm.

Although this has already been partly described in the previous section, several assumptions made in that section will be verified in this section. Also, the complete E.S.R. microwave circuit will be described. Finally, the theory of the double modulation spectrometer will be given to show how the modulation depth of the D.C. magnetic field effects the definition of sensitivity given in the previous section.

The signals which come from the E.S.R. absorption are usually much smaller than the incident microwave power which stimulates them. In the system used in this work a reflection cavity is used and this will reflect some of the incident microwave power. In order to prevent this reflection swamping the E.S.R. signal some further microwave circuitry is used to remove any reflection. This circuitry consisted of a magic tee and a matching arm (see figure 3.2).

In a similar way to the maser cavity described in section 1.5, the E.S.R. cavity has a 'Q' factor given by equation 5.27. If R_o is the characteristic impedance of the waveguide, then any reflection at the E.S.R. cavity is given by equation 1.51. Using the equivalent circuit of the E.S.R. cavity shown in figure 5.1, the equation 1.54 can be written for the E.S.R. cavity as:-

$$\rho_{r\ (E.S.R.)} = \frac{\alpha' - 1}{\alpha' + 1} \qquad 5.31$$

where $\alpha' = \dfrac{m'^2 R_o}{R_e}$

and R_e is the series resistance of the cavity. Now if P_e is the

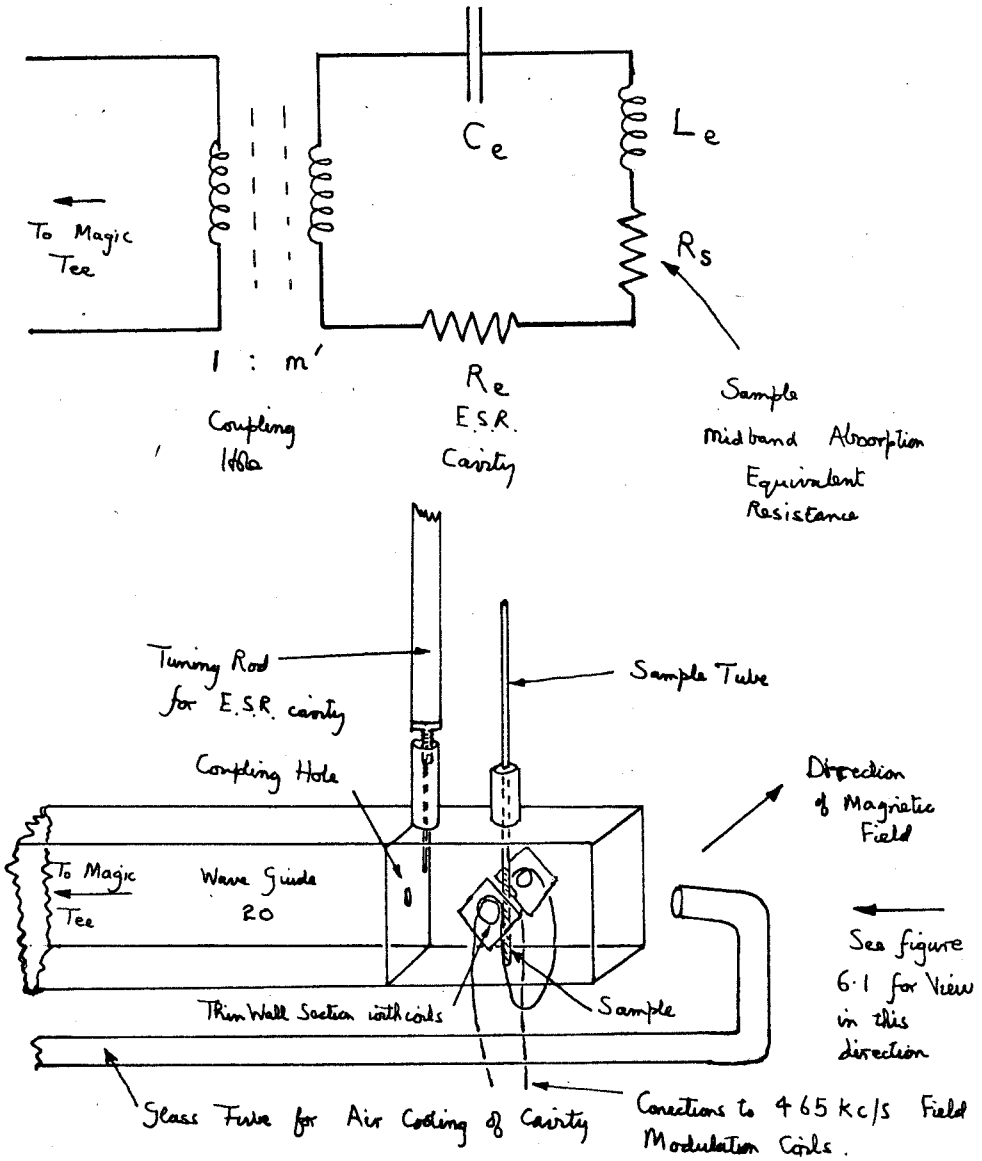

Figure 5.1 The Equivalent Circuit of the E.S.R. Cavity and a block diagram of the cavity showing the various parts discussed in chapters 5 and 6.

power entering the magic tee from the klystron (if matched) then this can be expressed as an input voltage V_o:-

$$V_o = \sqrt{P_e R_o} \qquad 5.32$$

Since this voltage is divided in the ratio 1 : $\frac{1}{\sqrt{2}}$ at the magic tee the voltage incident on the coupling hole of the E.S.R. cavity is $\sqrt{\frac{1}{2}} V_o$. Using equation 5.31, the amplitude of the reflected voltage at the coupling hole is:-

$$\frac{\alpha' - 1}{\alpha' + 1} \quad \frac{V_o}{\sqrt{2}} \qquad 5.33$$

If the absorption at $\omega = \omega_o$ due to the E.S.R. is represented by $\beta' = \frac{R_s}{R_e}$ in a similar way to the maser, then the reflected voltage would be:-

$$\frac{\alpha' - \beta' - 1}{\alpha' + \beta' + 1} \cdot \frac{V_o}{\sqrt{2}} \qquad 5.34$$

The change in reflected voltage can be obtained from equations 5.33 and 5.34 and is:-

$$\Delta V_R = \frac{\sqrt{2}\, V_o\, \alpha'\, \beta'}{(\alpha' + 1)^2} \qquad 5.35$$

This change, ΔV_R, is a maximum with respect to α' for $\alpha' = 1$. This is the condition for the E.S.R. cavity matched to the guide. Using this condition:-

$$\frac{\Delta V_R}{V_o} = \frac{\sqrt{2}\ \beta'}{4} = \frac{R_s}{2\sqrt{2}\, R_e} = \frac{\Delta Q}{2\sqrt{2}\, Q_e} \qquad 5.36$$

And, using equations 5.28 and 5.32 and 5.36, equation 5.210 can be derived:-

$$V_e = \sqrt{\frac{P_e R_o}{16}} \cdot \eta_e \cdot \chi_m'' \cdot Q_e = \frac{\Delta V_R}{\sqrt{2}} \qquad 5.37$$

The above equation was not proved in the previous section.

The remainder of the power coming into the magic tee is largely absorbed in the matching arm (shown in figure 3.2). If the E.S.R. cavity is not perfectly matched then any reflection can be reduced by the appropriate tuning of the matching arm. One disadvantage of this method of reducing reflection is that the reduction is only over a narrow bandwidth. If $\Delta\omega_e$ is the bandwidth of the cavity and R_j is the rejection (or reduction) factor of the matching arm then the bandwidth over which it operates is $\Delta\omega_j$ given by:-

$$\Delta\omega_j = \frac{\Delta\omega_e}{R_j} \qquad 5.38$$

This means that if either the cavity or the matching arm impedance change with ambient temperature, then both the amplitude and phase of the output will also change.

Most E.S.R. spectrometers use a principle of double modulation on the magnetic field. The chief reason for this is that a better sensitivity can be obtained using the system. In the double modulation system, the magnetic field is both swept slowly through the resonance and modulated at a higher frequency. This higher frequency was chosen to be equal to 465 Kc/s in this spectrometer so that the carrier signal frequency was sufficiently far from the maser frequency. This was discussed in section 3.4c. As far as the E.S.R. cavity is concerned, the sidebands at 465 Kc/s lie well within the bandwidth of the cavity. If the modulation of the D.C. magnetic field is small in

comparison to ΔH_e then the output voltage at the sideband frequency will be proportional to the first derivative of the absorption curve. (The next section will show how the absorption and derivative curves are distinguished) The amplitude of the output will be proportional to the amplitude of the modulation put on the D.C. magnetic field. When the modulation is such that the amplitude (kH_o) is just equal to half the line width of the E.S.R., sample ΔH_e then approximately the full sensitivity is available. The definition of sensitivity can now be extended to include double modulation spectrometer using equation 5.217:-

$$S_e = \frac{\Delta H_e}{k H_o} \cdot \frac{4 V_c \rho_e}{\omega_o Q_e \hbar \beta F_e} \sqrt{\frac{K^3 T^3 \Delta\nu F_{om}}{P_e}} \qquad 5.39$$

The signal to noise ratio for the derivative curve is further defined as the ratio of the peak to peak height of the signal to the R.M.S., height of the noise. If the bandwidth of the E.S.R., signal is ΔH_e and the absorption trace output has a height S' at $\omega = \omega_o$ and the peak to peak height of the modulation signal is S'_{mod} then:-

$$S'_{mod} \sim \frac{S'}{\Delta H_e} \qquad 5.310$$

for both Lorentzian or Gaussian lineshapes. Thus if $\Delta H_e = 1$ (which is effectively the condition for the measurement of S_e) the signal to noise ratio is the same for both the types of modulation, so that the equation 5.38 applies to both types. The main advantage of the double modulation is the E.S.R. signal can be distinguished from the K Band carrier signal after detection. A further point worth noting is that the resolution of the spectrometer increases as the modulation

decreases. Thus, in order to resolve hyperfine structure, a reduced sensitivity has to be tolerated. The resolution is approximately proportional to kH_o so that:-

$$S_e \cdot kH_o = \text{constant (using equation 5.39)} \qquad 5.311$$

This equation summarises the overall performance of any double modulation spectrometer.

5.4. The Detecting System.

The detecting system for the E.S.R. signal is made more complicated by the presence of the Maser A.F.C. signal. The object of this section is to show how the two signals are detected and distinguished. This system was first proposed by T.H.W.[5] In order to do this, a more detailed examination of the E.S.R. cavity and matching arm and the maser must be made. For brevity, all amplifier gains and detector conversion ratios have been neglected by using expressions which are proportional to the signals concerned. Also, phase has always been measured relative to the main signal in a group of signals.

The microwave circuit is shown in figure 5.2, and the first point that will be considered is the magic tee which has the E.S.R. cavity on one arm and the matching arm on the other. The signal entering the magic tee from the main klystron has the form:-

$$a_1 \sin(\omega_1 t + \phi)\ (1 + k_1 \sin(\omega_2 t + \phi_1)) \qquad 5.41$$

Where a_1 is the amplitude, ϕ is an arbitrary phase angle, ω_1 is the frequency ($\omega_1 = 2\pi .\ 23.87$ Gc/s in practice), k_1 is the modulation depth of the sidebands put on at the X Band modulator and ω_2 is the frequency of that modulation ($\omega_2 = 2\pi .465$ Kc/s in practice). a_1 corresponds to V_o in equation 5.32. k_1 is changed slightly by the frequency tripler, but this change is unimportant. ϕ_1 is the phase of the modulation signal relative to some fixed phase. When this signal enters the magic tee it is divided equally between the E.S.R., cavity and the matching arm. Both of these components will reflect some of the microwave signal back again to the magic tee. Assuming

Figure 5.2 Block Diagram of the Entire System described in chapters 5 and 6.

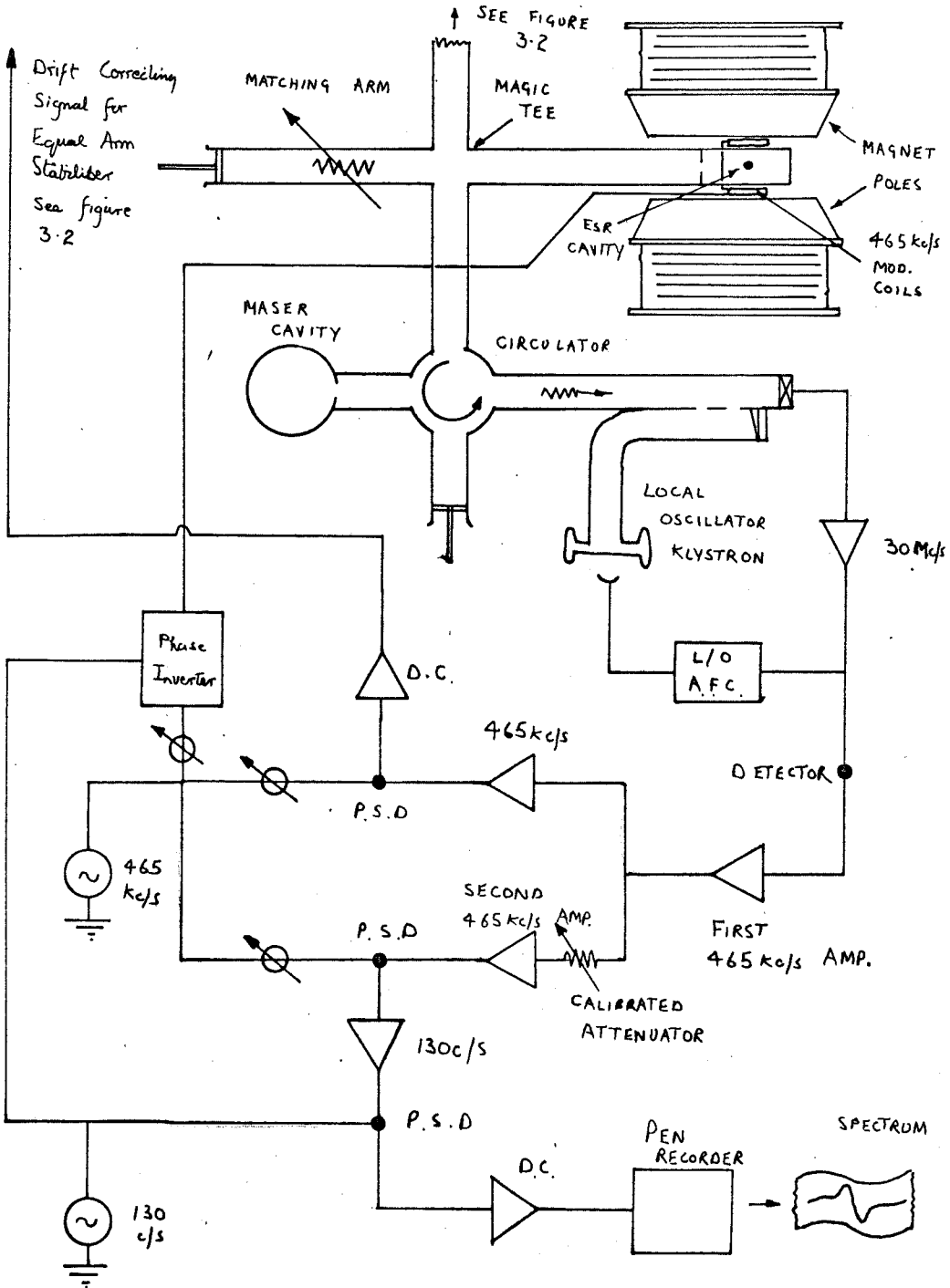

some slight mis-match at the E.S.R. cavity (which is true in practice) then using expression 5.41 the reflection will be of the form:-

$$a_2 \sin\omega_1 t(1 + k_2 \sin(\omega_2 t + \phi_1)) \qquad 5.42$$

Here the phase of the K Band signal has conveniently been assumed zero. The depth of modulation will be changed from k_1 to k_2 as the cavity has a finite bandwidth. Ideally, $a_2 \ll a_1$. The remainder of the signal which is not reflected at the coupling hole is absorbed in the cavity and it stimulates the E.S.R., absorption and dispersion signals. As the K Band carrier is normally much larger than the sidebands (i.e. both k_1 and $k_2 < 1$) then any E.S.R., signal stimulated by them can be neglected. The E.S.R. signals which arrive at the magic tee will be of the form:-

$$b_1(H_o) \sin\omega_1 t + b_2(H_o) \sin(\omega_1 t + \tfrac{\pi}{2}) \qquad 5.43$$

Where $b_1(H_o)$ is the amplitude of the absorption signal and $b_2(H_o)$ is the amplitude of the dispersion signal. As shown by the brackets both these functions are functions of H_o. The absorption signal is normally either a Lorentzian or Gaussian function. The dispersion signal can be obtained from the absorption signal by means of the Kronig-Kramer Relationship - see section 1.7. In the previous section, a double modulation spectrometer was described. The second modulation is put onto the D.C. magnetic field and in this case the frequency of this modulation is ω_2. In order to distinguish this modulation from the A.F.C. modulation a low frequency phase inversion is also added to this magnetic modulation. There will be two further signals arriving at the magic tee as a result of this magnetic modulation:-

$$b_1'(H_o)\ \sin\omega_1 t \cdot f(t) \cdot \sin(\omega_2 t + \phi_2)$$

$$b_2'(H_o)\ \sin(\omega_1 t + \tfrac{\pi}{2}) \cdot f(t) \cdot \sin(\omega_2 t + \phi_2) \qquad 5.44$$

As explained in the previous section, the amplitudes of these signals are the first derivatives with respect to H_o of the signals in expression 5.43. ϕ_2 is the phase of the modulation at ω_2 relative to some fixed phase. f(t) is the phase inverting signal for the modulation:-

$$f(t) = k_3 \cdot \frac{4}{\pi} \left\{ \sin(\omega_3 t) + \frac{1}{3}\sin(3\omega_3 t) + \frac{1}{5}\sin(5\omega_3 t) \ldots\ldots \right\} \qquad 5.45$$

Where k_3 is the modulation depth of the modulation on H_o and ω_3 is the frequency of the phase inversion ($\omega_3 = 2\pi \cdot 130$ c/s in practice). k_3 is proportional to k used in equation 5.39. The only other signal arriving at the magic tee is that reflected at the matching arm. This can be obtained from expression 5.41 and will be of the form:-

$$a_3\sin(\omega_1 t + \phi_3) \cdot (1 + k_1\sin(\omega_2 t + \phi_1) \qquad 5.46$$

Where a_3 is the amplitude of the reflection, ϕ_3 is the phase of the signal relative to the signal in expression 5.42.

All the signals given in expressions 5.42, 5.43, 5.44 and 5.46 recombine in the magic tee to give an output on the fourth arm. Neglecting, for convenience, a factor of 0.7, the output is:-

$$\begin{aligned} &a_2\sin\omega_1 t(1 + k_2\sin(\omega_2 t + \phi_1) \\ &+ a_3\sin(\omega_1 t + \phi_3) \cdot (1 + k_1\sin(\omega_2 t + \phi_1)) \\ &+ b_1(H_o)\sin\omega_1 t \quad + b_2(H_o)\sin(\omega_1 t + \tfrac{\pi}{2}) \\ &+ b_1'(H_o)\sin\omega_1 t \cdot f(t) \cdot \sin(\omega_2 t + \phi_2) \\ &+ b_2'(H_o)\sin(\omega_1 t + \tfrac{\pi}{2}) \cdot f(t) \cdot \sin(\omega_2 t + \phi_2) \qquad 5.47 \end{aligned}$$

In order to obtain the appropriate reduction (or rejection) of the carrier by the matching arm so that the 30 Mc/s amplifier (see figure 5.2) is not saturated the conditions are:-

$$a_2 R_j = (a_2 - a_3) < \sqrt{2}\, a_s$$

$$\phi_3 = \pi \qquad 5.48$$

Where R_j is the rejection factor (see equation 5.38) and a_s is maximum amplitude of carrier signal before the amplifier saturates.

The sidebands are also reduced by a slightly different factor so that the depth of modulation after the magic tee is:-

$$k_4 = \frac{a_2 k_2 - a_3 k_1}{a_2 - a_3} \qquad 5.49$$

All the components at the carrier frequency in expression 5.47 will not be amplified and will pass onto the detector crystal with some attenuation given by equation 1.54. These components are:-

$$a_2 R_j \sin\omega_1 t + b_1(H_o) \sin\omega_1 t + b_2(H_o) \sin(\omega_1 t + \tfrac{\pi}{2}) \qquad 5.410$$

Of the remainder of the components in expression 5.47 only those sidebands at the ammonia frequency will be amplified. In practice ω_o (which is the centre frequency of the maser) is equal to the upper sideband frequency $\omega_1 + \omega_2$. The components at the upper sideband frequency are:-

$$-\tfrac{1}{2} a_2 R_j k_4 \cos(\omega_o t + \phi_1)$$
$$-\tfrac{1}{2} b_1'(H_o) \cos(\omega_o t + \phi_2).f(t)$$
$$-\tfrac{1}{2} b_2'(H_o) \cos(\omega_o t + \phi_2 + \tfrac{\pi}{2}).f(t) \qquad 5.411$$

The maser will amplify the resultant of these three signals. The two requirements are that the A.F.C. signal is not disturbed by the

presence of the E.S.R. signals (i.e. so that the system remains frequency locked during the plotting of a spectrum) and secondly that the maser only amplifies the absorption signal. Both these requirements can be met if these conditions are maintained:-

$$a_2 R_j k_4 > b_1'(H_o) \text{ or } b_2'(H_o)$$
$$\phi_1 = \phi_2 \qquad 5.412$$

The maser has a gain G and a phase angle ϕ_m. This phase is usually quite small.

Using expression 5.411 the output of the maser is:-

$$-\tfrac{1}{2}a_2 R_j k_4 G\cos(\omega_o t + \phi_1 + \phi_m)$$
$$-\tfrac{1}{2}b_1'(H_o)G.f(t).\cos(\omega_o t + \phi_1 + \phi_m) \qquad 5.413$$

At this point the signals arriving at the K Band detecting crystal will be considered (see figure 5.2). In a similar way to the maser the detecting crystal detects the resultant of all the signals arriving from the circuit. As one of the signals is of much greater amplitude than all the others the detector will tend to only detect those signals in phase with this major signal and reject those in quadrature. The carrier frequency components, are attenuated slightly by the maser (in practice by a factor of 0.67) and they are given by expression 5.410. The first term in that expression is by far the largest signal to arrive at the detector. Thus only terms in phase with this signal will be considered. One further point is that the lower sideband term (frequency $\omega_1 - \omega_2$) can be neglected if the maser gain is changed from G to G'. This

change is fully explained in section 4.2 c). The components arriving at the detector in phase with the major signal are:-

$$0.67\ b_1(H_o)\ \sin\omega_1 t$$

$$+\quad a_2 R_j k_4 G'\ \sin\omega_1 t\ .\ \sin(\omega_2 t + \phi_1 + \phi_m)$$

$$+\quad b_1'(H_o).G'.f(t).\sin\omega_1 t.\sin(\omega_2 t + \phi_1 + \phi_m) \qquad 5.414$$

The detected output will be proportional to:-

$$0.67a_2R_j\ +\ 0.67b_1(H_o)\ +\ a_2R_jk_4G'\ \sin(\omega_2 t + \phi_1 + \phi m)$$

$$+\ b_1'(H_o).G'.f(t).\sin(\omega_2 t + \phi_1 + \phi_m) \qquad 5.415$$

The first two terms are the D.C. output of the detector following the 30 Mc/s amplifier (see figure 5.2). This is the normal video spectrometer output and as $a_2R_j > b_1(H_o)$ the former tends to swamp the E.S.R., signal in this type of spectrometer. This is the main reason for using the double modulation spectrometer. The other two terms in expression 5.415 are the maser A.F.C. and the double modulation E.S.R. signals respectively. The entire output of the 30 Mc/s amplifier is after detection passed through two similar 465 Kc/s amplifiers and P.S.D.s in parallel, (see figure 5.2) (P.S.D. = Phase Sensitive Detector) The output of both P.S.D.s is of the form:-

$$b_1'(H_o).G'.f(t).(\phi_1 + \phi_m + \tfrac{\pi}{2} - \phi_j)$$

$$+\ a_2R_j.k_4.G'.(\phi_1 + \phi_m + \tfrac{\pi}{2} - \phi_j) \qquad 5.416$$

where ϕ_j is the phase angle of the reference signal in the P.S.D. relative to some fixed phase. $j = 4$ or 5. In the first P.S.D.

(j = 4), the D.C. component only, is taken to produce the maser A.F.C. signal. The requirement of such a signal is that it is proportional to ϕ_m. This is achieved by the following condition:-

$$\phi_1 + \frac{\pi}{2} = \phi_4 \qquad 5.417$$

The A.F.C. signal is then proportional to:-

$$a_2 R_j . k_4 . G' . \phi_m \qquad 5.418$$

The output of the second P.S.D. (j = 5) is passed through a 130 c/s amplifier and P.S.D. (see figure 5.2). Using expression 5.416 and 5.45 the output will be proportional to:-

$$b_1'(H_o) . G' . k_3 . \frac{4}{\pi} . (\frac{\pi}{2} - \phi_6) . (\phi_1 + \phi_m + \frac{\pi}{2} - \phi_5) \qquad 5.419$$

where ϕ_6 is the reference phase angle of the reference signal relative to the initial phase inversion. The maximum signal is given by the following conditions:-

$$\phi_1 + \phi_m = \phi_5$$

$$\phi_6 = 0 \qquad 5.420$$

the final E.S.R. signal is then:-

$$\alpha \; b_1'(H_o) . G' . k_3 . \pi \qquad 5.421$$

The six phase conditions can be summarised as follows:-

$$\phi_1 = \phi_2 = \phi_4 - \frac{\pi}{2} = \phi_5 - \phi_m$$

$$\phi_3 = \pi \; , \; \phi_6 = 0 \qquad 5.422$$

These conditions are taken from equations 5.48, 5.412, 5.417 and 5.420. The practical details of setting up these conditions and maintaining them while a spectrum is being 'run' will be discussed in the next two chapters.

References Chapter 5

1. D.J.E. Ingram. "Free Radicals as Studied by Electron Spin Resonance". page 30 et seq. 1958

2. F. Bloch. "Nuclear Induction". Phys. Rev. 70 460 1946

3. A.E. Siegman. "Microwave Solid-State Masers". page 263. 1963

4. G. Feher, "Sensitivity Considerations in Microwave Paramagnetic Absorption Techniques". Bell System Tech. J. 36 449 page 454 1957

5. W.A. Gambling and T.H. Wilmshurst. "An Electron Spin Resonance Spectrometer using the Ammonia Maser as a Pre-Amplifier". Vol. 5, No. 4, 15th July 1963 Phys. Letters. page 228

Chapter 6

The Construction of the K Band Spectrometer

6.1. Introduction

The comments made at the beginning of Chapter 2 also apply to this chapter. The object of this chapter is to describe the additional microwave and electrical circuitry required to complete the K Band spectrometer. The majority of the circuitry has already been described in Chapters 2 and 3 as it formed the basis of the measuring circuit for the measurements on the ammonia maser.

The first section deals with the microwave circuit, which includes the E.S.R. cavity and matching arm. In view of the stringent frequency stability required from this circuit a sophisticated stabilising system was used. This is also described briefly.

The second section deals with the D.C. magnet. Some details are given about the power supplies and more details are given about the field stabilisation and sweep.

Finally, the electrical circuits which are used to detect and distinguish the E.S.R. signal from the maser A.F.C. signal are discussed. Also the phase inverter, which supplies the second modulation to the D.C. magnetic field is described. Where possible in this section the method of setting up the five phase conditions described in Chapter 5 section 4 will be discussed.

6.2. The Microwave Circuit.

6.2 a) The E.S.R. Cavity.

The E.S.R. cavity was designed and built by T.H.W. The cavity is shown in figure 6.1. Four features of the cavity will be described in this chapter. They are:-

i) The 'Q' factor and the coupling coefficient.

ii) The 465 Kc/s field modulation.

iii) The position and nature of the sample tube.

iv) The cavity tuning control.

i) The 'Q' factor of the cavity without a sample tube in the cavity was measured and found to be 5,000. With the sample tube present the 'Q' factor was found to be 3,000. This compares with a 'Q' of about 5,000 for an X Band spectrometer cavity with the sample tube in the cavity. Assuming that the 'Q' decreases as $\omega_o^{-\frac{1}{2}}$ (see Chapter 5 section 2) then a typical figure for a K Band spectrometer would be about 2,900. Thus the 'Q' measured is a reasonable figure.

The coupling of the cavity to the waveguide was fixed in this spectrometer. The coupling coefficient α' was equal to 4 when the sample tube was not in the cavity. Ideally, the value of α' should be unity when the sample tube was in the cavity. In practice it was found that the coupling varied from sample tube to sample tube. It would have been a lot easier to set up the microwave circuit if the coupling had been variable. In practice, any reflection due to mismatch had to be compensated for, by the matching arm.

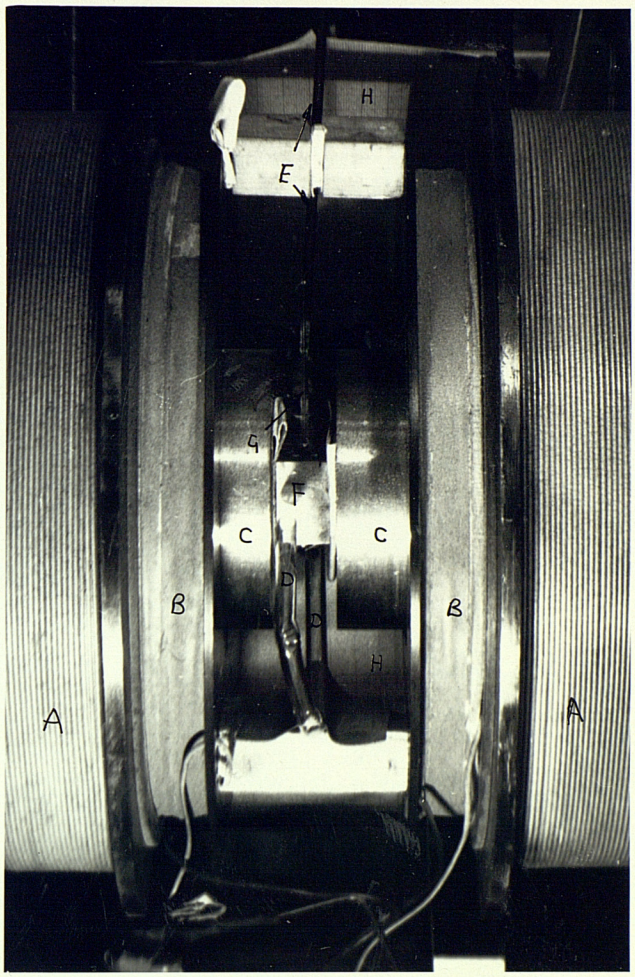

Figure 6.1 The E.S.R. Cavity showing position between the poles of the magnet. A Main Magnetic Coils, B sweep coils (for 50 c/s), C Magnet Pole Pieces, D Glass tube for Air Cooling, E Tuning Rod for E.S.R. Cavity, F E.S.R. Cavity (end wall), G E.S.R. Sample Tube(only top part, not containing sample) H Part of draught shield (the other part had been removed to show the cavity) See also figure 5.1 .

ii) The field modulation at 465 Kc/s was put onto the D.C. magnetic field by a pair of coils either side of the E.S.R. cavity walls. See figure 5.1. The cavity walls were 1 mm thick and the skin depth for electromagnetic radiation at 465 Kc/s is $2. 10^{-2}$ mm. The cavity walls were constructed so that a thin section of wall occurred in the vicinity of the coils (see figure 5.1). This thin section was made by cutting a diamond shaped hole in the cavity wall at the point where the coils would be attached and then covering this hole with some gold leaf (backed by paper for strength) which was only half a thousandth of an inch ($1.27. 10^{-2}$ mm) thick. This allowed the 465 Kc/s modulation to enter the microwave cavity. As the skin depth of electromagnetic radiation is about $3. 10^{-4}$ mm for the K Band signal, there was no leakage of radiation through this thin wall. The diagonal sections were designed so that the field pattern inside the cavity were not interfered with and also the 'Q' factor was unchanged.

As the thin wall was almost the thinnest gold leaf available this puts an upper limit on the frequency of a double modulation E.S.R. The other upper limits being the bandwidth of the E.S.R. cavity and the sample bandwidth.

iii) The sample tubes used were all 1 mm outside diameter and $\frac{1}{2}$ mm inside diameter. A brass tube was fitted on top of the E.S.R., to hold the same tube in place (fitted by the author). As approximately 1 cm of the sample tube was actually in the cavity, the maximum active sample volume is about $2. 10^{-3}$ cm^3. The volume of the cavity is 1 cm^3, so the maximum filling factor (assuming an ideal field configuration) is

$2.\ 10^{-3}$. When the sample tube is only partly filled, by, say, a very small crystal, the ratio of the sample volume to the maximum active sample volume may be as small as 10^{-3}.

The field mode used in the cavity was the H_{012} (TE_{012}) which has a maximum magnetic field along the axis of symmetry of the rectangular cavity. This is the most common mode for this type of spectrometer. The position of the sample was in this axis of symmetry (see figure 5.1).

iv) A method of manually tuning the E.S.R. cavity was used. This consisted of a glass rod which could be screwed in and out of the cavity. This glass rod changed the overall dielectric constant of the cavity medium (which is normally just the sample tube and air) and thus changed the resonant frequency. It did not change the degree of coupling appreciably. The glass rod was $\frac{1}{2}$ mm thick. In practice it was found that the resonant frequency changed very rapidly with the smallest change with the position of the glass rod. Also the rod was slightly eccentric, which made the frequency change, slightly cyclic. Thus the rod provided only a coarse frequency control. A fine tuning control is described in the next section.

6.2 b) The E.S.R. Cavity Temperature Control.

The resonant frequency of the E.S.R. cavity is a function of the temperature of the cavity walls. For a small range the frequency is inversely proportional to the temperature. The temperature of the cavity walls was normally well above ambient temperature, as the D.C. magnet nearby

dissipated about 1 KW of heat into the air. It was found that fluctuations in the cavity temperature caused by draughts etc., were sufficient to detune the E.S.R. cavity. That is, the resonant frequency changed an amount $\Delta\omega_j$ (which is defined in equation 5.38). Once the cavity resonant frequency had drifted this amount the 30 Mc/s I.F. amplifier became saturated and thus distorted any spectrum being plotted.

The first method of controlling this drift was to shield the E.S.R. cavity from draughts. This allowed the magnet to heat up the E.S.R. cavity and the air round it to a steady temperature of about $310^{\circ}K$. This method, although simple, proved surprisingly effective and the effects of the drift were reduced by a factor of about 10.

The second method of controlling the drift was an improvement on the first method. The E.S.R. cavity was shielded as in the first method and in addition a compressed air pipe was placed so that it allowed cold air to blow onto the cavity (see figure 6.1). Some electronic circuitry (which will be described later) was arranged so that this air was allowed to flow only when the cavity was above a certain critical temperature T_c. Where $T_c < 310^{\circ}K$. The action is as follows. The cavity is cooled by the air from $310^{\circ}K$ down to T_c at which point the air is switched off. The thermal time lag of the cavity will cause the temperature of the cavity to overshoot the value T_c and go to a lower temperature. However, the heat from the magnet will soon bring the cavity temperature back up to T_c again at which point the air is switched on again. This time there will be an

overshoot in the opposite direction as air corrects the drift. The optimum condition is reached when the rate of increase in temperature when the air is 'off' is equal to the rate of decrease of temperature when the air is 'on'. When the optimum conditions prevail the time period for the air switched on will be equal to the period 'off'. In practice this time period was about 6 seconds. In general the optimum conditions were achieved by changing the value of T_c. This circuit was thus difficult to set up as the entire E.S.R. microwave circuit and the electronic circuitry had to be tuned. Once it had all been tuned, the circuit worked quite well. The system eventually failed because the matching arm also changed with ambient temperature and in the present work there was no method of controlling these changes as well. In practice, it was found that the cavity had to be switched on for at least two hours before any stability was possible.

The electronic circuitry required to operate the air valve (made by Ether Ltd.) which controlled the compressed air flow was almost a complete A.F.C. system operating at 100 Kc/s. As several similar systems have already been described in this thesis so far, this system will be only briefly described. Two small 100 Kc/s frequency modulation sidebands were put onto the K Band signal. This was done by some amplitude modulation on the reflector of the main klystron (see figure 3.1), at 100 Kc/s. These sidebands did not interfere with any of the E.S.R. or maser circuitry to any noticeable extent (see figure 3.8). The sidebands were detected first by the mixer crystal and 30 Mc/s amplifier in the normal way. After further detection at the output,

the sidebands were amplified in a 100 Kc/s selective amplifier, followed by a P.S.D.

Now the rate of change of phase at the point where the E.S.R. microwave circuit is correctly tuned is equal to $(\Delta\omega_j)^{-1}$ (see equation 5.38) so that the phase changes rapidly $(\frac{\pi}{2})$ in the region $|\Delta\omega| \ll \Delta\omega_j$. This phase change produces a change in the voltage output of the P.S.D. Now as the phase change is proportional to the change in the resonant frequency of the E.S.R. cavity and hence inversely proportional to the cavity temperature, the voltage output of the P.S.D., can, with suitable phasing, be made inversely proportional to the temperature. In practice, the system was adjusted so that as the cavity temperature increased the output voltage of the P.S.D. decreased. The P.S.D. was connected to a transistor controlled relay which in turn operated the air valve. As soon as the output voltage of the P.S.D. went negative the air valve was switched on, which allowed air to flow onto the cavity.

Most of the 100 Kc/s A.F.C. system was built by T.H.W., and the remainder of the system and also the air control system were built by the author. The entire circuit is shown in figure 6.2.

6.2 c) The E.S.R. Bridge.

The E.S.R. Bridge consisted of a magic tee and the E.S.R. cavity and the matching arm. This is shown in figure 5.2. All these bridge components were made at Southampton University. The E.S.R. bridge (or microwave circuit) was designed to reject the K Band carrier signal reflected from the cavity. The matching arm consisted of an

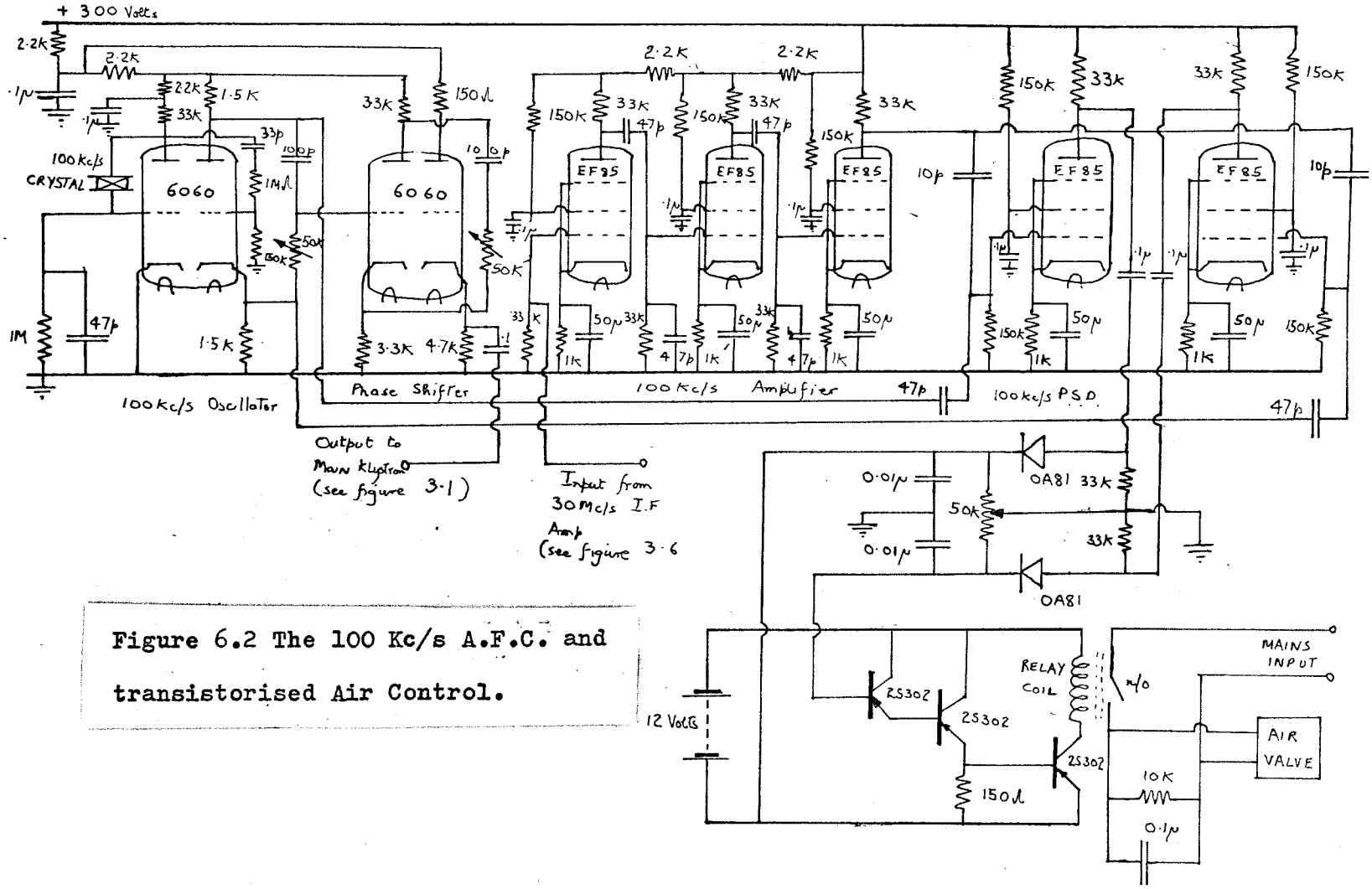

Figure 6.2 The 100 Kc/s A.F.C. and transistorised Air Control.

attenuator and a short circuit. The attenuator was capable of absorbing most of the signal entering the matching arm and the short circuit reflected the remainder of the signal at the right phase to reject the K Band carrier. It was shown in Chapter 5 section 3 that the setting of the matching arm determines the value of R_j, the rejection factor. It was also shown in Chapter 5 section 4 that the phase of the reflected signal is quite critical if the phase is measured relative to the phase of the reflection from the E.S.R. cavity. Equation 5.48 dictates that this phase (ϕ_3) must be equal to π. It was found in practice that this condition could be achieved, but both the attenuator and the short circuit were difficult to adjust. This was due to the coarseness of the screw threads in both these controls. A metal flange was fitted to the attenuator, by the author, to reduce play in the control. This greatly improved the adjustment.

Although most of the drift was due to changes in the cavity temperature, it was found that when that drift was compensated for (see last section) the system still drifted slightly. This drift was caused by changes in the temperature of the components in the matching arm. Fortunately, this drift was much less than the cavity drift and it could be tolerated during the plotting of a spectrum. It did mean, however, that the whole system needed retuning quite regularly.

The magic tee was used in a configuration which provided the best practical isolation between the incoming signal from the klystron and the outgoing signal to the detector. This was achieved by putting the incoming signal into the 'E' arm of the magic tee and taking the

signal for detection from the 'H' arm. Any leakage was removed by appropriate matching arm adjustment. In practice it was found that this leakage was sufficiently small to be neglected. The leakage was measured by putting matched loads in place of the matching arm and E.S.R. cavity, and measuring the output.

Finally, the rejection factor R_j was measured and found to be 33 dB (or 45 as a voltage ratio). It was also found that the reflected signal from the E.S.R. cavity was, for most samples, about 10 dB smaller than the incident signals. Thus the total rejection of the E.S.R. bridge was 43 dB, (or 140 as a voltage ratio). In terms of power, the incident power (if the E.S.R. cavity were matched) would be $1. 10^{-3}$ Watts. The figure of 10 dB measured suggests that α' was equal to 1.9. This could have been less if the coupling hole could have been adjusted - but as the value was very dependent on the nature of the sample, this mismatch was tolerated. If the cavity had been matched the power dissipated in the bridge would have been 2 mW. The mismatch caused slightly less power to be absorbed in the E.S.R. cavity. The value of α' was measured as follows. The matching arm was matched to the guide and the E.S.R. cavity was detuned (i.e. a short circuit). In this configuration the E.S.R. Bridge dissipates 1 mW and transmits 0.5 mW to the detector. Using the calibrated attenuator at the input to the E.S.R. bridge the transmitted power with the cavity tuned was observed to be 7 dB below this power. This gives a figure for α' of 1.9. Using the same calibrated attenuator the rejection factor of the bridge was found to be 33 dB as the transmitted power was 40 dB below

0.5 mW. The generator power when the bridge is tuned is then 2 mW (this is P_e in equation 5.210). In a similar way to the measurement of klystron drift (described in section 4.4 a)) the value of the bandwidth $\Delta \omega_j$ (see equation 5.38) was also measured and found to be equal to 105 Kc/s.

6.3. The Magnet Power Supplies and the Field Stabilisation and Sweep Controls.

The magnet used was a Newport 4" Pole magnet. The power supplies were also made by Newport. The pole gap was about 1". Although much higher fields are required in spectrometers with higher operating frequencies, this can often be achieved with the same type of magnet. This is because, as the frequency increases, the size of the E.S.R., cavity decreases and so the pole gap can also be decreased, and thus the maximum field of the magnet is increased.

It was found that the degree of field stability given by the commercial stabiliser was insufficient for this spectrometer. It can be seen that greater stability is required for these higher fields if the same resolution as, say, the X Band spectrometer is to be maintained. A modification of the commercial stabiliser was made by T.H.W. A circuit diagram is shown in figure 6.3. This stabiliser was basically a current stabiliser. This assumes that the current is proportional to the field under all conditions. (A more sophisticated type of stabiliser is to use a proton resonance, of Hall effect probe) In order to improve the high frequency response of the circuit a second feedback stabiliser was used for A.C. instability. The stabiliser also provided the means for a slow sweep to be put onto the magnetic field. The method of calibration is given in the next chapter.

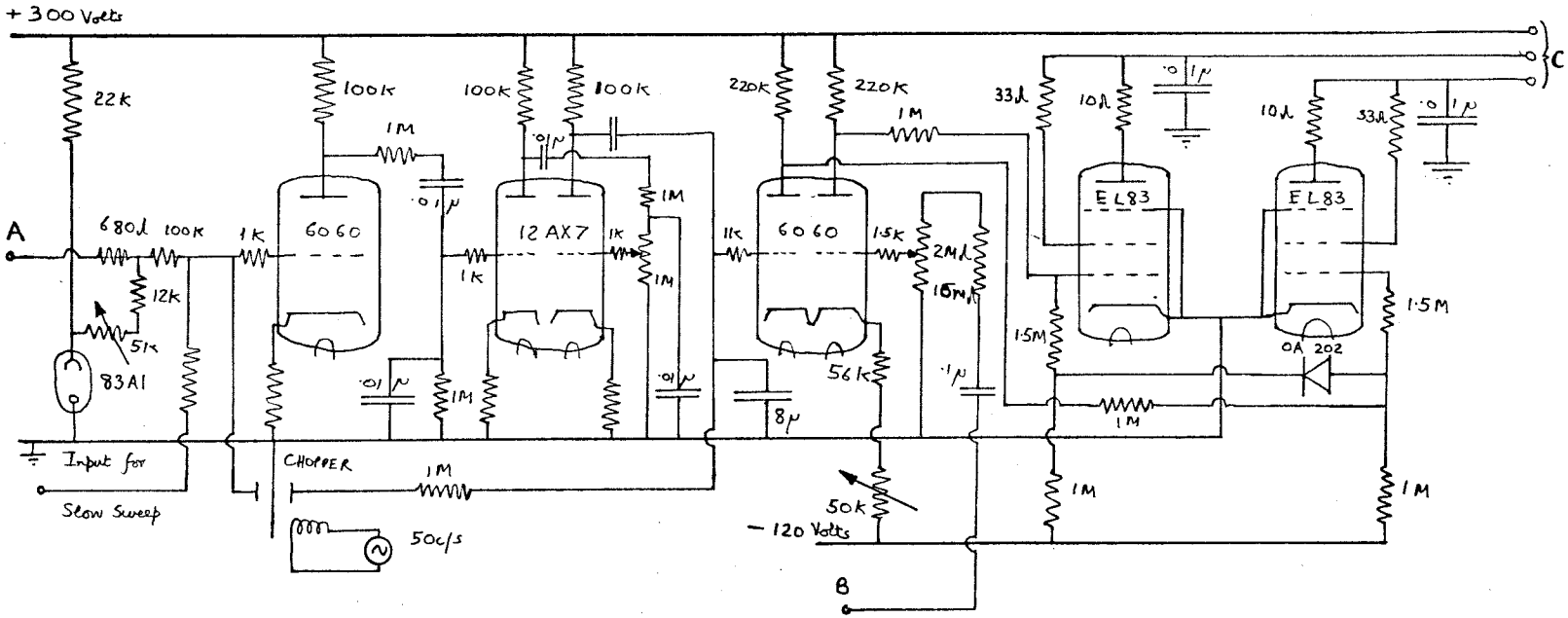

Figure 6.3 The Magnet Stabilisation Control

A Input for a Voltage proportional to the Magnet Current (from Power Supply)

B Input for a Voltage proportional to the Magnet Voltage (from Power Supply)

C Output to Magnetic Amplifier Control Circuit in Magnet Power Supply.

6.4. The Electrical Circuitry.

6.4 a) The 130 c/s Detection System.

In Chapter 5 and in the paper by T.H.W.[2], the method of detection is outlined. In Chapter 5, the five phase conditions for the detection of the E.S.R. signal are given. Only one of these conditions is concerned with the 130 c/s detection system. The 130 c/s detection system is fed from the output of the P.S.D. at the output of the second 465 Kc/s amplifier (see figure 5.2). The first part of the detecting system consisted of a 130 c/s selective amplifier which was originally built by T.H.W., but was later modified by the author using a bridged tee network as the selective circuit. The circuit diagram is shown in figure 6.4. The output of this amplifier was then passed through a transistorised 130 c/s P.S.D. The circuit diagram for the P.S.D. is also shown in figure 6.4. Finally, the output of the P.S.D. was passed through a D.C. amplifier and then via a low pass filter to a pen recorder, (made by Elliot). This D.C. amplifier was built by the author. A method of measuring the time constant of the filter at the output of the amplifier is given in the next chapter. This time constant is inversely proportional to the detector bandwidth $\Delta\nu$ (given in equation 5.211). The circuit diagram of the amplifier is given in figure 6.4.

The reference signal supplying the 130 c/s P.S.D. did not have a phase changing circuit in series with its supply. A special technique was devised for the setting up of the system. The technique also used the second 465 Kc/s amplifier and P.S.D. but it did not set

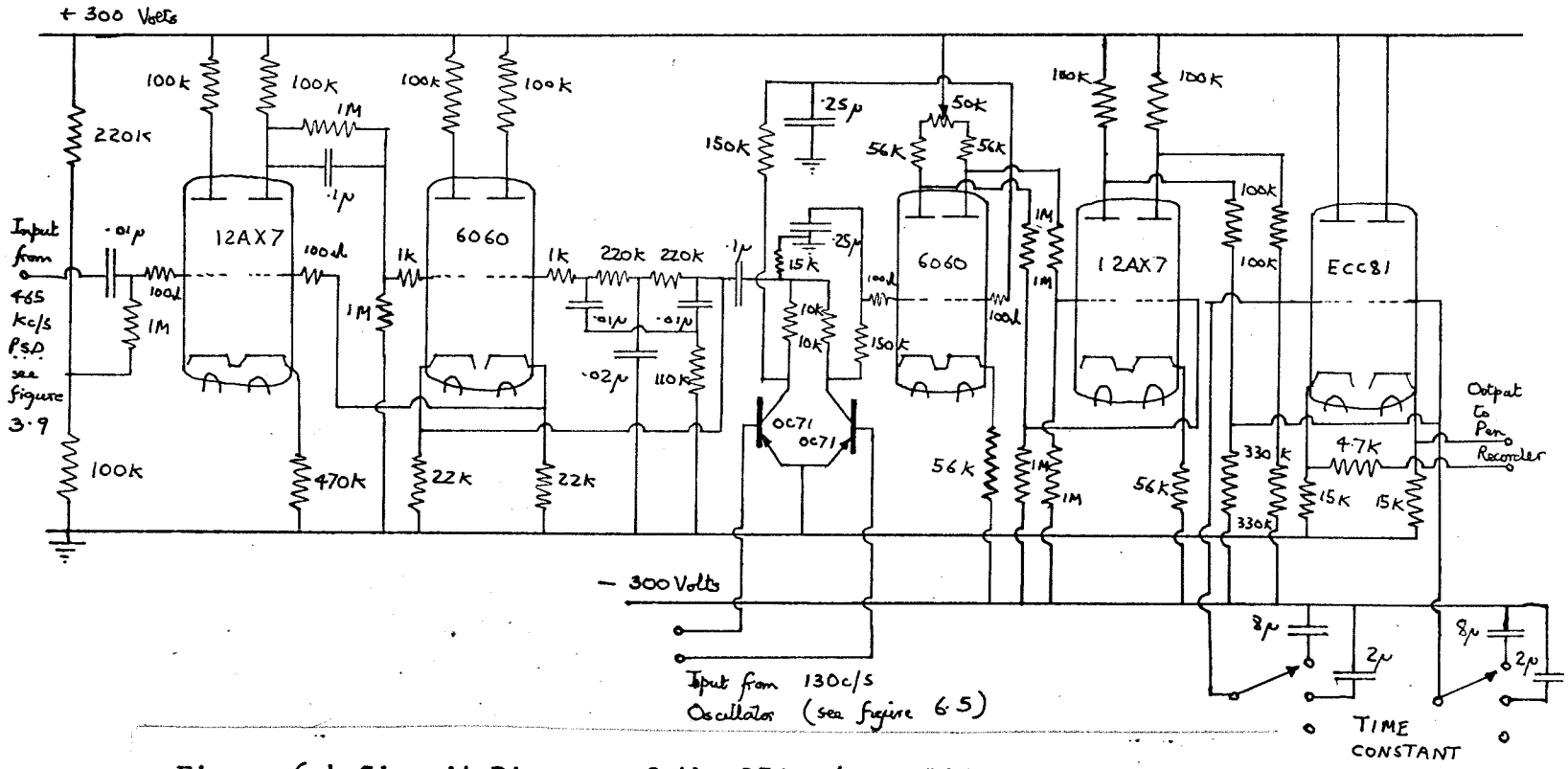

Figure 6.4 Circuit Diagram of the 130 c/s Amplifier and P.S.D.

and the D.C. coupled Amplifier supplying the Pen Recorder

up the correct conditions for that P.S.D. In Chapter 5 the phase condition for the 130 c/s detection system is given as $\phi_6 = 0$. This implies that the output of the system must be a maximum. It can be assumed that the phase shift in the 130 c/s modulation between the output of the 465 Kc/s phase inverter, right through the system, to the output of the P.S.D. following the second 465 Kc/s amplifier is either 0 or π. With this assumption, a small fraction of the output was taken from the output of the phase inverter and taken direct to the input of the second 465 Kc/s amplifier. The 130 c/s detection system could then easily be set up as follows. Both the 465 Kc/s phase inverter and the 130 c/s P.S.D. were supplied from the same oscillator (built by T.H.W. and modified by the author and shown in figure 6.5). If the frequency of this oscillator was changed slightly, the only signal which changed in phase appreciably was that signal going through the selective amplifier. Thus the frequency control (shown in figure 6.5) became, for a small range, the phase shifter for the reference signal to the 130 c/s P.S.D. The frequency control was adjusted so that the output from the 130 c/s detection system, as measured on the pen recorder, was a maximum. This method satisfied the condition $\phi_6 = 0$.

6.4 b) The 465 Kc/s Phase Inverter.

This phase inverter is shown in figure 6.5. The phase inverter consisted of two transistors which switched two 465 Kc/s signals, in antiphase, alternately. The sum of the two outputs from the transistor switches was a 465 Kc/s signal which changed in phase

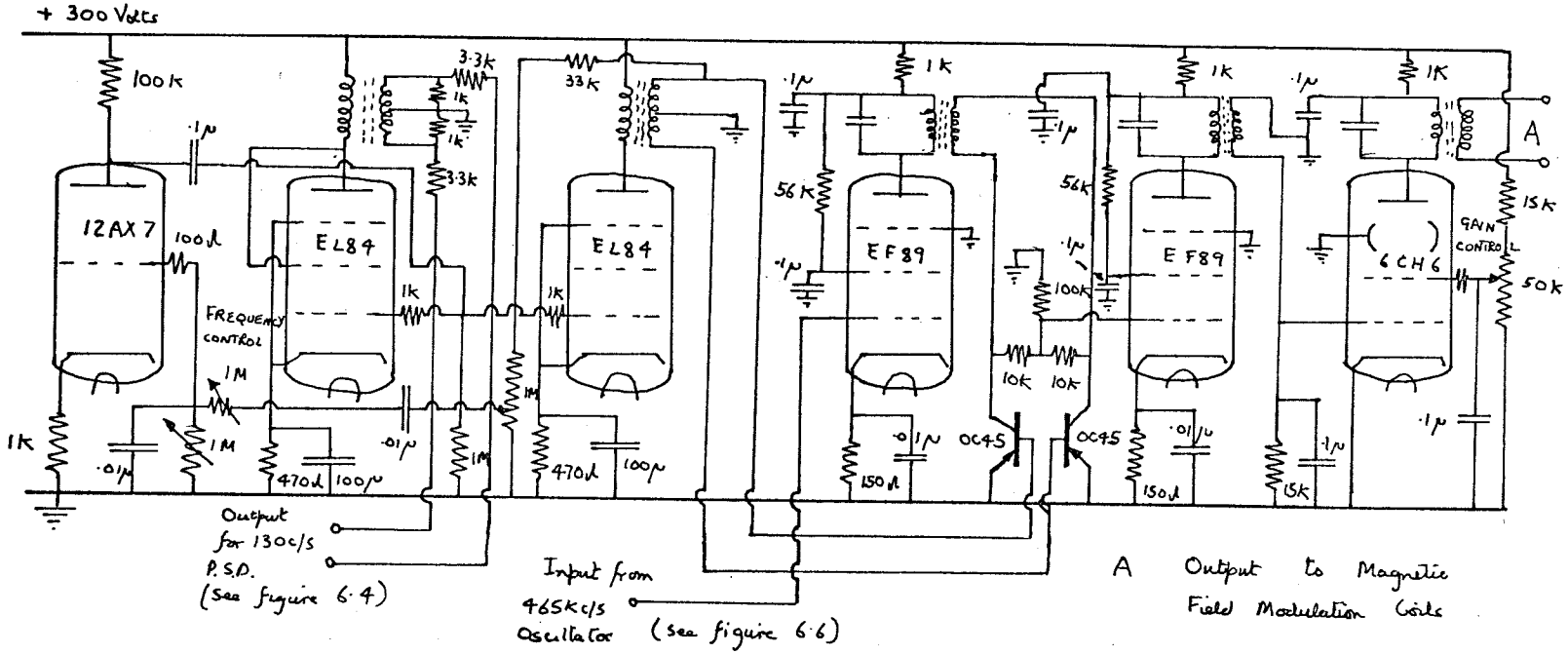

Figure 6.5 The Circuit Diagram of the 130 c/s Oscillator and the 465 Kc/s Phase Inverter.

by π at a frequency of 130 c/s. The phase inverter was driven by a 130 c/s oscillator (shown in figure 6.4). The output of the phase inverter was fed to a power amplifier which supplied sufficient power to modulate the D.C. magnetic field in the E.S.R. cavity. A gain control was fitted in the power amplifier so that the depth of modulation k could be adjusted (see equation 5.39 for a definition of k). This gain control also introduced a variable phase shift as it was adjusted so that for each setting of modulation depth the phase conditions had to be set up again. However, this would only be the phase conditions involving ϕ_2 and ϕ_5 (see equation 5.422).

The 465 Kc/s oscillator (shown in figure 6.6) was built by T.H.W. The oscillator had four outputs, three of them with phase changing circuits (range 0 - 2π) in series with their outputs. The output without the phase changing circuit was used to supply the X Band modulator and thus the phase of this output is ϕ_1 (see equation 5.41). One of the other outputs was used to supply the 465 Kc/s phase inverter. The phase changing circuit in this supply was used to set up the condition $\phi_1 = \phi_2$ (see equation 5.412). Another of the outputs was used to supply the P.S.D. following the second 465 Kc/s amplifier. The phase changing circuit is this supply was used to set up the condition $\phi_1 = \phi_5 - \phi_m$ (see equation 5.420). Finally, the last output was used to supply the P.S.D. in the maser A.F.C. circuit. The phase changing circuit in this supply was used to set up the condition $\phi_1 = \phi_4 - \frac{\pi}{2}$ (see equation 5.417). The practical details of how these conditions were set up are given in the next chapter.

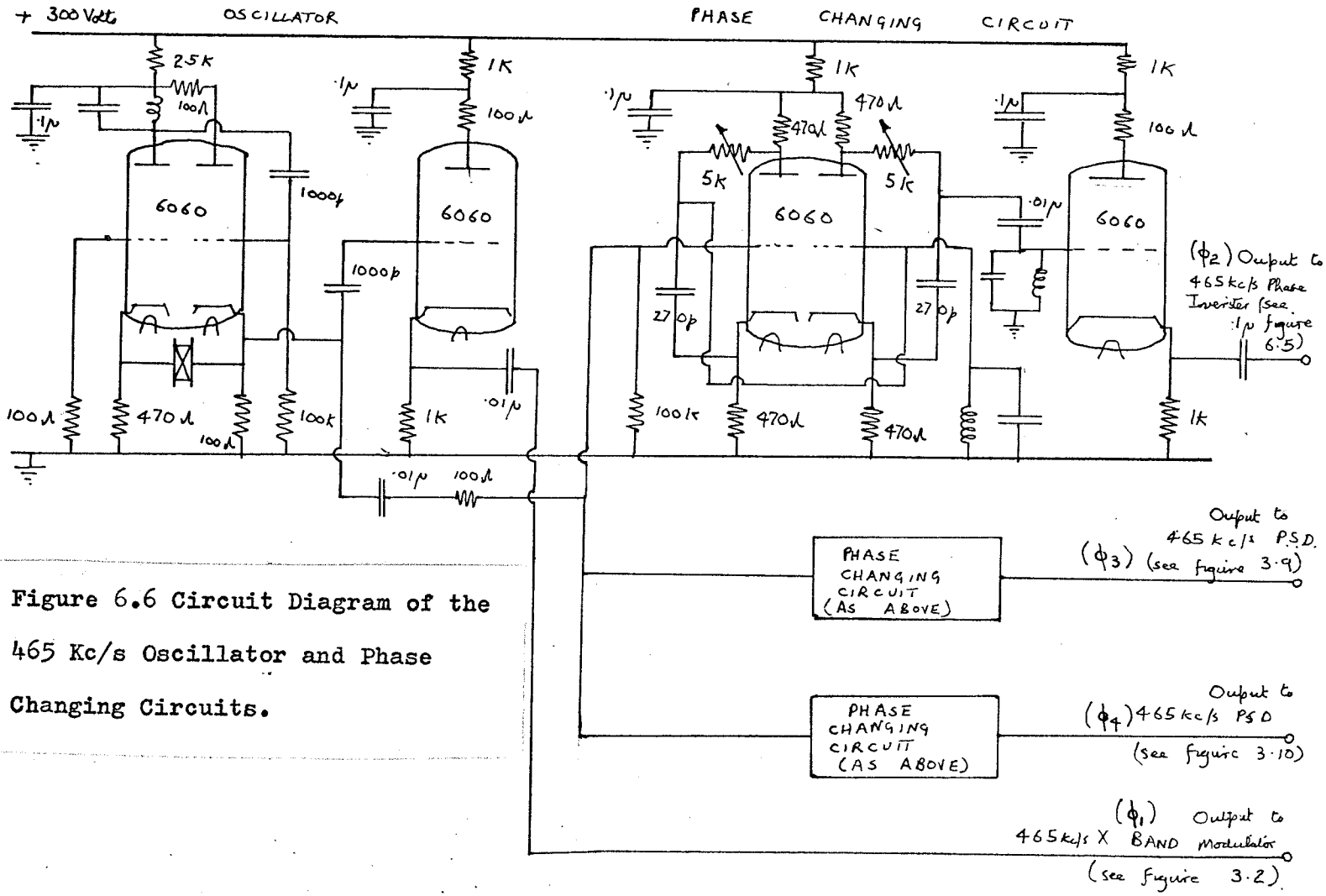

Figure 6.6 Circuit Diagram of the 465 Kc/s Oscillator and Phase Changing Circuits.

References Chapter 6

1. D.J.E. Ingram. "Free Radicals as studied by Electron Spin Resonance". page 49 1958

2. W.A. Gambling and T.H. Wilmshurst. "An Electron Spin Resonance Spectrometer using an Ammonia Maser as a Pre-amplifier".
Vol. 5, No. 4, 15th July Phys. Letters page 228 1963

Chapter 7

Sensitivity and Stability Measurements on Amplified E.S.R. Spectra

7.1. Introduction.

The objects of this chapter are first to give all the details of the calibration and setting up procedure which were required before any sensitivity measurement could be made. These calibrations included the field sweep of the magnetic field, the modulation depth of the magnetic field and the signal level of the maser A.F.C. The next object of this chapter is to show the improvement in signal to noise factor made by the maser. This measurement, linked with a measurement on sensitivity made it possible to estimate the overall sensitivity. This was compared with the sensitivity of other spectrometers. Finally, the last object of the chapter is to examine the stability of the entire system.

7.2. Determination of the Optimum Conditions for Operating the Spectrometer.

7.2 a) Determination of the Maser Gain required.

The maser gain can be measured from the E.S.R. spectra, by running the spectrometer with the maser switched 'on' and 'off'. The maser was switched off by disconnecting the maser A.F.C. and slightly detuning the equal arm stabiliser. With maser off, the E.S.R. spectrum of a sample could be traced out on the pen recorder by slowly varying the D.C. magnetic field. It was possible to keep the magnetic field constant so that the trace was at the 'top' of one of the E.S.R. spectrum peaks. As it was a derivative curve there were two such peaks. If the maser was then switched on by reversing the procedure described earlier in this paragraph, this peak was amplified. To achieve the maximum amplification the various phase conditions had to be set up (see section 7.2 c)). In order to get the trace on the pen recorder output, the attenuator between the first and second 465 Kc/s amplifiers had to be adjusted. After each adjustment, the various phase conditions had to be set up again, as the attenuator introduced a phase change. The maser gain could then be calculated from the trace heights and the change in attenuator value.

By increasing the level of either the maser A.F.C. signal or the E.S.R. signal the maser could be made to saturate. This could be detected by measuring the maser gain by the method described above and the focusser voltage V. Using figure 4.6, the unsaturated gain could be found for the value of focusser voltage measured and if this

was greater than the gain actually measured, then the maser was saturating.

As the maser itself tends to be unstable at very high gains, the actual gain used was normally in the region of 20 dB. This was a reasonable value for two other reasons. Figure 4.15 shows that, above this value of gain, the improvement in signal to noise ratio is small but the value of the input power required to saturate the maser rapidly decreases. So, in order to get a reasonable working range for the maser and an improvement of signal to noise near the theoretical maximum a value of gain of about 20 dB was used.

7.2 b) Determination of the Maser A.F.C. Signal Level required.

The maser amplifier could be saturated by the maser A.F.C. signal so that the E.S.R. signal was not amplified. On the other hand, sufficient A.F.C. signal was required to give a tolerable signal to noise ratio in the A.F.C. circuit. If P_s is the input power to the maser amplifier which just saturates the maser, then a convenient A.F.C. signal level was $\frac{1}{2}P_s$. This satisfied the first of the conditions in equation 5.412. The A.F.C. level could be changed using the calibrated attenuator at the input to the X Band modulator. The method of setting up the correct level was as follows. The system was set up of the peak of an E.S.R. spectrum with the maser on. (See previous section for method of setting up) The A.F.C. level was then changed and the various outputs of the E.S.R. spectrum were examined

for both signal and noise level. As the attenuator feeding the X Band modulator introduced phase change as it was altered, the various phase conditions had to be set up for each A.F.C. level. (See next section for the method of setting up the phase conditions) The result of the measurement is shown in figure 7.1.

It can be seen in figure 7.1 that for high signal levels the output of the E.S.R. spectrometer is reduced as the maser is saturated. Another sign of saturation was that the background thermal noise level was also reduced. For A.F.C. signal levels within a certain range the output level is almost constant and so is the noise level. Below this range of values, i.e. for small A.F.C. levels, the output level falls to zero. This is because the signal to noise level in the maser A.F.C. loop has become so small that the system is trying to stabilise on noise. As a result, the average gain of the maser is less. The noise level of the output was also increased as system was unstable. This was not because it is about to oscillate but because it was about to lose the locking condition.

Finally, it is worth noting that the effect of the E.S.R. bridge on the modulation depth of the A.F.C. signal was to increase it by about 10 - 15 dB. This effect was predicted by equation 5.49 where k_4 is the modulation depth of the A.F.C. signal entering the maser. As $k_2 > k_1$ then $k_4 > k_2 > k_1$ for large values of R_j. For each value of R_j the A.F.C. level had to be measured again.

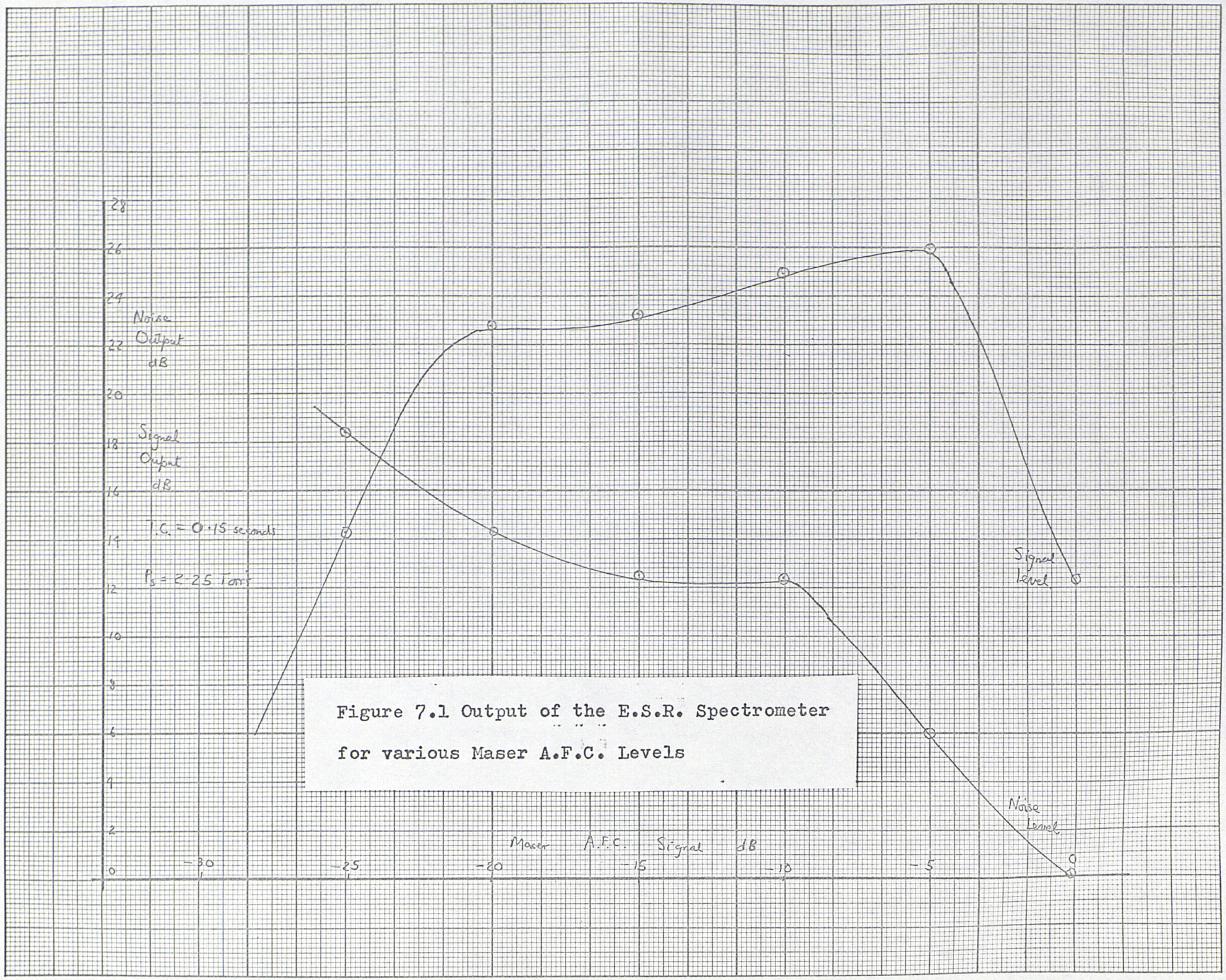

Figure 7.1 Output of the E.S.R. Spectrometer for various Maser A.F.C. Levels

7.2 c) Setting up the Five Phase Conditions.

The method used to set up one of the five phase conditions has already been described. In section 6.4 a) the method of setting up the condition $\phi_6 = 0$ was discussed. In section 6.2 c) the various circuit components used to set up the condition $\phi_3 = \pi$ were described. This condition was set up as follows. The E.S.R. cavity was tuned so that the D.C. output of the detector immediately following the 30 Mc/s amplifier was a minimum. Then the matching arm was adjusted so that the output was about 1.7 volts. In practice this voltage corresponded to an input signal power to the K Band crystal of about 10^{-7} Watts. This was the required signal level.

In section 6.4 b) the various phase changing circuits which were used to change the values of ϕ_2, ϕ_5 and ϕ_4 were described. The maser A.F.C. condition (see equation 5.417) will be discussed first. The output of the D.C. amplifier in the maser A.F.C. circuit was displayed on an oscilloscope. In general, this output (displayed against frequency) was the dispersion characteristic mixed with the emission characteristic for the ammonia maser (see section 1.7 and figure 1.8). The correct output was obtained by adjusting ϕ_4 so that the dispersion characteristic only was displayed. In order to achieve the A.F.C. locking condition it was found that the dispersion characteristic with a positive, rather than negative, slope in the centre portion was the correct output. Once this output had been obtained the A.F.C. could be locked on in the usual way. (See section

3.3 c)) The A.F.C. was found to operate quite satisfactorily, despite thermal drift in the E.S.R. cavity, which changed ϕ_3 and thus effected the dispersion shape. (See equation 5.48)

The E.S.R. conditions were more difficult to set up as they were dependent on more variables. These conditions are given in equation 5.422. They were more difficult because they were implicit functions of ϕ_3 and explicit functions of ϕ_m and both these phases were subject to drift. The phase ϕ_3 was subject to drift caused by the thermal drift in the E.S.R. cavity. The phase ϕ_m was subject to drift in the maser cavity and to drift in the main klystron frequency. The method of setting was as follows. The maser was switched off and the magnetic field adjusted to give a peak of the spectrum on the output trace. (See section 7.2 a) for the method for this) In practice the sample used was a carbon one as this had a line width of about 10 gauss and thus a reasonable spectrum could be traced (i.e. not too cramped or too broad) within the limits of the stability of the magnetic field stabiliser. The maser was then switched on and the phase changing circuits appropriate to ϕ_2 and ϕ_5 were adjusted to give the maximum output. These phase changing circuits were described in section 6.4 b). It was assumed that the small frequency change incurred in switching the maser on did not upset the condition $\phi_3 = \pi$. At this point all five conditions were set up. Drift in the maser phase ϕ_m did not effect the E.S.R. spectrum to a great extent. The major cause of phase drift was the term ϕ_3. Drift in the 130 c/s signal was also small.

7.2 d) Determination of the Field Modulation Depth.

The modulation depth was controlled by a gain control in the power amplifier energising the 465 Kc/s modulation coils round the E.S.R. cavity. This was described in section 6.4 b). Now the modulation required for the maximum sensitivity (without distortion) is given in equation 5.39. In that section it was shown that:-

$$S_e \propto \frac{\Delta H_e}{2 k H_o} \qquad 7.21$$

The maximum sensitivity was available when $\Delta H_e = 2kH_o$, where ΔH_e is the magnetic line width of the E.S.R. spectrum and kH_o is the modulation depth k times the D.C. magnetic field H_o. the possible range of values for k is thus:-

$$0 \leqslant k \leqslant \frac{\Delta H_e}{2 H_o} \qquad 7.22$$

If k is greater than this range then the E.S.R. spectrum is distorted. (This was explained in section 5.3) This distortion provided a useful method of finding k. A narrow line spectrum was used to do this. A single crystal of D.P.P.H. which had a line width of 2 gauss was used. The value of k was increased until distortion began. The distortion was twofold. The effective line width increased and the amplitude of the spectrum was changed. A convenient way to give dimensions to k is to put $k' = 2kH_o$. Then the units of k', the hybrid field modulation, are gauss. At the point where the distortion begins, $k' = \Delta H_e$, which in the practical example was 2 gauss. The output of the power amplifier was calibrated in gauss by plotting the output amplitude

against spectrum line width. This is shown in figure 7.2. The amplitude of the E.S.R. spectrum was also measured for the various values of k'. The line width was measured by a technique which is outlined in section 7.3. From figure 7.2, it can be seen that the line width increased with k' showing the distortion expected. However, up to a certain value the amplitude of the E.S.R. spectrum also increases with k'. In fact about 6 dB more signal is possible using distorted spectrum. For very large distortion the amplitude decreases as the effective line width increases.

Figure 7.2 Determination of the Depth of Magnetic Field Modulation

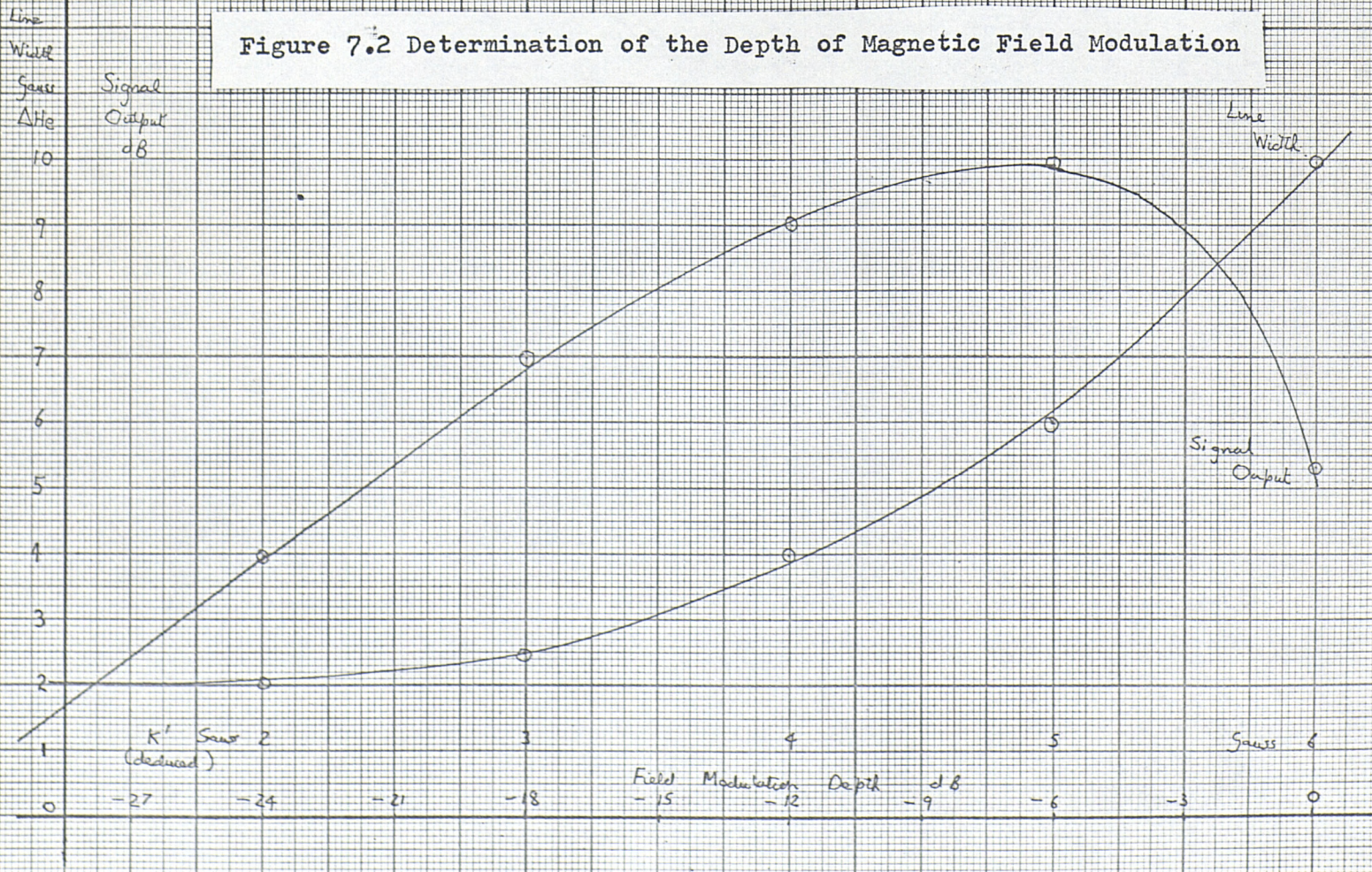

7.3. Calibration of the D.C. Magnetic Field.

The magnetic field was calibrated in two parts. In the first part, a method was used to set up the stabiliser so that the field at the centre of the sweep was known. In the second part, a method was used to calibrate the sweep. In the first part the field was measured using a proton resonance meter which is described by Ingram[1]. Using the proton resonance meter the magnetic field stabiliser was adjusted so that the centre point of the total possible field sweep was about 8,500 gauss. The centre of a spectrum of D.P.P.H. was 8,513 gauss. This spectrum was used to check this calibration.

The second part provided a means of calibrating the field sweep. As the operating frequency of the microwave signal in the spectrometer was accurately known, this calibration was used to calibrate the sweep using the relationship given in equation 5.23. The operating frequency was first adjusted to the ammonia frequency in the usual way, and the sweep voltage required to set the pen recorder to the centre of an E.S.R. spectrum of D.P.P.H. was noted. The operating frequency was then lowered by 10 Mc/s using the coarse control on the Equal Arm Stabiliser cavity (see section 3.2 b)). The sweep voltage required to give the centre of the trace was again noted. This was repeated for two further frequencies. The measurement of the frequency was done by using the calibrated X Band klystron reflector voltage. (See section 4.4 a)) These various voltages and frequencies are shown in figure 7.3. The general sweep

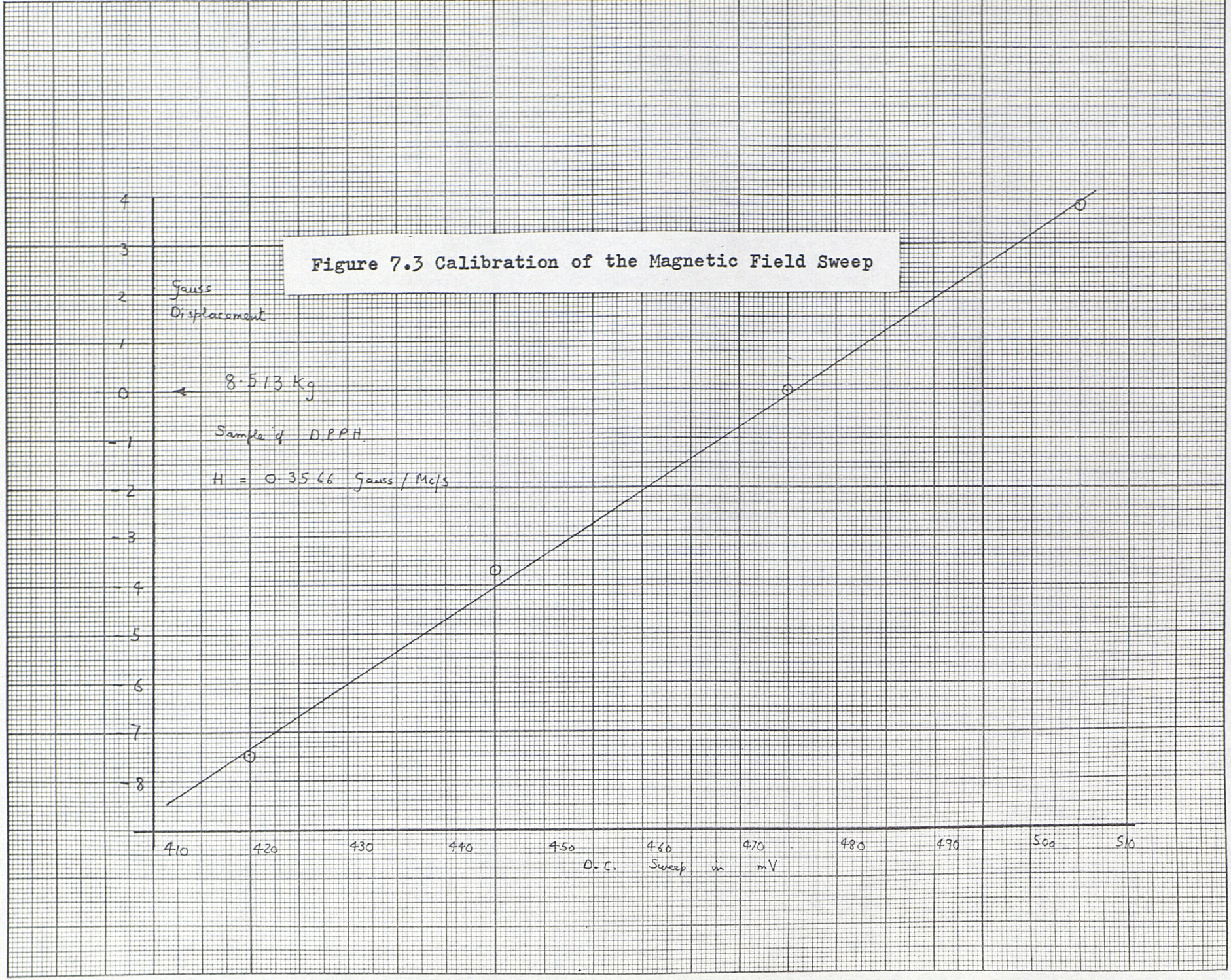

Figure 7.3 Calibration of the Magnetic Field Sweep

calibration figure is the slope of the line in figure 7.3. This slope is 143 gauss per sweep Volt. For small sweeps, the sweep voltage was measured on a Philips (GM 6020) Voltmeter to increase accuracy. If the drift in the stabiliser is assumed to be of the order of 1 mV of sweep voltage, then the field stability is of the order of 0.1 gauss.

It is worth noting the line broadening effect which is due to the magnetic field inhomogeneity. Ingram[1] discusses this broadening and the effect of possible broadening due to the high frequency of the magnetic field modulation. The field homogeneity for this magnet is about 0.1 gauss. This was estimated from the characteristic output of the proton resonance meter. Thus, there is little broadening effect due to field inhomogeneity for values of $\Delta H_e \geq 1$ Gauss. The broadening due to a modulation of 465 Kc/s is higher and is of the order of 0.3 gauss. Thus, this effect is also negligible for values of $\Delta H_e \geq 2$ Gauss. This broadening effect limits the upper frequency of modulation of most spectrometers.

Finally, the magnetic line width ΔH_e is usually defined as the width in gauss at half peak height of the absorption curve. In the double modulation spectrometer, the value measured is usually the width between the peaks of the derivative curve in gauss. This width is the distance between the points of maximum slope on the absorption curve. If $\Delta H_e'$ is the 'width' of the derivative curve the value of ΔH_e can be obtained from[1]:-

$$\Delta H_e = 1.17 \Delta H_e' \quad \text{Gaussian Line Shape}$$
$$\Delta H_e = 1.73 \Delta H_e' \quad \text{Lorentzian Line Shape} \qquad 7.31$$

7.4. Determination of Detector Bandwidth.

The measurement of the detector bandwidth was essential for measurement of the spectrometer sensitivity. As far as the present circuit was concerned the bandwidth of the detector was determined by the frequency response of the pen recorder and the time constant of the low pass filter at the input to the pen recorder. This was described in section 6.4 a).

The type of pen recorder used in this spectrometer was a simple moving coil ammeter movement. This recorder had all the usual faults of sticking on the paper and also jumping whenever the paper was uneven. To overcome these faults it was normal to work with quite a low signal to noise ratio at the output. For very low noise levels the apparent noise was smaller than the real noise due to the static friction of the pen being higher than the dynamic friction (i.e. sticking). The system was thoroughly tested for linearity so that there was no distortion for signals larger than one division on the trace. The pen recorder had a resonant frequency at about 0.85 c/s which had a loaded 'Q' factor of about 1.6.

Three time constant settings were available on the low pass filter (see section 6.4 a)). One of these settings gave just the pen recorder characteristic, as the time constant was small. The other two had much larger time constants. The overall response was measured by putting into the input of the D.C. amplifier feeding the pen recorder a low frequency sinusoidal signal, and measuring the amplitude on the pen recorder. The response of the three settings

is shown in figure 7.4. It can be seen in figure 7.4 that the pen recorder resonance effects, to a certain extent, all three response curves. A reasonable approximation to $\Delta\nu$, the detector bandwidth is the upper 3 dB point definition. Although this neglects the resonance effect it still gives reasonably accurate figure. The method gives values of $\Delta\nu$ as 1.48 c/s, 1.04 c/s and 0.16 c/s for the three positions on the low pass filter. These positions are equivalent to time constants of 0.1 seconds, 0.15 seconds and 1.0 second respectively.

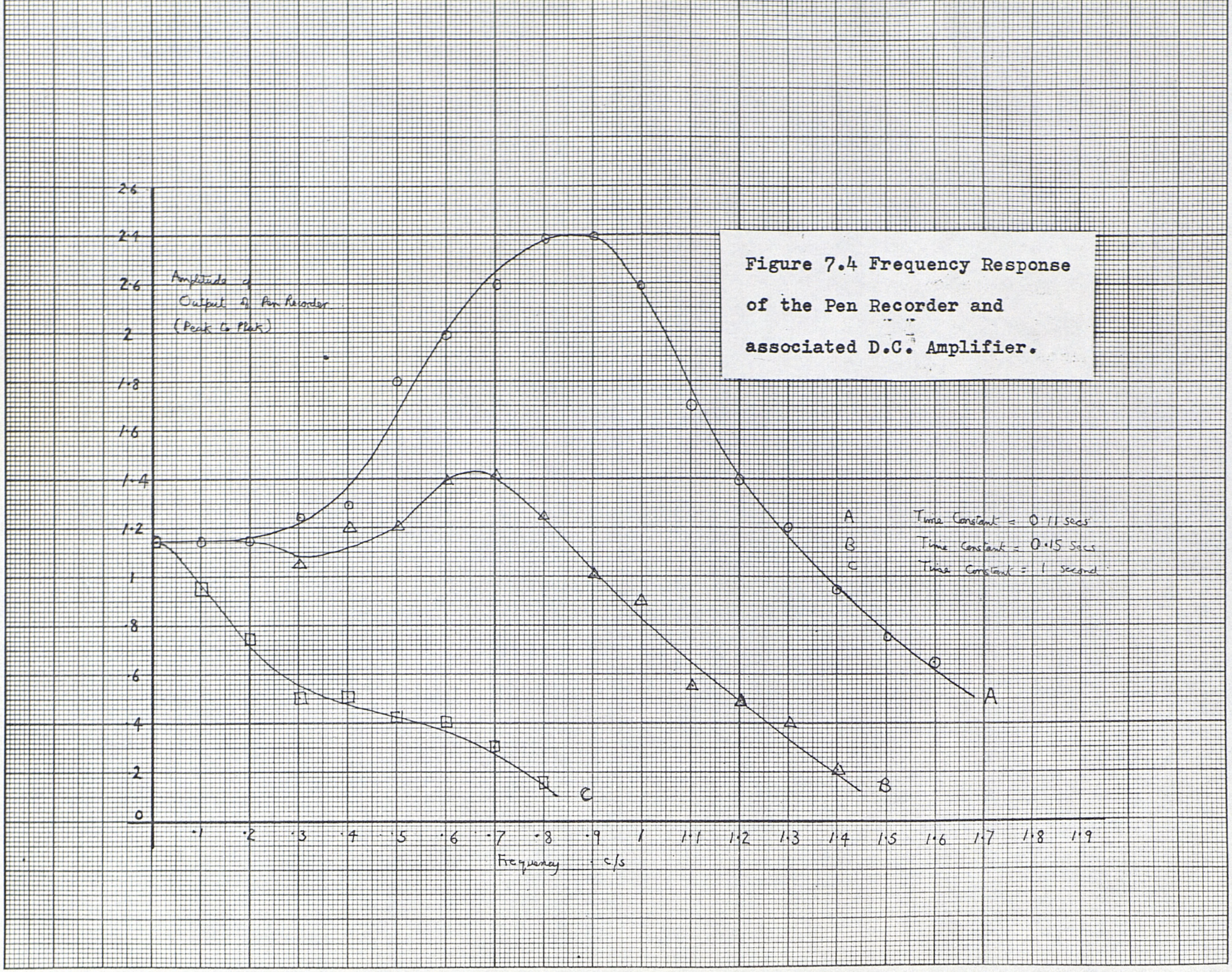

Figure 7.4 Frequency Response of the Pen Recorder and associated D.C. Amplifier.

7.5. Determination of the Sensitivity of the E.S.R. Spectrometer.

This section links most of the preceding sections of this chapter. The section begins with a full definition of sensitivity and then a measurement of generator power. Following this there is a brief discussion on the making of standard samples and the measurement of sensitivity. Finally, a comparison with both the theoretical value and practical values from other spectrometers is made.

The definition of sensitivity which was taken was that stipulated by 'Varian Associates'. This definition was adopted so that direct comparison between their spectrometer and the present system could be made. The sensitivity of a spectrometer depends on several factors which include - the line shape of the sample, the definition of noise output, the sample line width, the lossiness of the sample, the filling factor and the homogeneity of the modulating field. To eliminate some of these variables the following definitions were stipulated:-

i) Noise Level = $\frac{\text{The Peak to Peak Noise}}{2.5}$

ii) Signal Level = The Peak to Peak Signal Height (including noise)

iii) Optimum Field Modulation. It has been assumed that this is the modulation which just distorts the spectrum (see section 7.2 d)).

iv) Time Constant of the Detecting System = 1 Second.

v) Temperature of the System = Ambient temperature.

Before any measurement of sensitivity was made the power level was measured to find the value accurately. If the frequency tripler had been functioning properly the power entering the E.S.R. cavity (half the generating power in this present system) would have been 1 mW. It was found that the power was a factor of 10 below this at 0.1 mW. This power was measured by comparison with the power coming from the local oscillator which was 1 mW. Unfortunately, the makers of the frequency tripler (Microwave Associates) were unable to repair the device (it needed both retuning and a new crystal fitting) in time to repeat the measurements at the higher power.

Several standard samples were made using carbon which had been heat treated[1]. The standard samples below 10^{15} spins were diluted with chalk to make the weighing of the samples easier. It was found that the background E.S.R. signal from the glass sample tube swamped the sample E.S.R. signal below about $9.\ 10^{13}$ spins. The standard samples were checked on a Decca Spectrometer (situated at Southampton University) using 10 mW input power to the sample cavity. In order to obtain a convenient signal to noise level at the pen recorder, a standard sample of $4.\ 10^{14}$ spins was chosen for the sensitivity measurements.

The sensitivity was measured by obtaining the E.S.R. spectrum of this sample ($4.\ 10^{14}$ spins) with, and without, the maser operating. The figure was then reduced by the various factors outlined in the previous definition. They are :-

i) Signal to Noise 7 (without the maser)

ii) Time Constant Correction to 1 second 2.58

iii) Bandwidth of sample 10

iv) Signal to Noise 70 (with the maser)

This gives the sensitivity of the system as:-

$2.2 \cdot 10^{12}$ (without the maser operating)

$2.2 \cdot 10^{11}$ (with the maser operating)

These figures were taken from several measurements and an example of such a measurement is shown in figure 7.5.

The theoretical sensitivity can be obtained from equation 5.39:-

$$S_e = \frac{\Delta H_e}{k H_o} \quad \frac{4 V_c \rho_e}{\omega_o Q_e \hbar \beta_e F_e} \sqrt{\frac{K^3 T^3 \Delta\nu F_{om}}{P_e}}$$

The values used were:-

ΔH_e	The Magnetic Line Width of Carbon	=	10 Gauss
V_c	E.S.R. Cavity Volume	=	1 cm^3
ρ_e	The Sample Density	=	2.2 gm/cm^3
K	Boltzmann's Constant	=	$1.38 \cdot 10^{-23}$ joules/°K
T	The Sample Temperature	=	310°K
$\Delta\nu$	Bandwidth of the Detector (for a Time constant of 1 second)	=	0.16 c/s
F_{om}	The Overall Noise Figure (see next section for how this figure is obtained)	=	1.2
$kH_o = k'$	Magnetic Field Modulation	=	5 Gauss
ω_o	Spectrometer Microwave Frequency	=	$1.5 \cdot 10^{11}$ rads/secs.
Q_e	Loaded 'Q' of the E.S.R. cavity	=	3,000.
$\hbar$	(Plank's Constant). $\frac{1}{2\pi}$	=	$1.05 \cdot 10^{-34}$ joules sec.

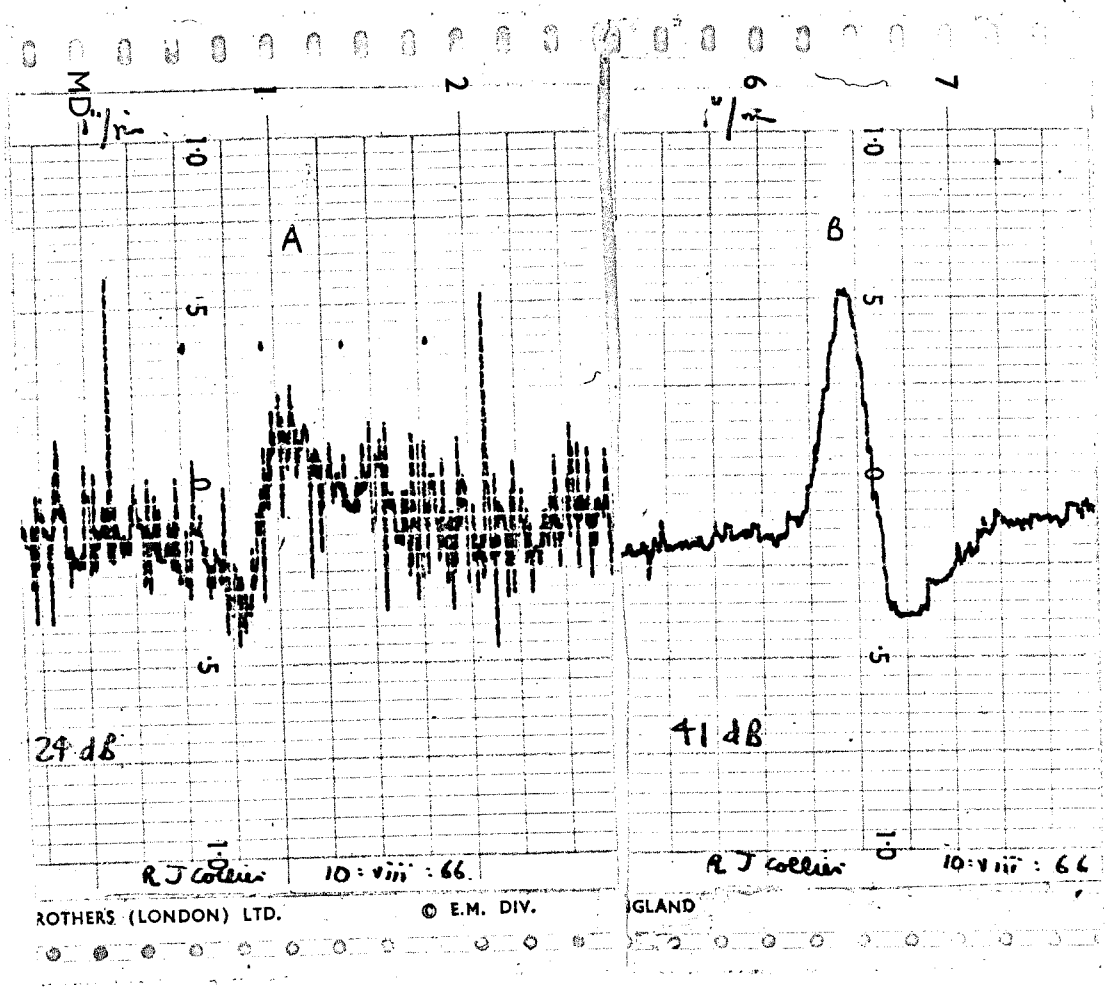

Figure 7.5 Sensitivity Measurements on the Carbon Standard Sample. A E.S.R. Spectrum of 4 . 10^{14} Spins without the Maser operating. B The same spectrum with the Maser operating.(the phase is changed in the output by π)

Line Width of Sample 10 Gauss Dectector Time

Field Modulation 5 Gauss Constant 0.15 Secs

(Spikes on spectrum A are field calibration marks)

β_e	Bohr Magnetron for an Electron	=	$0.927 \cdot 10^{-20}$ ergs/gauss
F_e	Field Distribution Factor for TE_{012} Cavity Mode	=	1
P_e	Generator Power	=	0.2 mW

The value of F_e given by Feher[2] is for the cavity mode TE_{101} and was the value 4. The theoretical sensitivity is $S_e = 1.2 \cdot 10^{11}$ spins if the maser is operating and $6.7 \cdot 10^{11}$ spins if the maser is not operating (using a value of $F_o = 38$). The practical sensitivity with the maser operating agrees with theoretical value quite closely. The difference is probably due to the lossiness and line shape of the sample which have been neglected so far. The practical sensitivity without the maser operating is much poorer than the theoretical value. This difference will be discussed in the next section.

In figure 7.6 an example of the various spectra obtained for different detector bandwidth settings are shown. In view of the general overall instability of the system, the spectra were normally taken over a period of about a minute. (The normal time would be about five minutes) As a result of this shorter 'sweep time' a smaller time constant was used in the detector so that a noise level, which could be measured easily, was obtained.

Finally, the sensitivity was compared with other spectrometers, insofar as information about the spectrometers was available. The 'Varian Associates' Spectrometer claimed a sensitivity of 2.10^{11} spins for the following data:-

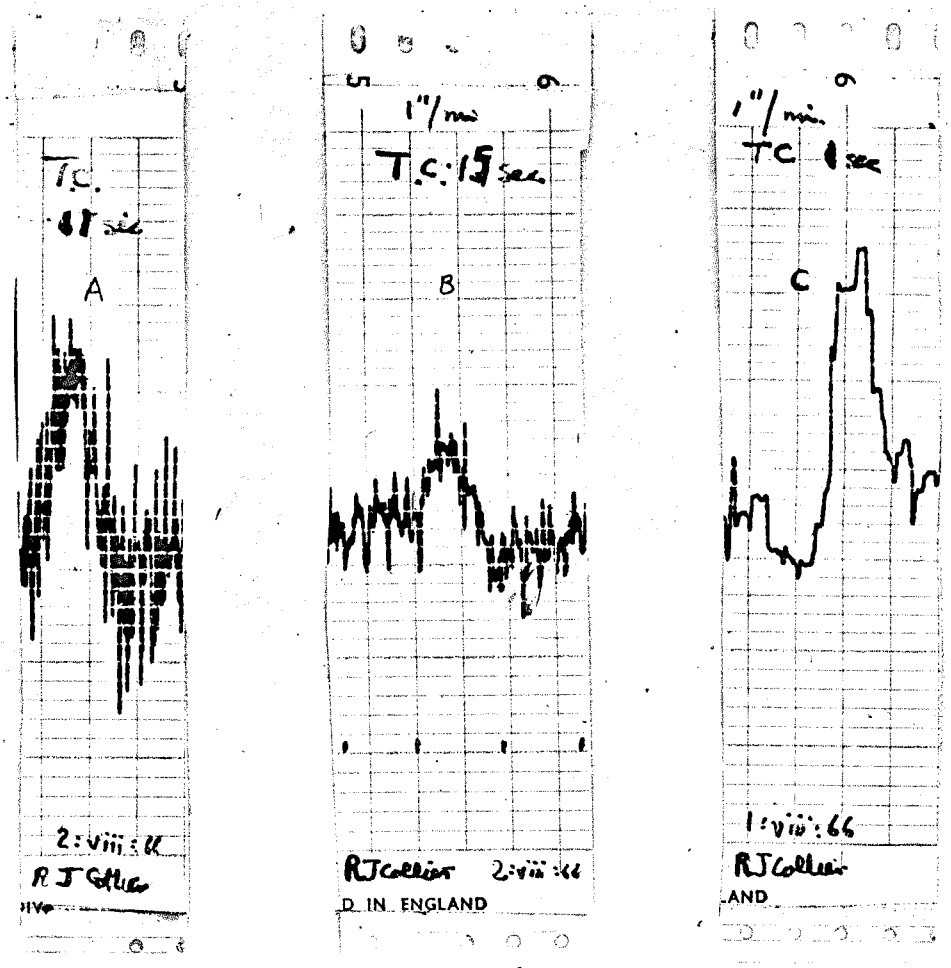

Figure 7.6 Sensitivity Measurements on a Standard Sample of Carbon. The Effects of Detector Time Constant. A E.S.R. Spectrum of carbon 4. 10^{14} Spins with a time constant of 0.11 Secs, B Same spectrum with a time constant of 0.15 secs. C Same Spectrum with a time constant of 1 second. Line Width 10 Gauss. Field Modulation 5 Gauss.

i)	Power Entering the Cavity	250 mW
ii)	'Q' of E.S.R. Cavity	7,500
iii)	Ambient Temperature Operation	
iv)	Microwave Frequency	10 Gc/s
v)	Cavity Mode	TE_{012}

Converting this sensitivity to a power of 0.1 mW power into the cavity, the sensitivity becomes 1. 10^{13} spins. Thus the apparent improvement at this power level is a factor of 45.5. Taking the theoretical improvement due to the maser as 5.62 (rather than the practical value - see next section) the improvement made by raising the operating frequency becomes a factor of 8. The theoretical factor of improvement can be obtained from the Feher[2] proportionality of $f^{\frac{7}{2}}$ and using the Varian Associates Q of 7,500. The factor is 18. If the practical value of Q was taken as 3,000 (rather than 5,000 which the figure of 7,500 at 10 Gc/s would become theoretically at 23,87 Gc/s) then the factor would be 10. Once again the difference here is probably due to the fact that both the lossiness and the line shape of the sample have been neglected.

The sensitivity of the 'Decca Ltd.' Spectrometer was measured by the author at Southampton University. Here the sensitivity was found to be 1.4. 10^{12} spins for the following data:-

i)	Power entering the Cavity	10 mW
ii)	'Q' of the E.S.R. Cavity	approximately 5,000
iii)	Ambient Temperature Operation	
iv)	Microwave frequency	10 Gc/s
v)	Cavity Mode	TE_{012}

Converting this sensitivity to a power of 0.1 mW the sensitivity becomes $1.4 \cdot 10^{13}$ spins. Clearly, this figure is similar to the 'Varian Associates' sensitivity if the lower 'Q' factor is taken into account.

In conclusion to this section, it is worth noting that for several samples which are measured by E.S.R. techniques, the saturation power is about 1 mW. Thus the present spectrometer, although not capable of such large powers as the X Band counterparts is clearly an improvement when only a small generator power is allowable. Unfortunately, it is not possible to quote the sensitivity of the present K Band spectrometer at say 1 mW as $7. 10^{10}$ spins or at 250 mW as $4.4 \cdot 10^{9}$ spins, as this has not been observed practically. Also, the main klystron noise (which has been assumed negligible so far), may well be the limiting factor as the generator power is increased.

7.6. Noise and Stability of the Spectrometer.

In the previous section the improvement in the signal to noise ratio obtained from the maser was greater than that predicted in section 4.5. Inspection of equation 5.419 shows that the output of the spectrometer was proportional to the product of two phases, because there were two P.S.Ds in series in the detection circuit. Any change in the frequency of the main klystron would produce a change in the spectrometer output, even if this change in frequency was very small. These changes appeared at the output as additional noise to the normal amplitude noise. This additional noise is called frequency noise. The frequency noise is caused by amplitude noise on the reflector of the main klystron. Causes of this noise were:-

1) Mechanical and Thermal noise effecting the equal arm stabiliser - especially the cavity of the stabiliser.
2) Amplitude noise generated in the modulation circuits supplying the equal arm stabiliser.
3) Noise from the main klystron power supply.

When the maser was operating, it was assumed that the majority of this noise was eliminated. This was particularly true when the maser gain was high and the A.F.C. was thus more efficient. Using equation 4.54 (the Friis formula) and the data from figure 7.5 where $G' = 300$ and $F_o = 38$ the figure for F_{om} becomes 1.2 (0.8 dB). This figure was used in the theoretical calculation made in the last section. The improvement in output of amplitude noise is given by equation 4.55.

In this practical example, this improvement would be the factor 5.63. As the practical improvement was the factor of 10 this suggests that the improvement in frequency noise is the factor 1.8 (or 2.5 dB). Use of the Friis formula is limited to only amplitude noise, so that an extended formula might be:-

$$F_{om} = 1 + \frac{F_o - 1}{G'} + \frac{F_n}{S_m} \qquad 7.61$$

where F_n is the equivalent amplitude noise figure of the frequency noise (in this case 1.8) and S_m is the increase in frequency stability (in practice about 100). The overall noise figure without the maser would then become 66 or 18.2 dB.

So far, no mention has been made of the amplitude noise produced by the two klystrons in the circuit. Extensive tests were made by T.H.W. to find the effect of noise from the local oscillator and the conclusion was that it could be neglected. Similarly, the noise on the main klystron can be neglected. This was discussed by Feher[2] and he showed that for small values of P_e (i.e. only a fraction of the power of the main klystron) the noise could be neglected. Even so, despite their claims this source of noise might well be the cause of the loss of sensitivity, with respect to the theoretical figure, discovered in the last section.

In section 4.4 d) the gain stability of the maser was discussed. It was found, in practice, that for higher values of maser gain the effect of the intermittent leak in the pressure system was almost reduced to zero. This would suggest that part of the

'spike' produced by the leak was a result of a slow response of the maser A.F.C. The response time of the A.F.C. decreased as the maser gain increased. The spectrum in figure 7.5 showed no signs of these 'spikes'. When some further spectra were run at lower maser gain values these spikes appeared. These are shown in figure 7.7. Besides the obvious way of eliminating the leak from the system, these spikes could be eliminated by:-

i) Decreasing the bandwidth of the detector

ii) Increasing the maser gain.

Finally, the drift in the E.S.R. bridge did not cause an increase in frequency noise but it did cause some of the spectra to be distorted. This was because the drift in phase changed the spectra from being the derivative of an absorption spectra to being the derivative of a dispersion spectra. This was eliminated to a large extent by the temperature control of the E.S.R. cavity. This was described in section 6.2 b). Figure 7.8 shows the spectrum of a carbon sample (not amplified by the maser) which was traced forwards and backwards consecutively. It can be seen that between the two spectra there is little or no change in phase.

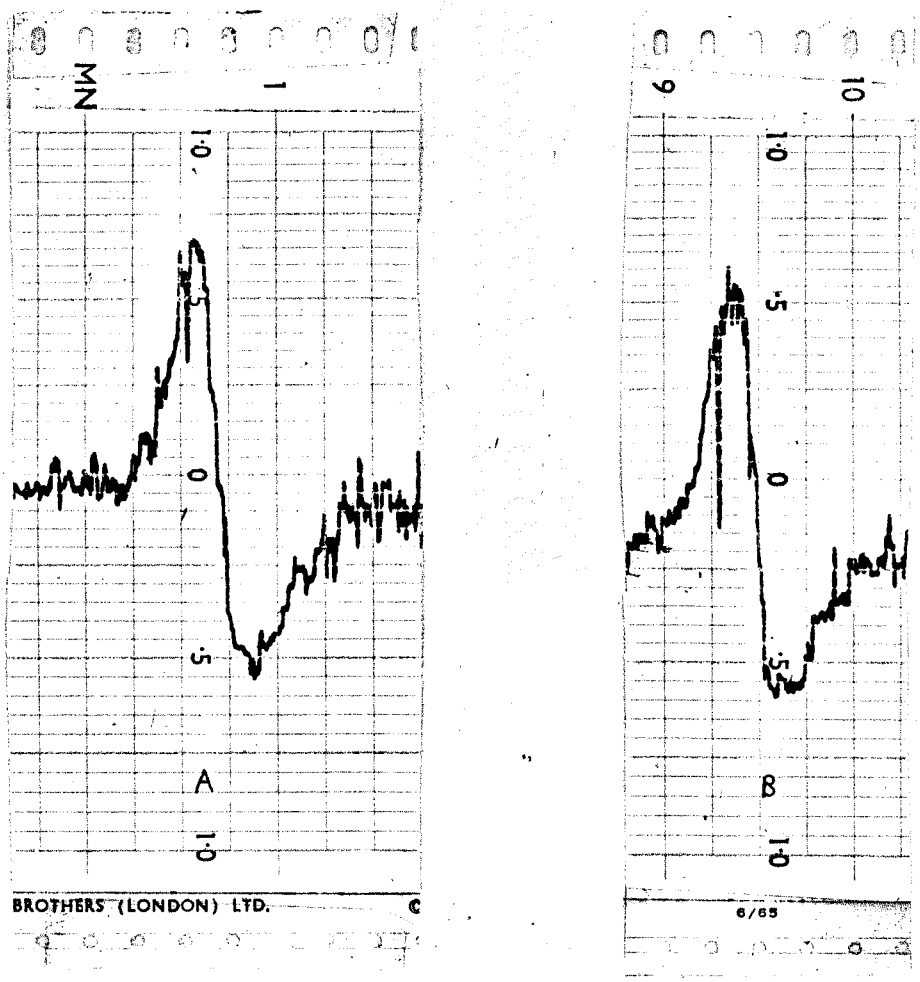

Figure 7.7 Stability of Amplified E.S.R. Spectra.

A Amplified E.S.R. Spectrum (Maser Gain 10 dB) of Carbon Sample ($\Delta H_e = 10$ Gauss) showing instability due to leaks in the maser chamber. B Same spectra later in time. Field Modulation 5 Gauss

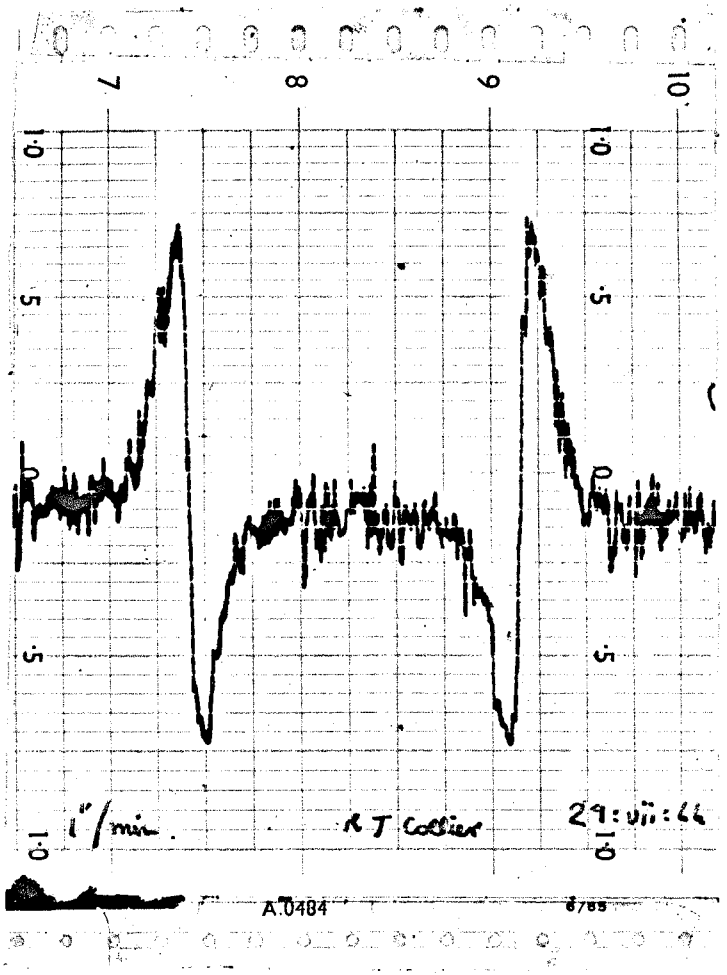

Figure 7.8 Phase Stability of Spectrometer. A Sample of carbon was examined twice as shown above. The E.S.R. Spectrum was traced in both directions of magnetic field sweep. There is negligible phase drift between the Spectra.

7.7. Saturation Effects.

The object of this section is to discuss, briefly, the effects of maser saturation on the amplified E.S.R. signals. This section is not dealing with the saturation effect which occurs when a large value of P_e is used, which for some samples the saturation power might be as small as 1 mW. The first saturation effect that will be considered is the saturation caused by an A.F.C. signal which is too large. The condition (5.412) that the E.S.R. signal is much smaller than the A.F.C. signal will be assumed, as this was normally the case. When the maser saturated the gain was reduced. The most noticeable effect was that the improvement in signal to noise ratio was reduced. As the small signal gain, even in saturation, is constant, the E.S.R. signal was still amplified but at reduced maser gain. In figure 7.9 there is an example of such a case. It can be seen that there is little or no distortion due to non-linear gain. This type of distortion does not change the value of the measured magnetic line width, but could change the value of the measurement of the number of spins.

The second saturation effect considered was the opposite case to the first. In this case the A.F.C. level was the normal one and the maser was not saturated, when there was no E.S.R. signal. The maser saturated, when the E.S.R. signal was passed through it. As before, a reduction in the improvement in signal to noise level was noticed and a little distortion. An example of such a spectrum is shown in figure 7.10. Unfortunately, the E.S.R. spectrum was not big enough

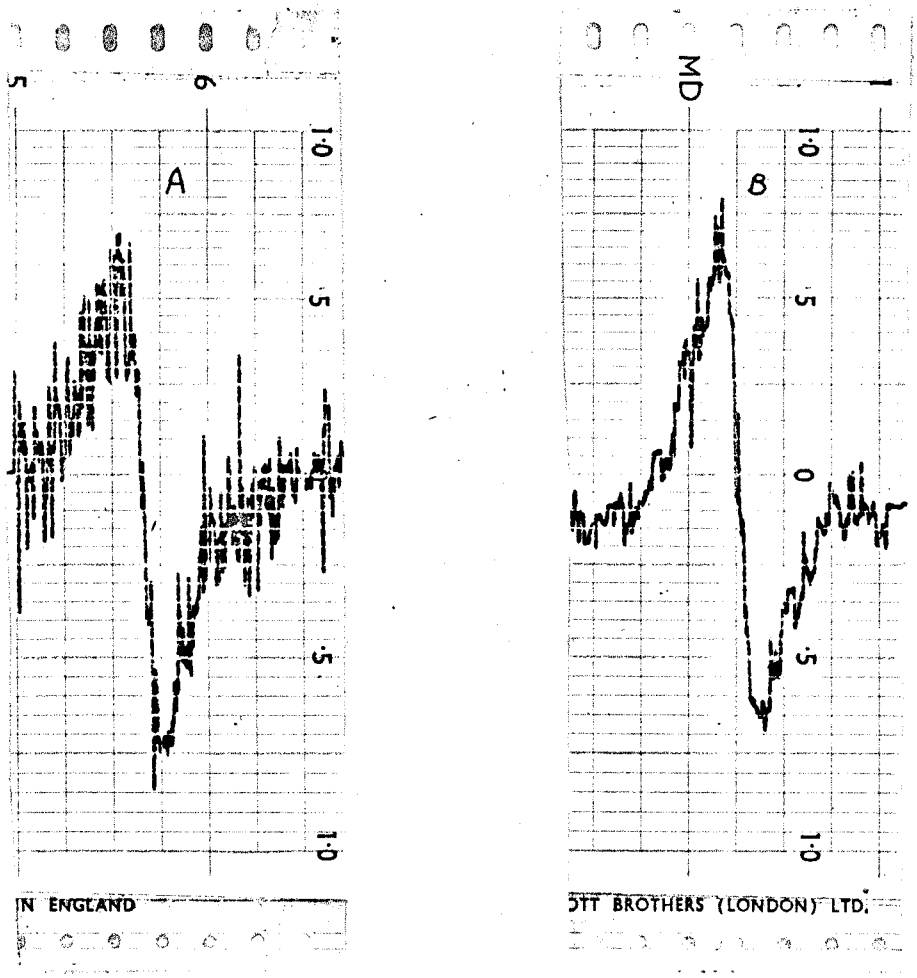

Figure 7.9 Saturation Effects caused by the Maser A.F.C. A Spectrum of Carbon without maser operating, B The same Spectrum amplified by the Maser. Gain of Maser = 10 dB. The Maser was saturated by the A.F.C. signal. The E.S.R. signal was much smaller than the A.F.C. Signal.

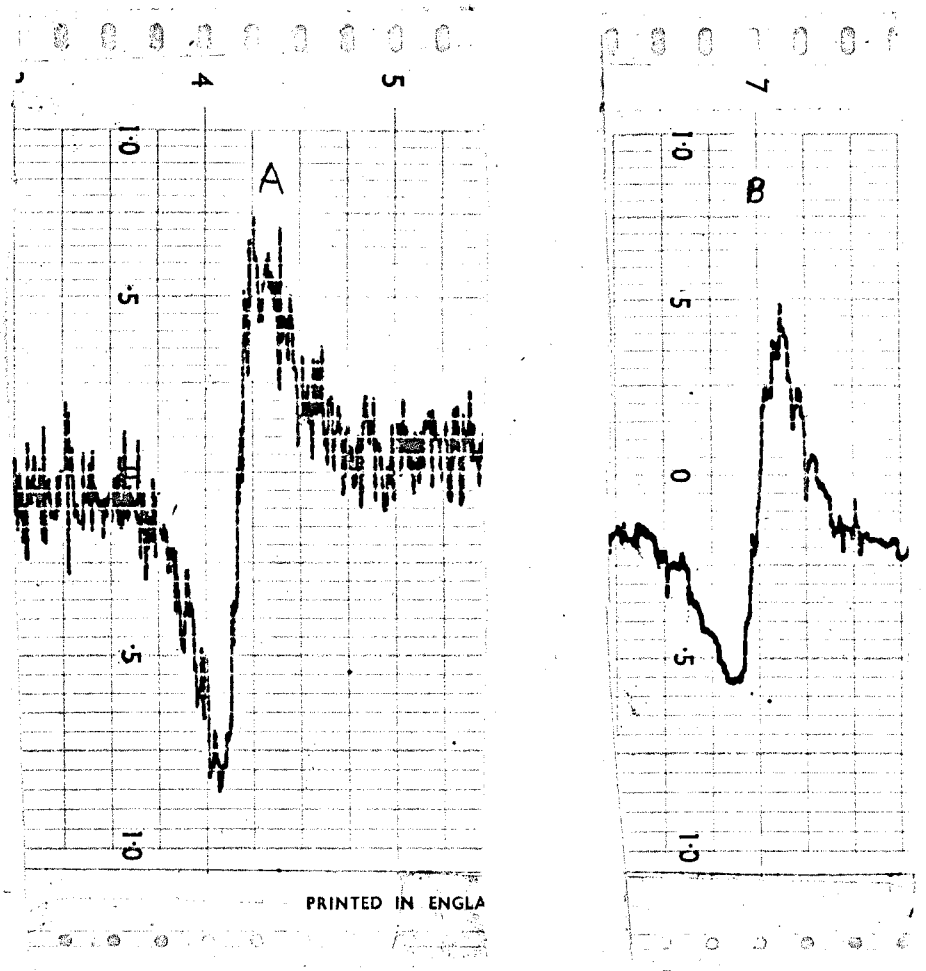

Figure 7.10 Saturation Effects caused by the E.S.R. Signal. A Spectrum of Carbon without the Maser Operating. B The same spectrum amplified by the Maser. The Maser was not saturated by the A.F.C. signal. The maser was saturated by E.S.R. signal. Maser Gain 17 dB.

to drive the maser well into saturation. Even so, there was a reduction is the noise performance and slight distortion. The theoretical curves in figure 1.11 for the saturated gain show that the gain falls off in saturation at approximately the rate of 10 dB for every increase in input of 40 dB. This shows that a very large increase in E.S.R. spectrum would be needed to really saturate the maser. Thus the chief effect of saturation is not one of distortion but of increase in noise.

References Chapter 7

1. D.J.E. Ingram. "Free Radicals as studied by Electron Spin Resonance". pages 98 & 121 1958

2. G. Feher. "Sensitivity Considerations in Microwave Paramagnetic Resonance Absorption Techniques". The Bell Syst. Tech. Jor., Mar. pages 451 & 465 1957

3. W.A. Gambling and T.H. Wilmshurst. "An Electron Spin Resonance Spectrometer using the Ammonia Maser as a Pre-amplifier". Vol. 5, No. 4, 15th July, Phys. Letters page 228 1963

Chapter 8

Conclusions

This thesis is in two distinct parts. The first part deals with the ammonia maser as an amplifier and the second part with the application of the amplifier to an E.S.R. spectrometer. Only a sparse theory of the ammonia maser amplifier existed at the commencement of this work, so it was decided to devote a large section of the work to working out and proving experimentally the theory of the amplifier. On the other hand, the E.S.R. spectrometer was covered by a large amount of literature which described most of the features of it's performance. For this reason, only a small section of the work was devoted to E.S.R. theory. The object of this chapter is to make comments on the various results and to suggest further work where possible.

Several of the results of the work on the ammonia maser are quite new to the field of ammonia maser amplifiers. As the application of the ammonia maser has been very limited, it is not expected that these results will change the position of the amplifier to any degree. The first results to be considered are the mid-band gain characteristics (shown in figures 4.4, 4.5 and 4.6). These results form a complete set of characteristics. Using the theoretical analysis, a method of calibrating the small powers involved in this work was developed. The range of these powers was 10^{-14} - 10^{-9} Watts. Further work in this field might be done on the limitations of the maximum stable gain of the maser amplifier. This

might be extended to any regenerative amplifier.

The second set of results to be considered are the various bandwidth characteristics. One of the results of this work was the resolution of the hyperfine components of the J = 3, K = 3 transition of the ammonia inversion spectrum. This has not been achieved before. This is shown in figures 4.7 and 4.8. The other characteristics are shown in figures 4.9, 4.10 and 4.11 and these include the development of an equivalent circuit of the maser. An unusual result was obtained from work on the frequency pulling effect of the main maser cavity. This effect is wellknown in the field of ammonia maser oscillators but has never been observed before in the context of the amplifier. All these results verified various sections of the theoretical analysis and the agreement between them was sufficiently good to suggest that the present theory is an accurate representation of the ammonia maser amplifier.

The third set of results was concerned with the stability and noise of the ammonia maser amplifier. Like all research using vacuum techniques this work was hampered with small leaks. These were incorporated into the general instability of the amplifier. The theoretical improvement in signal to noise ratio was also evaluated.

The majority of the work on the K Band E.S.R. spectrometer was spent in verification of the work done by T.H.W.[1] previously. However, it proved to be more than just a verification as several unique features were also developed in the course of the work. In order to avoid the ambiguity (prevalent in many publications) about

the sensitivity of the spectrometer, this factor was carefully defined at the outset of the work. It was found necessary to develop a complete theory of the detection technique in order to find the optimum operating conditions.

Some of the improvements made on this present spectrometer, by the author, include the increasing of the available generator power from 0.03 mW to 0.2 mW, the development of an E.S.R. cavity temperature control, the construction of an electronic locking system for the local oscillator klystron, the increasing of the maser gain by the use of a circulator, the development of the electronic modulation of the equal arm stabiliser and the calibration of the magnetic sweep. All these have been covered in the text.

The results of the E.S.R. work were compared with other spectrometers in section 7.5. In this spectrometer a sensitivity of $2.2 \cdot 10^{11}$ spins were obtained for a magnetic bandwidth of 1 Gauss and a generator power of 0.2 mW and a detector time constant of 1 second. The configuration used in the microwave circuit of the spectrometer was the 3 dB coupler - or magic tee - system. An improvement in sensitivity could be obtained with a higher order coupling if better matching could be obtained with the E.S.R. cavity. The effects of the maser amplifier were clearly demonstrated in figure 7.5 and the improvement in signal to noise reduction was a factor of 10. This was a reduction in both amplitude and frequency noise. The various effects produced by the saturation of the maser are demonstrated in figures 7.9 and 7.10. The stability of the spectrometer is shown in

figures 7.7 and 7.8. As far as the use of the maser is concerned the main disadvantage was not the narrow bandwidth but rather the small saturation power. In fact the narrow bandwidth was an advantage as it reduced frequency noise and provided a frequency standard for the spectrometer.

The improvement in sensitivity as a result of increasing the operating frequency from the conventional X Band to the K Band was not demonstrated as clearly as the maser effect. A spectrometer with a similar cavity at X Band would have a sensitivity of about $1. 10^{13}$ spins for the same generator power and magnetic line width. Thus the improvement in sensitivity appears to be lower than that anticipated by Feher[2] for a constant sample volume. This is partly due to the better noise figures (without maser preamplifiers) of spectrometers at X Band as compared with K Band. The improvement in this present work due to raising the operating frequency is thus a factor of about 8. Several reasons for this effect have been suggested in the text of Chapter 7.

Further work on E.S.R. spectrometers could be done in several fields. The first would be to investigate the way in which the filling factor and the 'Q' factor for the various cavity modes effected the sensitivity. The second would be to investigate the other low-noise amplifiers which are now available as possible preamplifiers for E.S.R. spectrometers. Although not all these forms of low noise amplifier have been developed at K Band aat the present time, they exist at X Band. Examples of such amplifiers

are the ruby maser, the parametric amplifier and the parametric up-converter. The ruby maser has the disadvantage that it requires liquid helium. If it were used in a spectrometer where the E.S.R. cavity was cooled to liquid helium temperatures this would not be a disadvantage. The sensitivity at $4^{o}K$ could be as impressive as $3.\ 10^{8}$ spins. The other two amplifiers require high pump powers at frequencies greater than the signal frequency, even this will not be a disadvantage as better Q Band klystrons are developed.

Thus the main objects of the work have been achieved with several interesting side features which could lead on to further useful work in this field.

References Chapter 8

1. W.A. Gambling and T.H. Wilmshurst. "An Electron Spin Resonance Spectrometer using the Ammonia Maser as a Preamplifier".
Vol. 5, No. 4, 15th July, Phys. Letters page 228 1963

2. G. Feher. "Sensitivity Considerations in Microwave Paramagnetic Resonance Absorption Techniques".
The Bell Syst. Tech. Jor., March page 460 1957